To Diana

ProQuest Number: 10609396

ProQuest 10609396

ProQuest LLC.
789 East Eisenhower Parkway
P.O. Box 1346
Ann Arbor, MI 48106 – 1346

DENSE SKYRMION STRUCTURES

by

PATRICK JONES

A THESIS SUBMITTED FOR THE DEGREE OF PH.D.

UNIVERSITY COLLEGE LONDON

1

ABSTRACT

The Skyrme Model is used to investigate dense baryonic matter.

A general review of skyrmionic crystalline arrays thus far investigated, reveals the existence of a universal delocalising phase transition as the density of baryonic matter is increased. At low densities the skyrmions localise on the lattice points, while at high densities they become delocalised and an array of half skyrmions remains. This phase transition is believed to represent the restoration of chiral symmetry of high densities.

Numerical solutions of static arrays with fcc, bcc and intermediate symmetries are considered as a function of density. The fcc array is found at high densities to be the most stable of all the arrays so far considered. As the density is decreased the fcc array becomes unstable against deformations to arrays with intermediary symmetries. This instability occurs at a critical density slightly greater than that of the delocalising phase transition.

A single skyrmion on a three sphere has an analogous delocalising phase transition as the volume of the sphere increases. Generalising this simple model of a skyrmion on a three sphere, to a skyrmion on an elliptical three surface, we identify that varying the shape of this sphere is analogous to deforming the fcc array. It is shown that the deformation transition occurs at the same critical volume as the delocalising phase transition. Beyond this density there are a large number of unstable modes, suggestive of a solid to liquid phase transition. There

also exists a first order phase transition, corresponding to a phase separation.

The relevance of The Chiral Bag Model to dense crystalline skyrmionic matter is discussed and its possible future application is outlined.

ACKNOWLEDGEMENTS

CONTENTS

CHAPTER 1

INTRODUCTION

CHAPTER 2

INTRODUCTION TO THE SKYRME MODEL

CHAPTER 3

DENSE SKYRMIONC MATTER IN A CRYSTALINE FORM

CHAPTER 4

SKYRMIONIC MATTER ON A CLOSED SURFACE OF VARYING CURVATURE

CHAPTER 5

CHIRAL BAGS WITHIN DENSE SKYRMIONIC MATTER

CHAPTER 6

CONCLUSIONS

LIST OF TABLES AND FIGURES

CHAPTER 1

INTRODUCTION

1.1 General Introduction

In this thesis, I will present the results of my investigations involving dense skyrmionic matter systems, which are believed to pertain to dense baryonic matter systems. We shall see that there exist a number of differing forms of skyrmionic matter and that I have employed a variety of differing techniques in order to establish an understanding of each.

The most direct of these approaches involves the brute force technique, of numerically obtaining results for dense skyrmionic matter in its crystalline form and I shall present numerical results for infinite crystalline arrays of skyrmionic matter. In particular, I consider a fcc array, a bcc array and a series of arrays of intermediate symmetries. The discovery of the existence of these arrays of skyrmionic matter and their respective numerical results, have already been reported in reference [1] .

I shall also extend some of the results obtained by Manton [2] for a single skyrmion on a three sphere, S^3_{phy}. I shall generalise this simple model of dense skyrmionic matter, to more general shaped physical space. Using an ellipsoidal

shaped space as an example, I demonstrate the significance of the curvature and the symmetry of physical space in a dense skyrmion environment. This model is constructed so that its relation to dense crystalline skyrmionic matter can be revealed.

A final approach to understanding of the nature of skyrmionic matter will be outlined, in which the Chiral Bag Model is invoked in order to include an explicit quark content within crystalline skyrmionic matter and to establish the physical relevance of such dense baryonic matter.

In the remainder of this chapter, we shall briefly outline historically, the development of the Skyrme Model and finally, the manner in which the rest of this thesis has been organised.

The Skyrme model was originally proposed by Skyrme [3] in 1961, as a phenomenological description of the nucleon and this model has recently attracted much interest. The model describes the nucleon as a topological soliton of an extended version of the Non-Linear Sigma Model. This revolutionary approach to nuclear physics, attempts to describe the fermionic nature of nucleons in terms of bosonic pion fields.

Skyrme [3] was able to deduce many of the properties of his model, by assuming that a spherical symmetric solution existed within his model. He showed that such a solution gave a reasonable picture of a nucleon. The spherically symmetrical hedgehog solution, he viewed as a classical degenerate combination of nucleons and deltas. Fixing the mass of the soliton to that of the nucleon led

8

to an energy distribution, with a *r.m.s.* of $\sim 0.5 fm$, he also deduced that the correct asymptotic form for the one-pion exchange potential between nucleons emerged. He proposed that the topologically conserved winding number of these hedgehog skyrmions, be identified with the baryon number.

Though Skyrme's work was generally ignored during the 60's and 70's, it has recently received a revival of interest. Indeed, much of this new interest stems from the realisation within theoretical physics, that such a topological non-trivial solution of the non-linear bosonic field theories, can be used to describe fermionic particles. Indeed, within other simpler models [4], the relationship between fermion number and topological charge, originally predicted by Skyrme in 1961, was demonstrated.

Attempts to understand hadronic physics from a Q.C.D. stance, had naturally led to a series of effective meson models with similarities to the Skyrme model. Indeed, T'Hooft [5] showed, assuming confinement, that the $1/N_c$ expansion of Q.C.D. leads to an effective Lagrangian in the low energy sector, containing only mesons. Witten [6] later argued that baryons then emerge as solitons in the large N_c limit of Q.C.D.. This reasoning naturally led physicists to look for an effective model for low energy mesonic sectors, which support solitonic solutions. Since the lowest mass meson is the pion and the Non-Linear Sigma model is known to describe low energy pionic physics successfully, this model certainly represents a natural starting point. Hence, Skyrme's extension of the Non-Linear Sigma Model, by introducing his Skyrme term, is now viewed as the first and simplest

term in a truncated infinite series of mesonic terms, which extends the Non-Linear Sigma so as to support non-trivial solitonic solutions. Thus, the Skyrme Model is now viewed as an effective model for low energy Q.C.D. mesonic physics. However, no derivation of this exists.

The bag approach to nuclear physics presents an instructive alternative to such effective low energy Lagrangians. This model directly attempts to understand the relationship between such effective Lagrangians and Q.C.D.. In the model quarks and gluons are governed by Q.C.D. and placed within a spherical cavity. In the Chiral Bag Model [7][8], the exterior of the bag's mesonic degrees of freedom are governed by the Skyrme or similar low energy effective models. The quarks are assumed to be confined to the interior of the bag and mesons to the exterior by the boundary conditions on the bag surface. Imposition of conservation of axial current across the surface of the bag, connects the two dynamical regions and leads to the so called, chiral boundary conditions. Assuming the existence of a spherically symmetric mesonic field, leads to a hedgehog form with a spherical cavity cut out at its centre, in which spherically symmetric, massless Dirac fermion wave functions, obeying the Dirac Equation, have been obtained [7][9]. This object is then viewed as a baryon with the short distance quark degrees of freedom explicitly present. Thus, this elegant, effective, low energy model has developed as a generalisation of the pure skyrmionic description of a baryon.

Balachandron et al [10] and Witten [11] in 1982, showed Skyrme's identifica-

tion of baryon number with winding number of the soliton was indeed correct. In order to make physical predictions for properties, Adkin's etal[12] developed a projection procedure to obtain physical N and Δ states from the classical hedgehog solution. They showed that such an approach produces a reasonable description of the $N\Delta$ mass splitting, nucleon magnetic moments, nucleon charge radii and the coupling constant ratio for πNN and $\pi N\Delta$.

More recently, attempts have been made to understand the interaction between two skyrmions [13][14]. By considering the interactions between two hedgehogs with relative spin-isospin degrees of freedom, they numerically studied the skyrmion-skyrmion potential at finite separations. Invoking the quark hedgehog model, they demonstrated that mesons which couple to hedgehogs, are precisely those which are known to have couplings to nucleons. This model for the two nucleon system was thus shown to successfully describe the nucleon-nucleon potential.

More recently there have been considerable developments in the extension of this model to finite baryon number systems and their application to light nuclear matter systems. Thus, in Chapter 2, having described the Skyrme model and outlined its success in describing a single baryon, we go on to discuss many of the recent and fascinating results obtained for the two baryon system and other finite baryon number systems. These results have shown that the the model seems versatile enough to model single baryons, the deutron and the two nucleon potential.

In Chapter 2 we also briefly introduce Manton's simple model of baryonic matter on a three sphere. The results of this model bear a striking similarity to those which we discuss in Chapter 3 for skyrmionic matter in a crystalline form. Both models reveal, that as the average baryon density of skyrmionic matter is increased, it generally undergoes a phase transition from an uncondensed phase, in which skyrmionic matter's baryon density is well localised in space, to a condensed phase in which skyrmionic matter's baryon density is more evenly distributed throughout space.

For a skyrmion on a three sphere we see that this phase transition occurs as we reduce the volume of physical space and in the uncondensed phase the skyrmion is localised about a point in space, while in the condensed phase it becomes completely delocalised over the whole of space. For skyrmionic matter in its crystalline form, as the average baryon density of the crystal is increased, this phases transition is shown to correspond to an uncondensed array of spherical skyrmions centred at the points of an infinite lattice, becoming a condensed array of half skyrmions.

In Chapter 3 we outline the differing lattices and orientations of skyrmions on these lattices, which have to date been numerically investigated. We also show the manner in which these lattice arrangements of periodic skyrmions are deduced from the analytic form of the asymptotic skyrmion-skyrmion potential. This construction also leads us to discover that there exist other crystalline arrays of skyrmions which maximise the asymptotic attraction between neigh-

bouring skyrmions within the lattice, which have date gone unnoticed. We show that these new simple cubic arrays of skyrmions represent a simple generalisation of the rectangular array which Jackson et al [15] investigated as an alternative to Klebanovs [16] original cubic array of skyrmions. We see that this generalisation of the Jackson et al array, corresponds to a simple continuous relative isospin-rotation of the skyrmions within successive parallel planes. Comparing the asymptotic binding energies of this generalised array to the Jackson et al array, by summing the net asymptotic potential of an individual skyrmion within the array over increasingly distant nearest neighbours, reveals that as the relative isospin-rotation angle of skyrmions within successive planes is varied, the net the asymptotic attraction of progressively increasing numbers of nearest neighbours does not change. Hence we appear, at least asymptotically, to have discovered a genuine zero mode of the Jackson et al array.

We also present in Chapter 3 the arrangements of the fcc array, bcc array and an array of intermediate symmetry. Numerically we show how the binding energy of these arrays increases as their densities are increased. The manner in which these calculations were performed is first described and then we show that their results reveal that a condensed fcc array of skyrmions, corresponding to a simple cubic array of half skyrmions, has an energy which is just 3.8% above the energy lower bound and thus, that it represents the most bound crystalline array of skyrmions so far considered.

We also investigate the effect that bulk deformations have on the fcc array of

skyrmionic matter by varying the length of the fcc cube in one direction, while keeping the other lengths fixed. The results reveal that the fcc lattice becomes unstable with respect to these bulk deformations at a density close to that at which the phase transition to a condensed array of half skyrmions occurs and that at high densities the fcc array is stable, while at low densities it is unstable to bulk deformation.

The striking similarity of the behaviour of skyrmionic matter on a three sphere and within a crystalline environment, as the average baryon density is increased, leads one to believe that the curvature of the sphere results in a self interaction of a skyrmion which closely resembles the interactions experienced by skyrmions within dense crystalline skyrmionic matter. Thus, in Chapter 4 we attempt to uncover what might be the simple analogue of bulk deformations of crystalline skyrmionic matter, for a single skyrmion on a curved physical space. Having detailed the geometric interpretation of the Skyrme Model's energy functional and reviewed Manton's [2] elegant formalism for considering such general shaped physical spaces, we consider the effect of an infinitesimal variation in the shape of the sphere S^3_{phy}, by varying its metric. This deformation in the shape of physical space we argue should provide the correct analogue of bulk deformations of the fcc array of skyrmions. We are able to prove that with respect to fluctuations of the metric on the sphere, that the the sphere shape is stable up to volume equal to that at which the delocalising phase transition occurs. Thus, we are able to demonstrate that this is the direct analogue the bulk deformations we consider

14

in our flat space array calculation.

To illustrate this result and also to enable us to consider finite variations in the shape of the sphere, we generalise this sphere to an elliptically shaped three dimension surface. By varying the volume and the eccentricity of this ellipse, we obtain numerically, the energy of a single hedgehog on a physical space whose curvature varies locally. In some detail, we the outline the effect that the curvature has on the skyrmion and show in general, that all our results can be explained using very simple arguments. These show that skyrmions prefer to sit on regions of space with the same curvature as that of the target space, the isospin three sphere. Moreover, if a skyrmion is forced to choose between regions of space in which the curvature is greater or less than this optimal value, they prefer the regions of lower curvature. The other effect which determines the regions of space that skyrmions prefer, is that they particularly dislike being stretched over large regions of space and thus localise as the volume of physical space increases substantially. Finally, by considering a hedgehog skyrmion on a more general shaped closed surface, with radius that is allowed to vary in one dimension from point to point, we show that the insights gained from the elliptical example enable us to explain all of the numerical results of the minimisation calculation we performed. This calculation involved minimising the energy of a variational ansatz for the map and radius variable at fixed volume and with the curvature constrained to be negative semi-definite. This latter constraint we deduce to be necessary, in order to avoid certain pathological problems in minimising the

15

energy functional with respect to variations in the shape of physical space.

In Chapter 5, we attempt to extend the crystalline skyrmionic calculations of Chapter 3 by incorporating explicit quark degrees of freedom within the minimal energy condensed fcc array. Thus, initially we outline the fundamentals of the Chiral Bag Model's description of a baryon. We then propose the manner in which the Chiral Bag Model's two phase description of baryonic matter, with its explicit quark content, can be incorporated consistently within the condensed fcc half skyrmion array. We demonstrate that there exists the possibility of cubic bag being cut out of this field in a consistent manner, which is in itself, a non-trivial result due to the discontinuities at the edges of this cube. Having established that cubic bags can exist and having argued that these bags are the most relevant to the condensed fcc array, we the outline a calculation which could be performed numerically and which would involve solving the Dirac equation for the ground state up and down quark wave function within the cubic bag. The results of this calculation would then reveal the particle content within this cubic bag and suggest the physical interpretation that should be placed on skyrmionic crystalline matter.

We go on to present an appealing argument, based on analogies with the spherical bag, to assess the effects that the interior quark vacuum will have on physical quantities. In particular we concentrate on its contribution to the baryon number which is required in order that the total baryon number of valence quarks, exterior mesonic field and quark vacuum give a total baryon number which has

an integer value, since clearly this is a physical requirement of any reasonable model of baryonic matter. For the spherical bag, this net contribution to the baryon number is indeed an integer value [17] and thus we show the manner in which this cancelation occurs in this case. We then attempt to demonstrate that a similar cancelation should occur for our cubic bag. These suggestive arguments are appealing, though inconclusive.

We also note in this chapter, that since the condensed fcc array is composed of tetrahedral four skyrmion units, these might represent α particle like structures within dense skyrmionic matter. This suggestion is further justified by comparing the structures of these tetrahedral units with the true minimal energy four skyrmion field configuration [18]. Recently it was proposed, that this minimal energy four skyrmion field configuration should represent the Skyrme Model's description of an alpha particle.

Finally, in Chapter 6 we give a number of concluding remarks concerning the results outlined in the previous chapters.

References

[1] L.Castillejo, P.S.J.Jones, A.D.Jackson, J.J.M.Verbaarschot, A.Jackson
Nucl. Phys. A501 (1989) 801

[2] N.S.Manton, Commun. Math. Phys. 111 (1987) 469

[3] T.H.R.Skyrme, Nucl. Phys. 31 (1962) 556

T.H.R.Skyrme, Proc. Roy. Soc. London 262 (1961) 237

T.H.R.Skyrme, Proc. Roy. Soc. London 260 (1961) 127

T.H.R.Skyrme, Nucl. Phys. 31 (1962) 550

[4] A.S.Goldhaber, Phys. Rev. D16 (1977) 1815

[5] G.t'Hooft, Nucl. Phys. B72 (1974) 461

G.t'Hooft, Nucl. Phys. B72 (1974) 461

[6] E.Witten, Nucl. Phys. B160 (1979) 57

[7] A.Chodos and C.B.Thorn, Phys. Rev. D12 (1975) 2783

[8] C.G.Callen, R.F.Dashen and D.J.Gross, Phys. Lett. 78B (1978) 307

G.E.Brown and M.Rho, Phys. Lett. 82B (1979) 177

G.E.Brown, M.Rho and V.Vento, Phys. Lett. 84B (1979) 383

[9] V.Vento, M.Rho, E.B.Nyman, J.H.Jun and G.E.Brown, Nucl. Phys. A345
(1980) 413

[10] A.P.Balachandran, V.P.Nair, S.G.Rajeev and Astern, Phys. Rev. Lett. 49 (1982) 1124

[11] E.Witten, Nucl. Phys. B223 (1983) 422

E.Witten, Nucl. Phys. B223 (1983) 433

[12] G.S.Adkins, C.R.Nappi and E.Witten, Nucl. Phys. B228 (1983) 552

[13] A.D.Jackson and M.Rho, Phys. Rev. Lett. 51 (1983) 751

[14] A.Jackson and A.D.Jackson, Nucl. Phys. A457 (1986) 687

[15] A.D.Jackson and J.J.M.Verbaarschot, Nucl. Phys. A484 (1988) 419

[16] I.Klebanov, Nucl. Phys. B262 (1985) 133

[17] J.Goldstone and R.L.Jaffe Phys. Rev. Lett. 51 (1983) 1518

[18] E.Braaten, S.Townsend and L.Carson 'Novel Structure of Static Multisoliton Solutions in the Skyrme Model' Uni. of Minnesota preprint (1989)

CHAPTER 2

INTRODUCTION TO THE SKYRME MODEL

2.1 The Skyrme Model

It is now believed that Quantum Chromodynamics, (Q.C.D.), provides the fundamental description of strong interactions. Thus, in principle the structure of baryons and mesons should be derivable from this $SU(3)$ colour gauge theory of quarks and gluons. Due to its non-abelian nature, the $Q.C.D.$ vacuum is paramagnetic and gives rise to strong infrared forces. At short distances, colour anti-screening takes place, resulting in an effective coupling constant tending to zero. In this perturbative phase quarks and gluons are asymptotically free [1][2]. However, at large distances the coupling constant grows and only colour singlet states exist asymptotically. This non-perturbative regime at low energies, with colour confinement, is relevant to nuclear physics. Since here perturbative methods are inappropriate, lattice calculations aimed at numerically solving $Q.C.D.$ have been developed in an attempt to uncover the nature of this phase. However, these calculations are far from making physical predictions and contain many difficulties yet to be resolved.

Thus, phenomenological models of low energy hadronic physics have been

developed. At low energies the dominant quark degrees of freedom of $Q.C.D.$ are the lightest quark fields. These are the up and down quarks, with current quark masses of about $10MeV$. Neglecting these masses, massless, two flavour $Q.C.D.$ is chiral invariant, with the global symmetry

$$U(2)_L \times U(2)_R \cong SU(2)_L \times SU(2)_R \times U(1)_V \times U(1)_A, \qquad (2.1.1)$$

where L and R denote the left the right symmetry groups, V refers to the vector and A to the axial vector symmetry groups. At the quantum level, it is well known that the $U(1)_A$ symmetry group is explicitly broken by the A-B-J anomaly [3] [4] leaving the global invariance group

$$SU(2)_L \times SU(2)_R \times U(1)_V. \qquad (2.1.2)$$

The Chiral Symmetry group $SU(2)_L \times SU(2)_R$ is then spontaneously broken down to $SU(2)_V$, via the Nambu-Goldstone mechanism. The resulting three massless pseudo-scalar particles are the pions. Thus, the vacuum carries axial charge and pions are able to decay to the vacuum. This leads to the Goldberg-Teimann relation between the axial form factor for the nucleon g_a and the pion decay constant f_π. This physically appealing scenario is consistent with the symmetries of $Q.C.D.$. However, due to the non-perturbative nature of $Q.C.D.$ at low energies, little information can be deduced from $Q.C.D.$ about g_a and f_π.

It is clear that Chiral Symmetry is fundamental to low energy strong interactions. Due to the smallness of the pion mass, about $130MeV$, as compared to the mass of the nucleon is about $1GeV$, one would also expect Chiral Symmetry

21

to hold approximately on physical grounds.

Thus, one is led to believe that the Non-Linear Sigma Model [5], which incorporates all the essential features of chiral symmetry breaking, would provide a good model of the low energy mesonic physics as dominated by pions. Moreover, the expansion of $Q.C.D.$ in the number colours N_c, developed by t'Hooft, suggests that at low energies, assuming confinement, $Q.C.D.$ becomes a theory described by an effective mesonic field [6]. Since at low energies the dominant chiral degrees of freedom are pionic, the Non-Linear Sigma Model should provide a first approximation to this effective low energy theory, even though N_c is not infinite but three.

Thus, Skyrme's proposal that the Non-Linear Sigma model be used to describe low energy mesonic interactions [5] has been justified many times over. It provides a model which describes Chiral Symmetry breaking and is also consistent with soft pion threshold theorems [7]. Its Lagrangian reads

$$L_2 = \frac{f_\pi^2}{2}(\partial_\mu \sigma \partial^\mu \sigma + \partial_\mu \vec{\pi} \partial^\mu \vec{\pi}), \qquad (2.1.3)$$

with the non-linear constraint,

$$\sigma^2 + \vec{\pi}^2 = f_\pi^2, \qquad (2.1.4)$$

where f_π is the pion decay constant, $\vec{\pi}$ is the iso-triplet pion field and σ the scalar sigma field of the $[1/2, 1/2]$ representation of $SU(2)_L \times SU(2)_R$. Thus the theory is manifestly chiral invariant.

In the trivial vacuum the pion fields are not excited and the sigma field

22

attains a constant value f_π throughout space. The introduction of an explicit chiral symmetry breaking term, generates masses for the pions which are viewed as fluctuations of the sigma field along the valley of a 'mexican hat' potential. Such a mass term is

$$L_m = -m_\pi^2 f_\pi^2 \sigma, \qquad (2.1.5)$$

where m_π is the pion mass and the coefficient has been chosen so as to generate a pion mass term to leading order in the weak pion field limit. The inclusion of this term also leads to the correct form for the P.C.A.C. [8] relation for the divergence of the axial current. Not only does this model satisfy the low energy requirements of Chiral Symmetry, but it has also been found to describe well, the self interaction and propagation of pions in the exterior of a nucleus [7].

The configuration space of this model possesses a non-trivial topological structure resulting from its non-linear nature. This observation led Skyrme to propose that it's non-trivial field configuration be identified as classical baryons [5].

It is convenient to introduce the quaternionic representation of $SU(2)$, in order to understand the topology of this configuration space. Thus we write

$$U(t, \vec{x}) = \frac{1}{f_\pi}(\sigma(t, \vec{x}) + i\vec{\tau}.\vec{\pi}(t, \vec{x})), \qquad (2.1.6)$$

with constraint (2.1.4) becoming

$$U(t, \vec{x})U(t, \vec{x})^+ = 1, \qquad (2.1.7)$$

where $U(t, \vec{x})$ is an $SU(2)$ valued matrix. In terms of this field variable we can

23

represent the Non-Linear Sigma Model Lagrangian as:

$$L_2 = \frac{f_\pi^2}{4} Tr(L_\mu L^\mu),\qquad (2.1.8)$$

where

$$L_\mu \equiv U(t,\vec{x})^+ \partial_\mu U(t,\vec{x}).\qquad (2.1.9)$$

At a fixed time t_0, the field $U(t_0,\vec{x})$, maps physical space R^3 into $SU(2)$, whose group manifold is isomorphic to a three sphere, S^3. For a static field configuration the energy is given by:

$$e_2 = -\int d^3x L_2.\qquad (2.1.10)$$

On physical grounds it is natural to consider only finite energy fields. Thus, the derivative of $U(\vec{x})$ must vanish outside some finite region, in order that (2.1.10) be finite. Hence, we are led to consider static configurations satisfying the natural boundary condition that $U(\vec{x})$ takes a constant value at spacial infinity, which on physical grounds, we choose to be its trivial vacuum value. That is, we have the boundary condition

$$U(|\ \vec{x}\ |\to \infty) = 1.\qquad (2.1.11)$$

This boundary condition compactifies physical space R^3, to a three sphere, S^3 and so topologically the field $U(\vec{x})$ is a map

$$U(\vec{x}) : S^3 \mapsto S^3.\qquad (2.1.12)$$

24

It is well known that such mappings are classified topologically into homotopy classes. The set of mappings (2.1.12), is classified by the third homotopy class of a three sphere,

$$\Pi_3(S^3) \cong Z, \qquad (2.1.13)$$

which is iso-morphic to the additive group of integers Z, the winding number of the mapping. Thus, if we consider only continuous fields, then the configuration space is disconnected and the time evolution of a configuration can be view as a homotopic deformation. Moreover, this disconnected topology of configuration space, means the winding number of a configuration is a conserved quantity independent of its dynamics. The winding number of a static field configuration, $U(\vec{x})$, is defined to be

$$B = \frac{1}{2\pi^2} \int d^3x \frac{\varepsilon^{0\,\mu\,\nu\,\rho}}{12} Tr(L_\mu L_\nu L_\rho). \qquad (2.1.14)$$

At the origin we require the condition

$$U(|\,\vec{x}\,|) = -1 \qquad (2.1.15)$$

be satisfied. This, together with condition (2.1.11), results in a continuous map $U(\vec{x})$, mapping the whole of physical space onto the whole of the target space S^3, an integer number of times. Thus B, as given by equation (2.1.14), takes only integer values when $U(\vec{x})$ satisfies boundary conditions (2.1.11) and (2.1.15). It has been shown that associated with this topological conservation there is a

current,[18]

$$B^\sigma = \frac{\varepsilon^{\sigma\mu\nu\rho}}{24\pi^2} Tr(L_\mu L_\nu L_\rho), \qquad (2.1.16)$$

which is conserved independently of the dynamics and the winding number (2.1.14) and is its corresponding charge.

Skyrme proposed that this current be identified with the baryon current and hence the baryon number with the winding number of a configuration [5]. Thus, baryons are described as topological solitons of the sigma and pion fields. Furthermore, he proposed that the fermionic nature of baryons in this soliton picture, results as a consequence of the skyrmion's non-trivial topological nature. This was shown later to be possible by Finkelstein et al [9]. Moreover, much of the resurgence of interest in the Skyrme Model, stems from Witten's observation of the mesonic fields [10], that in an effective mesonic theory of $Q.C.D.$ in the large N_c limit, baryon number should be identified with the winding number.

Finite energy static field configurations of the Non-Linear Sigma Lagrangian (2.1.8), are however, unstable. This can be seen if we consider rescaling a static field, $U(\vec{x})$. The energy of this field will be reduced by shrinking it to a point, since the static energy functional e_2, scales with length. Thus, finite energy configurations are unstable to rescaling to a point.

To remedy this instability, Skyrme proposed that an additional term be included in the Lagrangian, which is fourth order in the derivatives of the fields [5]. Such a term scales with inverse length and stabilises finite energy field con-

26

figurations against rescaling to a point. Thus, Skyrme considered an extended chiral symmetric model, with Lagrangian given by [11]

$$L = L_2 + L_4, \qquad (2.1.17)$$

where the additional Skyrme Term,

$$L_4 = \frac{-1}{32e^2} Tr[L_\mu, L_\nu]^2, \qquad (2.1.18)$$

has a dimensionless parameter e, characterising the size of the finite energy configurations. The energy of a static field configuration is now given by

$$E = e_2 + e_4, \qquad (2.1.19)$$

with

$$e_4 = -\int d^3x L_4. \qquad (2.1.20)$$

This energy is minimised with respect to scale transformations, when both the e_2 term (2.1.10), and the e_4 terms (2.1.20), are equal.

To this order, the additional fourth order term is the unique term yielding a positive definite Hamiltonian, that is only second order in time derivatives of $U(t, \vec{x})$.

A skyrmion is now taken to be a static, non-trivial finite energy field configuration, minimising the energy function (2.1.19). It has a topologically conserved charge and its winding number is to be identified with its baryon number. As we shall show later, (see chapter 4), the energy of a static configuration of winding

27

number B, is bounded from below by

$$E \geq 6\pi^2 \frac{f_\pi}{e} \mid B \mid .$$
$$(2.1.21)$$

Thus, finite energy configurations are locally stabilized as a result of the underlying global topology of configuration space.

The detailed structure of these skyrmionic solutions is determined by the highly non-linear Euler Equation, which results from functional minimisation of the Skyrme Model's energy function with respect to the field variables. Except for fields possessing a high degree of symmetry, finding analytic solutions to this equation poses a virtually intractable problem.

Skyrme [5] was thus led to consider the spherically symmetric hedgehog ansatz,

$$U(\vec{x}) = \exp(i\frac{\vec{\tau} \cdot \vec{x}}{\mid \vec{x} \mid} f(r))$$
$$(2.1.22)$$

for the fields. This field configuration, in terms of the sigma and pionic fields, takes the form

$$\sigma(r) = f_\pi \cos f(r),$$
$$\vec{\pi}(\vec{x}) = f_\pi \frac{\vec{x}}{\mid \vec{x} \mid} \sin f(r).$$
$$(2.1.23)$$

The ansatz greatly simplifies the resulting equation of motion, which becomes an ordinary non-linear equation for the profile function $f(r)$.

The hedgehog ansatz couples the spatial and isospin degrees of freedom. $U(\vec{x})$ commutes with the grand-spin generator $K = J + I$, (where $J = S + L$ is the

total angular momentum generator and I is the isospin generator), but not with J or I separately. This leads one to suspect that K will be a conserved quantum number for the quantized hedgehog and that it is a scalar in grand-spin space. Since this configuration has positive parity, it's quantum numbers are 0^+.

Substituting the hedgehog ansatz (2.1.22), into the energy functional (2.1.19), gives the energy for a hedgehog field

$$E = 4\pi \int_0^\infty dr r^2 \{\frac{f_\pi^2}{2}(\dot{f}^2 + 2\frac{\sin^2 f}{r^2}) + \frac{1}{2e^2}\frac{\sin^2 f}{r^2}(\frac{\sin^2 f}{r^2} + 2\dot{f}^2)\}, \quad (2.1.24)$$

where we have performed the trivial angular integration and $\dot{f}$ denotes the derivative of $f(r)$ with respect to the radial coordinate, r.

Upon functionally minimizing the energy for the hedgehog configuration (2.1.22), with respect to its profile function $f(r)$, the Euler Equation is given by:

$$(\frac{1}{4}\tilde{r}^2 + 2\sin^2 f)\ddot{f} + \frac{1}{2}\tilde{r}\dot{f} + \sin 2f \dot{f}^2 - \frac{1}{4}\sin 2f - \frac{\sin^2 f \sin 2f}{\tilde{r}^2} = 0, \quad (2.1.25)$$

where we have introduced the dimensionless variable $\tilde{r} = ef_\pi r$, of reference [12].

The hedgehog solutions of this equation are also solutions of the general Euler Equation, obtained from a general field variation of the energy functional (2.1.19), subject to the non-linear constraint (2.1.4). This was shown to be the case [13] for any field configuration possessing a high degree of symmetry, such as the hedgehog ansatz.

Integer winding number configurations can be obtained by numerically integrating this equation subject to the boundary conditions:

$$f(0) = B\pi,$$

$$f(\infty) \;=\; 0, \qquad\qquad\qquad (2.1.26)$$

to give a baryon number B configuration. We note that for a field taking its trivial vacuum value at spatial infinity, the winding number of such fields is dependent only on the boundary condition at the origin. The interpolating function between the two points is determined by the Euler Equation (2.1.25).

For hedgehog configurations, the resulting energy was found to be $864MeV$ for $B = 1$ and $2523MeV$ for $B = 2$ [19]. Here we have taken the parameters of the model to have values $f_\pi = 64.5MeV$ and $e = 5.45$, as used by Adkins et al [12]. They were determined by employing a semi-classical quantization technique, which enables physical baryon states to investigated. The collective spinning modes of the Skyrme Lagrangian generate classical angular momentum. Upon quantizing these collective coordinates, states of definite spin and isospin and hence physical baryon states, can be investigated. The parameters were subsequently fixed so as to reproduce, independently, the nucleon and delta(1236) masses. This approach fails to reproduce the $NN\pi$ coupling constant, giving a value $g_{NN\pi}$ approximately 30% too small.

For the $B = 1$ hedgehog, from equation (2.1.16), the baryon density is given by:

$$B^0(r) = -\frac{1}{2\pi^2}\frac{\sin^2 f}{r^2}\dot{f}. \qquad\qquad (2.1.27)$$

The exact solution yields a r.m.s. baryon number radius of about half a fermi.

Skyrme's proposal that the $B = 1$ hedgehog should represent a generalised

classical baryon, thus leads to a reasonable mass and a r.m.s radius for the nucleon.

Since this is a model of a baryon, the hedgehog field should be quantized as a fermion for it to make sense. However, the Skyrme fields are bosonic. It was proposed by Skyrme [5] and later demonstrated by Finkelstein et al [9], that topological excitations of non-trivial field configurations are capable of carrying half integer angular momentum. For such an effective theory of $Q.C.D.$ with an odd number of colours, Witten [10] further confirmed Skyrme's proposal, that a skyrmion field has a fermionic nature. Thus Adkins et al procedure involved quantizing the $B = 1$ hedgehog as a fermion.

To study physical baryon states, it is necessary to obtain states of definite spin and iso-spin from the hedgehog state, a hedgehog state being an admixture of states of equal spin and iso-spin. Quantizing the spinning modes of the Skyrme Lagrangian allows these to be isolated. The Skyrme Lagrangian is invariant under a global iso-rotation of the pion fields produced by AUA^+, where $A = a_0 + \vec{a}.\vec{\tau}$ is a constant $SU(2)$ valued matrix. This also leaves the boundary conditions for the hedgehog unchanged. The iso-spin degrees of freedom of the hedgehog are coupled to spatial rotations by the hedgehog ansatz and these rotational modes generate classical angular momentum. Thus, this iso-spin collective coordinate is taken to be the dominant effective degrees of freedom of the hedgehog. Thus, spinning the hedgehog adiabatically and allowing the collective coordinate A to vary in time, one can semi-classically quantize the zero modes of the skyrmion

31

as a fermion. This amounts to quantizing the hedgehog like a rigid rotor, with the hedgehog being a symmetric top. The resulting hedgehog states are partially characterized by the conserved quantum number K, which takes integer values from zero upwards. These states have equal half integer values of S and I, with the nucleon states having $S = 1/2$ and $I = 1/2$. The tower of grand-spin states thus contains the nucleons, deltas and higher resonances. The masses of the nucleons and deltas, as already stated, are then used to fix the parameter e.

2.2 The B=2 Sector Of The Skyrme Model and Beyond

This elegant picture of a skyrmion as a generalized baryon was further extended to the $B = 2$ sector. The physics of this sector are characterised by the nucleon-nucleon potential and the existence of a $B = 2$ bound state, the deutron. In the initial studies a product ansatz, of two $B = 1$ hedgehogs, $U_H(\vec{x})$, was employed [5],

$$U(\vec{x}_1, \vec{x}_2) = U_H(\vec{x}_1)U_H(\vec{x}_2). \qquad (2.2.1)$$

It has been shown [11] that for such a product, the baryon number is additive and hence, such a configuration has $B = 2$.

In the limit of large separation between the two hedgehogs this ansatz is valid, as the overlap of their localised baryon densities is insignificant. However,

32

as the skyrmions approach each other at finite separations, this overlap becomes significant and results in a large distortion of their fields which this ansatz is not able to describe. Thus, as the hedgehogs approach each other, the product ansatz becomes an increasingly less valid approximation for the true $B = 2$ minimal energy configuration. Hence, the product ansatz as been used to describe asymptotic nucleon-nucleon interactions. Indeed, Skyrme [5] himself originally addressed this problem and deduced an analytic expression for the asymptotic potential between two hedgehogs by employing this ansatz.

For two hedgehog skyrmions centred at the points $\vec{x}_1$ and $\vec{x}_2$, which are well separated, the field configuration is described by two undistorted hedgehogs with a relative isospin rotation of their pion fields, which can be represented as

$$U(\vec{x}_1, \vec{x}_2) = U_H(\vec{x}_1) A U_H(\vec{x}_2) A^+, \qquad (2.2.2)$$

where $A = a_0 + \vec{a}.\vec{\tau}$ and $U_H(\vec{x})$ is a $B = 1$ hedgehog solution. The resulting potential, defined as the difference between the energy of the $B = 2$ product configuration and twice the energy of the $B = 1$ skyrmion,

$$V = E_{B=2} - 2E_{B=1}, \qquad (2.2.3)$$

in the asymptotic limit is given by

$$V(\vec{r}_{12}) = 2C\{\frac{3(\vec{a} \cdot \vec{r}_{12})^2 - \vec{a}^2\vec{r}_{12}^2}{|\vec{r}_{12}|^5}\}, \qquad (2.2.4)$$

where C is a positive constant and $\vec{r}_{12} = \vec{x}_1 - \vec{x}_2$. This potential represents the asymptotic one pion exchange potential between the two skyrmions, which in the

zero pion mass limit considered here, goes with the inverse separation distance cubed. This is indeed similar to the form of the nucleon-nucleon tensor potential.

Equation (2.2.4) for the potential, shows that the tensor force between two well separated hedgehogs is optimally attractive when the conditions $\vec{a}^2 = 1$ and $\vec{a}.\vec{r}_{12} = 0$ are satisfied. To understand the non-isotropic nature of the potential, one should note that the product ansatz (2.2.2), represents two hedgehog skyrmions relatively rotated about the axis $\vec{a}$, by an angle θ, with $\mid \vec{a} \mid = sin(\theta/2)$. Thus, the optimal relative isospin orientation condition, corresponds to the two hedgehogs being relatively rotated about an axis perpendicular to their line of centre, by an angle π. The resulting configuration has the $\vec{\pi}$ fields of the hedgehog centred on $\vec{x}_1$ pointing radially outwards, while those of the hedgehog centred on $\vec{x}_2$ point radially inwards, having been rotated through an angle π, about an axis perpendicular to $\vec{x}_1 - \vec{x}_2$. This configuration of hedgehogs is such that their respective $\vec{\pi}$ fields match smoothly along their line of centre and this non-frustrated arrangement minimises the $\vec{\pi}$ field gradients and hence optimises the attraction.

We shall later see that the detailed non-isotropic structure of this potential has been used to construct optimally attractive arrangements of hedgehogs [14], in order to deduce optimal rarified crystaline arrays of skyrmions. Since this is the starting point from which we shall proceed to study dense crystaline matter, the subject of the next chapter, we shall at this point note only that the sign of this potential depends entirely upon relative isospin orientation of the hedgehog

34

fields and is thus strongly anisotropic.

Skyrme's asymptotic result (2.2.4), employing the product ansatz (2.2.2), has since been extended using numerical techniques to give the potential (2.2.3) at all separations [15]. These studies revealed the skyrmion-skyrmion potential to give a reasonably successful description of the phenomenological nucleon-nucleon potential.

In the small separation limit, the product ansatz (2.2.2) is no longer valid due to significant field distortion and an alternative description for the $B = 2$ configuration is certainly required. Thus Verbaarschot et al [16] were led to solve directly, for the exact minimal energy, $B = 2$ configurations at all separations, using a numerical relaxation technique. They found the minimal energy field configuration occurred at a separation at which the overlap of the hedgehog fields would be large. It was realised [17] that a finite reflection symmetry of the pion fields at large separations becomes a continuous axial symmetry of this minimal energy configuration. The appearance of new symmetries as the density of skyrmion matter is increased to its optimal configuration over and above that of the well separated skyrmion configuration, has since been seen to be the rule rather than the exception. While at large separation for the $B = 2$ configuration, an identification of two individual skyrmions is valid, this is not so for the minimal energy field configuration. Here both skyrmions completely lose there identity as a consequence of their close proximity and as a result of the substantial field deformations this involves.

35

These additional symmetries are important in themselves, due to the additional restrictions they place upon collective coordinate semi-classical quantization of the zero modes of skyrmions and result in selection rules for their quantum states. Thus, in the $B = 2$ case they were shown to result in the appearance of a non-degenerate ground state with the quantum numbers of the deutron [18]. However, the binding energy of this ground state was found to be unrealistic, as was expected, due to the naive semi-classical quantization of only the zero modes of the classical solution, which neglects the important degrees of freedom describing nuclear break up. In order to overcome the restricted nature of this quantization procedure, it is necessary to identify the degrees of freedom for nuclear separation. However, due to the non-renormalisability of the Skyrme Model, a semi-classical quantization procedure is still required.

Hence Atiyah and Manton [19] have recently developed a technique by which a non-trivial truncation of a skyrmion field's infinite number of degrees of freedom is possible. Their procedure of integrating over time lines for instanton fields in four dimensional Euclidean space, leads to non-trivial field configurations which are not minimal energy solutions. However, in both the $B = 1$ and $B = 2$ sectors their parametric forms give good approximations to the true minimal energy field configurations, possessing all the known symmetries of the true solutions. Moreover, their parametric $B = 2$ configuration is capable of representing the minimal energy configurations at all separations and hence nuclear break up. Unfortunately, their techniques become highly complex in the higher baryon

number sectors and their construction was based on the numerically discovered symmetries of the true field configurations. But it does now seem possible that a realistic evaluation of the binding energy of the $B = 2$ ground state will be possible and that in this sector the true economy of the Skyrme Model description will be realised, incorporating a description of both the bound state system and nuclear collisions.

Recently Carson et al [20] found numerical minimal energy $B = 3, 4, 5$ and 6 solutions and found these also to have a significant binding energy relative to isolated skyrmion configurations of the same baryon number. These fields also possess a high degree of symmetry, as revealed by the baryon density plots given by Carson et al. One thus expects that these fields may lead to a description of their corresponding baryon number light nuclei.

2.3 A Simple Model Of Dense Skyrmionic Matter

Given the successes of the Skyrme Model as described here, it is natural to try and discover what its predictions are for infinite baryonic matter systems. In particular, regular static crystalline arrays of skyrmions have been investigated and the results reveal new forms of baryonic matter at high densities. Since the classical spherical hedgehog skyrmions contain nucleons, deltas and higher resonances, whose properties are obtained by projecting out the relevant spin and

isospin content, it is interesting to see what the Skyrme Model predictions are for dense baryonic matter. Due to economical dual description of both baryonic structure and baryonic interactions, the model presents a means of describing the radical changes which occur when the density of baryonic matter is increased. The subject of Chapter 3 will be to review the results of these calculations and to present our own result for an fcc arrangement of skyrmionic matter.

An important insight into the nature of dense skyrmionic matter has been gained with the realisation of a simple alternative and complementary model of dense baryonic matter to that of the flat space arrays.

The flat space static array calculations we shall later review, require one to solve numerically for the minimal energy field configuration at a given average baryon density. For these arrays, a set of twisted periodic boundary conditions are imposed and the resulting minimal energy fields can be generated by lattice translations from the solution within a representative unit cell. Even so these calculations are tedious, it being technically difficult to obtain converged solutions.

The complementary model initiated by Manton[21] of dense baryonic matter, replaces flat physical three dimensional space by a three sphere . Now a skyrmion is a mapping of a three sphere of radius L, $S^3_{phy}(L)$, onto a three sphere, S^3_{iso}, of radius one. Due to the similar shapes of both the domain and target spaces, mathematical results are simpler to obtain than for flat space arrays and analytic solutions are even possible. The analogue of the average baryon density variable

for flat space arrays on $S_{phy}^3(L)$, is given by $B/2\pi^2 L^3$ for a static solution of winding number B and thus for a given baryon number we can find solutions at all average baryon densities by varying the radius L, of this sphere. A single $B = 1$ skyrmion on $S_{phy}^3(L)$ will have a self interaction due to the curvature of space and this is believed to give a good model of the interactions of skyrmions within flat space crystalline baryonic matter. This will also be true in the higher baryon number sector on $S_{phy}^3(L)$.

The results of calculations within both the $B = 1$ and $B = 2$ sectors have indeed been shown to have remarkable similarities to those obtained numerically for flat space arrays. Of course, even though analytical results are possible within the $B = 1$ sector, direct physical results are not possible with this simpler model since real physical space is flat not spherical.

For the moment we shall describe the $B = 1$ sector results on $S_{phy}^3(L)$ and leave the drawing of parallels with the physical flat space arrays until we present results in the next chapter.

The Skyrme Model's static energy functional on $S_{phy}^3(L)$ in Manton's dimensionless units[21] reads,

$$E = \int_{S_{phy}^3(L)} dV [g^{ij}K_{ij} + \frac{1}{2}\{(g^{ij}K_{ij})^2 - (g^{ij}K_{jl})^2\}], \qquad (2.3.1)$$

where g_{ij} are the components of the metric on $S_{phys}^3(L)$, with i, j running from 1 to 3 and

$$K_{ij} = \partial_i \phi^a \partial_j \phi^a, \qquad a = 1, 2, 3, 4 \qquad (2.3.2)$$

where the dimensionless fields satisfy the constraint $\phi^a \phi^a = 1$. In equation (2.3.1) dV is the measure on $S^3_{phy}(L)$. The dimensionless units of length and energy can be related to physical units by rescaling the dimensionless energy unit by $f_\pi/2e = 5.92 MeV$ and the dimensionless length unit by $1/ef_\pi = 0.561$ fermi.

Using the standard extension of polar coordinates for physical space,

$$0 \leq \mu \leq \pi, \qquad\qquad 0 \leq \theta, \phi \leq 2\pi \qquad\qquad (2.3.3)$$

the metric components, g_{ij}, are diagonal with elements,

$$g = \left(L^2, L^2 \sin^2 \mu, L^2 \sin^2 \mu \sin^2 \theta\right). \qquad\qquad (2.3.4)$$

The $B = 1$ field configuration we shall assume to be of the hedgehog form. This gives,

$$
\begin{aligned}
\phi^0 &= \cos f(\mu) \\[1em]
\phi^1 &= \sin f(\mu) \cos \theta \\[1em]
\phi^2 &= \sin f(\mu) \sin \theta \cos \phi \\[1em]
\phi^3 &= \sin f(\mu) \sin \theta \sin \phi.
\end{aligned}
\qquad (2.3.5)
$$

In order to ensure the hedgehog has winding number one, we have the boundary conditions for the profile function

$$f(0) = 0, \qquad\qquad f(\pi) = \pi. \qquad\qquad (2.3.6)$$

The matrix K_{ij} is now diagonal with elements

$$K = \left(\dot{f}^2, \sin^2 f, \sin^2 f \sin^2 \theta\right), \qquad\qquad (2.3.7)$$

40

where $\dot{f}$ denotes the derivative of $f(\mu)$ with respect to μ and hence the static energy functional takes the form

$$E(f) = 4\pi \int_0^\pi d\mu \sin^2 \mu \{L(\dot{f}^2 + 2\frac{\sin^2 f}{\sin^2 \mu}) + \frac{\sin^2 f}{L \sin^2 \mu}(2\dot{f}^2 + \frac{\sin^2 f}{\sin^2 \mu})\}, \quad (2.3.8)$$

where we have performed the trivial θ, ϕ integrations. The Euler Equation for the minimal energy hedgehog field is obtained from a functional variation of $E(f)$ with respect to $f(\mu)$ and is

$$(L^2 + 2\frac{\sin^2 f}{\sin^2 \mu})\ddot{f} + L^2 \frac{\sin 2\mu}{\sin^2 \mu}\dot{f} + \frac{\sin 2f}{\sin^2 \mu}\dot{f}^2 - \frac{\sin 2f}{\sin^2 \mu}(L^2 + \frac{\sin^2 f}{\sin^2 \mu}) = 0. \quad (2.3.9)$$

Examination of this Euler Equation, which is an ordinary second order differential equation, reveals that that there exists a trivial solution

$$f(\mu) = \mu \qquad\qquad (2.3.10)$$

at all values of L. This solution is the trivial mapping of $S^3_{phy}(L)$ onto $S^3_{iso}(1)$. The energy (2.3.8) of the trivial map is then given by

$$E = 6\pi^2(L + \frac{1}{L}). \qquad\qquad (2.3.11)$$

This attains a minimum energy at $L = 1$, when it is simply the identity mapping, of two three spheres of radius one, which saturates the lower bound with a value of the energy $12\pi^2$. This completely delocalised solution has the full 0(4) symmetry of the Skyrme Model and is an isometry of S^3.

The baryon density for a hedgehog skyrmion is given by

$$B^0(\mu) = \frac{1}{2\pi^2} \frac{\sin^2 f}{L^3 \sin^2 \mu} \dot{f}, \qquad\qquad (2.3.12)$$

41

which for the trivial map (2.3.10), reduces to $1/2\pi^2 L^3$ and is a constant over physical space. Thus, on a three sphere the trivial skyrmion represents a completely delocalised baryon over the whole of space.

As the radius of physical space is increased beyond one, the energy of the trivial solution (2.3.11) grows, becoming linear at large L. At infinite volume the trivial solution thus has infinite energy. At some intermediary volume, this solution, which is an absolute minimal energy solution at $L = 1$, might be expected to become unstable with respect to another solution which does have a finite energy in the infinite volume limit and which would correspond to the flat space hedgehog as the curvature of physical space becomes zero in this limit.

This is indeed the case and it as been demonstrated that the trivial map becomes unstable to a hedgehog solution of equation (2.3.9), above a volume corresponding to a critical value of $L = L_c = \sqrt{2}$. The transition at $L = L_c$ is of second order and instability of the trivial map has been shown to be due to the existence of infinitesimal conformal modes which are the paths of steepest descent in energy from the trivial map at $L = L_c$. Thus, up to a volume of $L = \sqrt{2}$, the trivial delocalised solution is a local minimum of energy and beyond this critical radius it is a local maximum. The local conformal modes result in the minimal energy hedgehog solution beyond L_c, this becomes increasingly localised about one of the poles of $S^3_{phy}(L)$ as L increases. Thus, there are two hedgehog solutions in this region of L corresponding to localisation centred upon either pole. These two solutions are degenerate in energy and transformed into

each other by the transformation

$$f(\mu) \mapsto \pi - f(\pi - \mu).\qquad(2.3.13)$$

In the limit of infinite volume the hedgehog skyrmion is centred on one of the poles, being well localised and having a finite energy corresponding to that of the flat space hedgehog [22].

The instability of the trivial map with respect to infinitesimal conformal modes, for values of L greater than $\sqrt{2}$, in general produces a localisation of the skyrmion about any point on $S^3_{phy}(L)$. However, the hedgehog form (2.3.5) is only consistent with the skyrmion localising about either pole and hence gives a two-fold degeneracy of localised solutions.

Manton [21] further demonstrated that the trivial map solution on $S^3_{phy}(L)$ is an absolute minimum of energy for volumes of physical space less than or equal to that of the target three sphere. Beyond these volumes, for an arbitrary space, this is no longer the case, as we shall demonstrate in Chapter 4 when we investigate the effect of generalising the shape of this sphere. The global stability of the trivial map up to the critical volume for the sphere is however, still a realistic possibility which up until now has not been demonstrated.

These results show that dense baryonic matter undergoes a localising-delocalising phase transition at some critical baryonic density. The phase transition described here is of second order and of the standard 'pitch fork' type. Here of course, the term 'phase transition' is some what misleading, since we are only considering

the potential energy surface generated by varying the average baryon density and have not included kinetic effects. Since all our results are thus at zero kinetic energy, there is no temperature involved and strictly speaking this is not a phase transition.

Similar results were also found for the $B = 2$ [23] sector of this model, with a second order phase transition occurring a some critical radius and the low density phase having two spherical skyrmions centred on opposite poles of the sphere.

These phase transitions have been interpreted as representing the restoration of Chiral Symmetry at high densities [24], in the sense that for both the $B = 1$ and 2 systems the average values of the sigma field $< \sigma >$ and pion field $< \pi >$, are zero in the high density phase. This interpretation was further justified by the observation that for the $B = 1$ solutions at the transition point, the formation of the high density phase is associated with the disappearance of the three Goldstone modes.

This simple model thus provides us with an insight in to the nature of the different forms of baryonic matter at high densities which the Skyrme Model predicts. Indeed, for flat space arrays of skyrmions, similar delocalising phase transitions have been discovered as we shall describe in Chapter 3.

Recently Wirzba et al [25] obtained analytically, the complete mode spectra for the $B = 1$ trivial background field. Moreover, the classification of the modes for the localised $B = 1$ background was given and these modes were calculated numerically. This development enables one to further understand the

effective degrees of freedom of dense skyrmionic matter and gives the possibility

of performing finite temperature calculations for dense skyrmionic matter.

References

[1] H.D.Politzer, Phys. Rev. Lett. 30 (1973) 1346

[2] D.J.Gross and F.Wilczec, Phys. Rev Lett. 30 (1973) 1343

[3] S.Alder, Phys. Rev. Lett. 117 (1969) 2426

[4] J.Bell and R.Jackiw, Nuov. Cimento 60A (1969) 47

[5] T.H.R.Skyrme, Proc. Soc. London 260 (1961) 127

T.H.R.Skyrme, Proc. Soc. London 262 (1961) 237

T.H.R.Skyrme, Nucl. Phys 31 (1962) 556

[6] G.t'Hooft, Nucl. Phys. B72 (1974)461

G.t'Hooft, Nucl. Phys. B75 (1974) 461

[7] T.D.Lee, 'Chiral Dynamics', Gordon and Breech, N.Y. (1972)

[8] V.Vento, M.Rho, E.B.Nymann, J.H.jun and G.E.Brown,

Nucl. Phys. A345 (1980) 413

V.Vento, Ph.D. Thesis Stony Brook

[9] D.Finkelstein and J.Rubinstein, J. Math. Phys. 9 (1968) 1762

[10] E.Witten, Nucl. Phys. B160 (1979) 57

[11] An excellent review of the Skyrme Model is given in:

I.Zahed and G.E.Brown, Phys. Rep. 142 (1986) 1

U.G.Meisner and I.Zahed, Adv. Nucl. Phys. 17 (1986) 143

G.Holsworth and B.Schweisinger, Rep. Prog. Phys. 49 (1986) 825

U.G.Meisner, Phys. Rep. 161 (1988) 213

[12] G.S.Adkins, C.R.Nappi and E.Witten, Nucl. Phys. B228 (1983) 552

[13] R.S.Palais, Commun. Math. Phys. 69 (1979) 19

[14] I.Klebanov, Nucl. Phys. B262 (1985) 133

[15] A.D.Jackson and M.Rho, Phys. Rev. Lett. 51 (1983) 751

A.Jackson and A.D.Jackson, Nucl. Phys. A457 (1986) 687

[16] J.J.Verbaarschot, T.S.Walhout, J.Wambach and H.W.Wyld,

Nucl. Phys. A468 (1987) 250

[17] V.B.Kopeliovich and B.E.Stern, J.E.T.P. Lett. 45 (1987) 203

N.S.Manton, Phys. Lett. B192 (1987)177

J.J.Verbaarschot, Phys. Lett. B195 (1987) 235

[18] E.Braaten and L.Carson, Phys. Rev. D56 (1986) 1897

[19] M.F.Atiyah and N.S.Manton, 'Skyrmions From Instantons'

D.A.M.P.T. preprint (1989)

[20] E.Braaten, S.Townsend and L.Carson, 'Novel Structures of Static

Multisoliton Solutions in the Skyrme Model' Uni. of Minnesota

preprint (1984)

[21] N.S.Manton, Commun. Math. Phys. 111 (1987) 469

[22] A.D.Jackson, C.Weiss, A.Wirzba and A.Lande, "Accurate Variational
Forms for Multi-Skyrmion Configurations" Stony Brook preprint (1988)

[23] A.D.Jackson, A.Wirzba and L.Castillejo, Phys. Lett. B198 (1987) 315
A.D.Jackson, A.Wirzba and L.Castillejo, Nucl. Phys. A486 (1988) 634

[24] H.Forkel, A.D.Jackson, M.Rho, C.Weiss and A.Wirzba, "Chiral Symmetry
Restoration and the Skyrme Model", Stony Brook preprint (1989)

[25] A.Wirzba, 'The Mode Spectrum and the Stability Analysis of
Skyrmions on a 3-Sphere' Nordita preprint (1990)

CHAPTER 3

DENSE SKYRMIONIC MATTER
IN A CRYSTALLINE FORM

3.1 Multi-Skyrmion Crystals

In Chapter 2 we have seen that the Skyrme Model provides a topological description of a generalized classical baryon which is both elegant and physically reasonable, with maximum discrepancies of around 30%. Moreover, the large N_c expansion of $Q.C.D.$, suggests that one loop corrections to these classical results will be of order $1/N_c$ and with the physical value of N_c being 3, these discrepancies seem reasonable at the classical level.

This description of baryons was also seen to lead to a skyrmion-skyrmion potential, possessing many of the salient features of the phenomenological nucleon-nucleon potential [1][2]. Moreover, within the $B = 2$ sector, the existence of a ground state, with the quantum numbers of the deutron, has also been demonstrated [3], though the stability of this bound state has yet to be conclusively established. It has even been suggested by Carson et al [4], that the model offers the possibility of describing the $B = 4, 5$ and 6 light nuclear systems, the classical skyrmion solutions having already been calculated numerically.

These successful developments in the application of the Skyrme Model to light nuclear systems have been mirrored by progress within the realm of infinite baryonic matter systems. Indeed, it is natural to believe, that within this sphere the model may provide an economical description of infinite baryonic matter and that it may provide a description of heavy nuclei or neutron star matter.

The economy of the description offered by the Skyrme Model for such systems, follows from the manner in which both the structure and interactions of baryons are placed on a similar footing from the outset. For infinite baryonic matter, this provides the opportunity of describing the radically different forms of baryonic matter expected to exist at high and low densities.

In Chapter 2 we also discussed Manton's [5] results for a skyrmion on $S^3_{phy}(L)$ and this revealed two distinct forms of skyrmionic matter that exist at high and low average baryon density. At low densities the skyrmion's baryon density is well localised about a point in space, while at high densities it is completely delocalised over the whole of space. The economy provided by the Skyrme Model's description of baryonic matter, results here in a single description of both phases of matter. This would not have been the case had two differing models been required to describe these two differing phases.

The insight gained from the understanding of the simple $S^3_{phy}(L)$ model, has provided a further insight, by which many of the features of the numerically obtained flat space array results have been interpreted. It thus appears, that there exist 'universal' features of dense skyrmionic matter which are common to

both the crystalline and $S^3_{phy}(L)$ environments.

The beauty of the $S^3_{phy}(L)$ model of skyrmionic matter is its simplicity, enabling one to obtain analytical results which have subsequently revealed the existence of a second order phase transition and this is due to the presence of a local conformal instability. An analogous conformal instability in flat space has also been proposed, in order to explain the existence of an analogous transition from a condensed to an uncondensed array of skyrmions and we shall see later that this proposal would seem to have been numerically justified.

Klebanov [6] pioneered the attempts to construct infinite arrays of skyrmionic matter and recently this field has attracted increased attention. His model was based on the belief, that a classical array of crystalline skyrmions might describe the dense neutron matter which exists at the core of a neutron star.

The idea that dense neutron matter has a crystalline form was proposed by Smith et al [7]. They investigated a pion condensate model of a neutron star and suggested that at short distances the dominant forces of interaction within dense neutron matter are the tensor force and hard core repulsions between neutrons. This tensor force is strongly anisotropic and for an optimal spin configuration is attractive. Thus, a crystalline array of neutrons, with an optimally arranged spin configuration, will enhance the size of the tensor attraction. However, within a disordered system, the tensor force experienced by a neutron will be averaged out to zero. Thus, the tensor force strongly prefers an ordered configuration of neutrons to a disordered neutron superfluid, while hard core repulsion cannot

distinguish between the two. However, the high quantum zero point energy, associated with a crystalline array of localised neutrons, will work against the formation of such crystalline matter.

Klebanov was thus led to consider an infinite cubic crystalline array of skyrmions, based in part on the cubic array of neutrons proposed by Smith et al. It is not however possible within this model, to estimate the effect of the zero point motions of skyrmionic matter, due to the non-renormalisability of the Skyrme Model.

The asymptotic form of the tensor potential between two skyrmions is highly anisotropic and their topological nature enforces strong repulsive forces at high densities. Hence we see, that the two dominant nucleon-nucleon interactions in neutron matter have analogies within the Skyrme Model at the classical level.

The argument that led Klebanov to deduce the structural form that an infinite array of skyrmions should take, was based upon the insights which had previously been gained from the understanding of the interaction between two $B = 1$ hedgehogs at large separations.

As we have already mentioned, Skyrme [8] deduced the analytic form of the asymptotic tensor potential between two $B = 1$ hedgehogs. Klebanov re-expressed this in the form given in Chapter 2, (2.2.4). This expression reveals the anisotropic nature of the tensor potential. The resulting optimal arrangement of two hedgehogs is one in which their respective pion fields are relatively iso-rotated about an axis lying in a plane perpendicular to their line of centre by

an angle π.

Thus, in order to picture this arrangement, we imagine that both $B = 1$ hedgehogs are situated on the x axis and located at $x = \pm\infty$. Presuming that the one at $x = -\infty$ is unrotated and thus has its pion field pointing radially outwards from its centre, the optimal field configuration has the pion fields of the hedgehog located at $x = +\infty$, iso-rotated about an axis lying in the (x, y) plane through an angle π. Without loss of generality, we can choose this axis to be the z axis, then the hedgehog at $x = +\infty$ has its pion field in the (x, y) plane pointing radially inwards, while along the line parallel to the z axis, which passes through its centre, its pion field points outwards. Thus, on transversing the x-axis from the centre of the hedgehog located at $x = -\infty$, to the centre of the hedgehog located at $x = +\infty$, the pion field on this axis flows in the positive x direction. Thus, this optimal arrangement has the pion fields of these two hedgehogs relatively non-frustrated. All other non-frustrated optimal arrangements of two hedgehogs are related to this configuration by a combination of constant global space and iso-space rotations. These rotations leave the Skyrme Lagrangian invariant and are thus symmetry transformations of a skyrmion field.

Klebanov realised that it was reasonable to assume that at low densities Skyrmionic matter is composed of well separated spherical hedgehogs. This being the case, an optimal orientation arrangement of these hedgehogs will give an asymptotic tensor interaction which is attractive and will thus result in the skyrmion array having significant binding.

In order to construct optimal arrays of skyrmions, it is useful to imagine placing hedgehogs at the points of an infinite lattice. In this way, Klebanov deduced that in order to maximise this binding, one should demand that nearest neighbouring hedgehogs be optimally orientated. The pion fields of neighbouring hedgehogs will run smoothly in to each other and neighbouring hedgehogs will have their pion fields relatively non-frustrated.

To illustrate this, let us first consider a simple cubic array of skyrmions. We choose a particular lattice point to define our origin and the lattice spacing to be a. At each point on the lattice there is situated a hedgehog, which at the origin we choose to be unrotated so that its pion field points radially outwards. We shall now consider those hedgehog skyrmions located on points within the plane $z = 0$. If we move to the hedgehog located at the point $(a, 0, 0)$, we should require that the pion field of this hedgehog be iso-rotated about an axis lying in the (y, z) plane by an angle π, in order to produce a non-frustrated pion field arrangement along the x axis. Without loss of generality, we choose at this point that the hedgehog be rotated about the z axis by an angle π. On moving along the line $x = a$, from the point $(a, 0, 0)$ towards the point $(a, a, 0)$, the pion field will flow in the negative y direction. Thus, the hedgehog located at the point $(a, a, 0)$ should have its pion field either iso-rotated about the y axis or be unrotated. In either instance, its pion field along the line $x = a$ will flow outwards from its centre at the point $(a, a, 0)$ in the y direction and the resulting pion fields of the hedgehogs at $(a, 0, 0)$ and $(a, a, 0)$ will be relatively non-frustrated.

Thus, we see that there are two choices of rotation axis at the point $(a, a, 0)$ which result in a relatively non-frustrated arrangement of the pion field of the hedgehogs located at the points $(a, 0, 0)$ and $(a, a, 0)$. If we choose the axis of rotation to be the y axis, then on moving along the line $y = a$, from the point $(a, a, 0)$ towards the lattice point $(0, a, 0)$, the pion field of the hedgehog at $(a, a, 0)$ will flow inwards along the line $y = a$ and thus the hedgehog at $(0, a, 0)$ should have its pion fields pointing outwards along this line. However, on moving from the unrotated hedgehog at the origin to the point $(0, a, 0)$, the pion field flows in the positive y direction and hence, at the point $(0, a, 0)$ they should flow inwards. Thus, the hedgehog at $(0, a, 0)$ should have its pion field on the line $y = a$ pointing outwards, while on the y-axis they should be pointing inwards. Hence, at the point $(0, a, 0)$, the hedgehog pion fields must be iso-rotated about the x-axis by an angle π, in order that its pion field be non-frustrated relative to the pion fields of the other hedgehogs at the origin and the point $(a, a, 0)$.

In Figure (3.1.1a) this arrangement has been depicted and we have indicated the direction of the axis at each of the lattice points for this square plaquette in the positive (x, y) plane at $z = 0$, about which the hedgehog at that point is iso-rotated by an angle π. We have indicated, that the pion fields of the hedgehog located at the origin are unrotated and point radially outwards, by drawing a circle at the origin. This figure shows clearly for an optimal arrangement, that moving to a neighbouring lattice point involves an iso-rotation about an axis perpendicular to the direction we move in by an angle π.
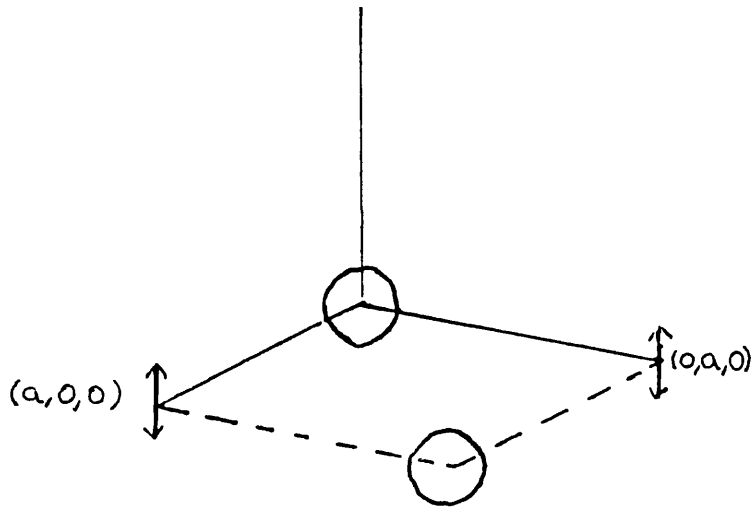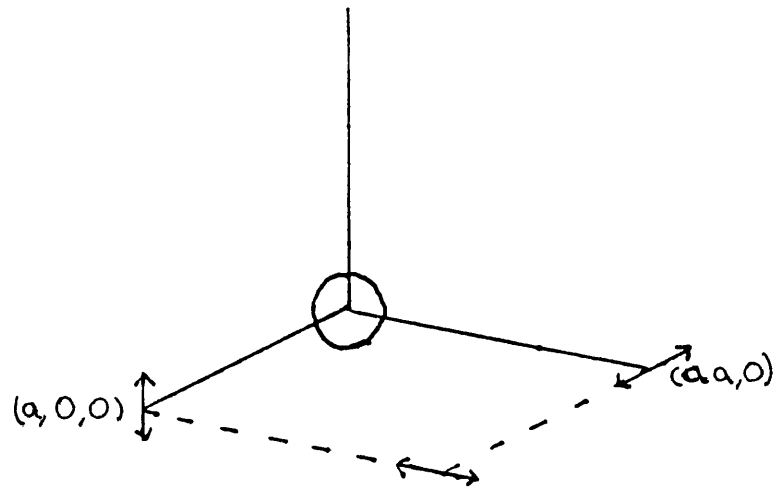
Figures (3.1.1a) and (3.1.1b): Non-frustrated arrangement of four hedgehogs in the $z = 0$ plane, on the vertices of a square plaquette. Arrows indicating the rotation axis about which the pion fields of the hedgehogs are iso-rotated by an angle π.

The alternative choice for an unrotated hedgehog at the point $(a, a, 0)$, requires that the hedgehog located at the point $(0, a, 0)$ have its pion field flowing inwards along the line $x = a$ and inwards along the y-axis. Hence, the hedgehog at the point $(0, a, 0)$ will have its pion fields iso-rotated about the z axis by an angle π. This arrangement is indicated on Figure (3.1.1b).

These two arrangements, of four hedgehogs around a square plaquette, with neighbouring hedgehogs having their pion fields relatively non-frustrated, are essentially unique. Other optimal arrangements will be related to these two arrangements by global spatial and iso-spatial rotations.

To simplify matters, we assume that the relative pion field arrangement that we choose within a plaquette, is repeated in all successive plaquettes in the (x, y) plane and that no mixing of these two arrangements occurs. In this manner, we see that a neighbouring plaquette will be related to the original by a global rotation, in such a way that they are the same on the line on which they meet. Hence, on translating the plaquette of Figure (3.1.1a), by a lattice spacing a in the x direction, we require that the pion field within the plaquette be iso-rotated about the z axis by an angle π, while a translational along the y axis involves an iso-rotation about the x axis by an angle π.

For the plaquette arrangement in Figure (3.1.1b), a lattice translation of a distance a, in the x or y directions, will involve an iso-rotation about the z axis through an angle π.

We now consider the lattice point $(a, 0, a)$. For both of our plaquette arrange-

57

ments in the (x, y) plane, we have to choose, for a hedgehog located at the point $(a, 0, a)$, to iso-rotate about an axis lying in the (x, y) plane by an angle π. We have also to make the similar choice at the point $(0, 0, a)$ and these two axes should be chosen such that they are perpendicular to each other.

For plaquette (3.1.1a) however, for the hedgehog located at the point (a, a, a), we have to choose either not to iso-rotate its pion field or, to iso-rotate its pion field about the z-axis by an angle π and similarly at the point $(0, a, a)$. Choosing to iso-rotate the pion field about the z-axis, at the point (a, a, a), requires that at the point $(0, a, a)$, we choose an unrotated hedgehog in order to avoid frustration of the respective hedgehog's pion fields. But at the point $(0, 0, a)$, we must make the choice of the x-axis to iso-rotate about and finally, at the point $(a, 0, a)$, we must choose to iso-rotate about the y-axis. In this way, this arrangement ensures that all pion fields are non-frustrated as we move along the edge of the cube and this arrangement is illustrated in Figure (3.1.2a)

The alternative choice at the point (a, a, a) of an unrotated hedgehog, also results in a unique arrangement in a similar manner and is shown in Figure (3.1.2b)

The first of these cubes, Figure(3.1.2a), has on the face lying in the $x = 0$ plane, a pion field arrangement which is similar to that indicated in Figure (3.1.1b) in the $z = 0$ plane. Thus, this arrangement is related by global spatial and iso-spatial relations, to the arrangements which result from this choice of base plaquette in the (x, y) plane.

(a)

(0,0,u)

(a,0,0)

(0,a,0)

(b)

(c)
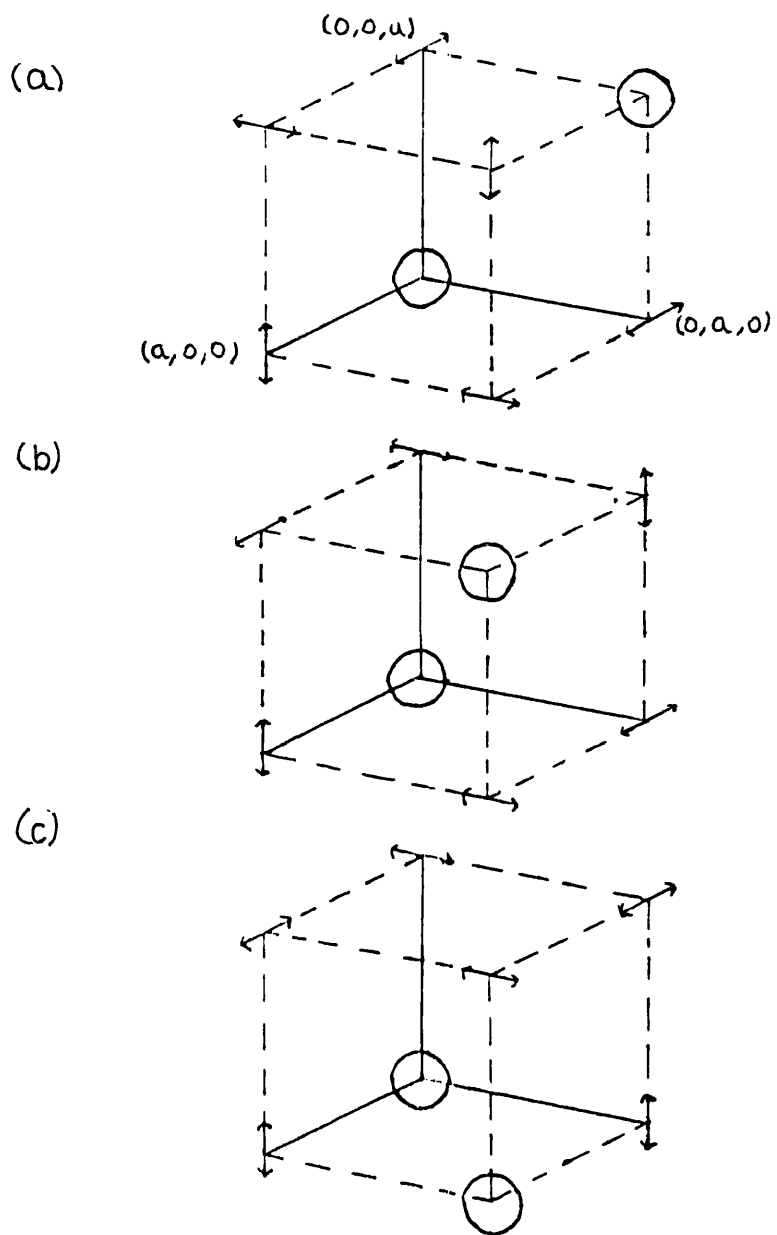
Figures (3.1.2a), (3.1.2b) and (3.1.2c): Non-frustrated arrangement of eight hedgehogs at the vertices of a cube. (a) and (c) correspond to the Jackson et al arrangement and (b) corresponds to the Klebanov arrangement.

The second of the arrangements, indicated in Figure (3.1.2b), corresponds to the cubic cell arrangement considered by Klebanov, if we assume translation symmetry in the z-direction. Thus, a translation of a in the z-direction will involve an iso-rotation about the y axis by an angle π.

For the second choice of the x,y base plaquette, Figure (3.1.1b), we have an infinite variety of possible options for orientation of pion fields within the plaquette in the $z = a$ plane, all of which would be relatively non-frustrated. The Jackson [9] choice is shown in Figure (3.1.2c). This generalisation of the Jackson arrangement, can be generated from Jackson's arrangement, by performing a global iso-rotation on the pion fields about the z axis by an angle θ, for all those hedgehogs within the plaquette lying in the $z = a$ plane.

To see this, consider the relation between the two neighbouring layers parallel to the (x,y) plane. This relation is such that the pion fields along the edges of the cube, parallel to the z-axis, point upwards. Thus, within the (x,y) planes at $z = 0$ and $z = a$, we are free to 'globally' iso-rotate the hedgehogs within these planes about the z-axis, without breaking the condition of non-frustration of the pion fields along lines of centre. These other lattice arrangements appear to have gone unnoticed and thus, have so far not been investigated.

Having fixed the relative field orientation within one cubic cell, for simplicity we choose to demand the whole lattice be generated from successive repetitions of these representative cells by lattice translation and corresponding iso-rotations. This translation symmetry, coupled to iso-rotations, can be expressed as a set

of twisted boundary conditions which relate the pion fields within neighbouring cells. These conditions shall be given in the next section.

As an alternative to a cubic array, an fcc array, with its increased number of nearest neighbours to twelve, has been investigated. Once more we can construct this arrangement in a similar manner. We shall prove that there is only one unique arrangement which satisfies Klebanov's condition of relative non-frustration of the pion field of nearest neighbouring hedgehogs.

We choose our hedgehog at the origin to be unrotated and so its nearest neighbours in the positive octant are located at the points $r_1 = (a/2, a/2, 0)$, $r_2 = (a/2, 0, a/2)$ and $r_3 = (0, a/2, a/2)$. Initially we shall consider just this octant. The pion fields of the hedgehogs, located at the point $r_i (i = 1, 2, 3)$, will be iso-rotated by an angle π, about an axis $\hat{\bar{a}}_i (i = 1, 2, 3)$, chosen such that it satisfies the non-frustration condition $\hat{\bar{a}}_i . \vec{r}_i = 0$, where $\vec{r}_i$ is the position vector of the point r_i.

Thus, the pion fields of the hedgehog at the origin are relatively non-frustrated to the pion fields of its nearest neighbours at the points r_i. However, all these nearest neighbours of the hedgehog at the origin, are also nearest neighbours to each other. Thus, we require that the pion fields of these three hedgehogs are also relatively non-frustrated to each other. In order to establish the generalisation of Klebanov's non-frustration condition, for the pion fields of two skyrmions which are both iso-rotated, we must unrotate the pion fields of one of the hedgehogs, while keeping their relative orientations fixed. Thus, we perform a global rotation

on all four of these hedgehogs, such that the hedgehog at r_i becomes unrotated. That is to say, we performed an iso-rotation about the axis $\hat{\vec{a}}_i$, through an angle π, on the pion fields of all four hedgehogs. To deduce the new direction of the iso-rotation axis, after performing this global iso-rotation of the hedgehog located at r_2, we need to observe that under a global rotation, about an axis $\hat{\vec{a}}$ by an angle θ, a skyrmion field U is transformed to

$$(\cos\theta/2 + i\hat{\vec{a}}.\vec{\tau}\sin\theta/2)U(\cos\theta/2 - i\hat{\vec{a}}.\vec{\tau}\sin\theta/2). \qquad (3.1.1)$$

Hence, if $\theta = \pi$ we have that,

$$U \mapsto \hat{\vec{a}}.\vec{\tau}U\vec{\tau}.\hat{\vec{a}}. \qquad (3.1.2)$$

Since before we perform the global rotation, the hedgehog at the point r_2 has its pion fields iso-rotated about the axis $\hat{\vec{a}}_2$, we should consider the expression,

$$(\hat{\vec{a}}_1.\vec{\tau})(\hat{\vec{a}}_2.\vec{\tau}) = (\hat{\vec{a}}_1.\hat{\vec{a}}_2) + i(\hat{\vec{a}}_1 \times \hat{\vec{a}}_2).\vec{\tau}, \qquad (3.1.3)$$

in order to deduce its new axis of iso-rotation. We then see that we have two possibilities. Since the hedgehog at r_2 must now be non-frustrated relative to the unrotated hedgehog at r_1, it must be iso-rotated about some axis by an angle π. Therefore, from (3.1.2) and (3.1.3), we deduce that $\hat{\vec{a}}_1.\hat{\vec{a}}_2 = 0$ and that the pion fields of the hedgehog located at r_2 are now rotated about the axis $\hat{\vec{a}}_1 \times \hat{\vec{a}}_2$. We can similarly deduce that the non-frustration condition, for the pion fields of the hedgehog located at the point r_3, relative to the pion field of the unrotated hedgehog located at the point r_1, leads to the condition $\hat{\vec{a}}_1.\hat{\vec{a}}_3 = 0$ and that the

axis of iso-rotation of the pion field of the hedgehog located at r_3, is $\hat{\bar{a}}_1 \times \hat{\bar{a}}_3$.
Since the unrotated hedgehog at the origin is now rotated about the axis $\hat{\bar{a}}_1$, we
again have the relative non-frustration condition $\hat{\bar{a}}_1.\vec{r}_1 = 0$, for the pion field of
the hedgehog located at the origin and at the point r_1.

These conditions imply that the vectors $\hat{\bar{a}}_1, \hat{\bar{a}}_2$ and $\hat{\bar{a}}_3$ form a mutually or-
thogonal set of unit vectors. We require one further subsidiary condition. After
performing the global iso-rotation, the pion field of the hedgehog located at r_2
is iso-rotated about the axis $\hat{\bar{a}}_1 \times \hat{\bar{a}}_2$ and the pion field of the hedgehog at r_1 is
unrotated. Therefore, in order for the pion fields of these two hedgehogs to be
relatively non-frustrated, the following condition must be satisfied,

$$(\hat{\bar{a}}_1 \times \hat{\bar{a}}_2).(\vec{r}_2 - \vec{r}_1) = \hat{\bar{a}}_3.(\vec{r}_2 - \vec{r}_1) = \hat{\bar{a}}_3.(-\hat{\bar{y}} + \hat{\bar{z}}) = 0. \qquad (3.1.4)$$

However, before we performed this global iso-rotation, we deduced that $\hat{\bar{a}}_i.\vec{r}_i = 0$
(for $i = 1, 2, 3$), from which we have, that

$$\hat{\bar{a}}_3.(\hat{\bar{y}} + \hat{\bar{z}}) = 0. \qquad (3.1.5)$$

Thus, from equations (3.1.4) and (3.1.5), we deduce that $\hat{\bar{a}}_3 = \hat{\bar{x}}$. Similarly we
can demonstrate that $\hat{\bar{a}}_2 = \hat{\bar{y}}$ and $\hat{\bar{a}}_1 = \hat{\bar{z}}$.

Hence, we have proven that there exists one unique arrangement of four neigh-
bouring hedgehogs which satisfies Klebanov's non-frustration condition for the
pion fields of all four neighbouring hedgehogs and this arrangement is indicated
in Figure (3.1.3a).
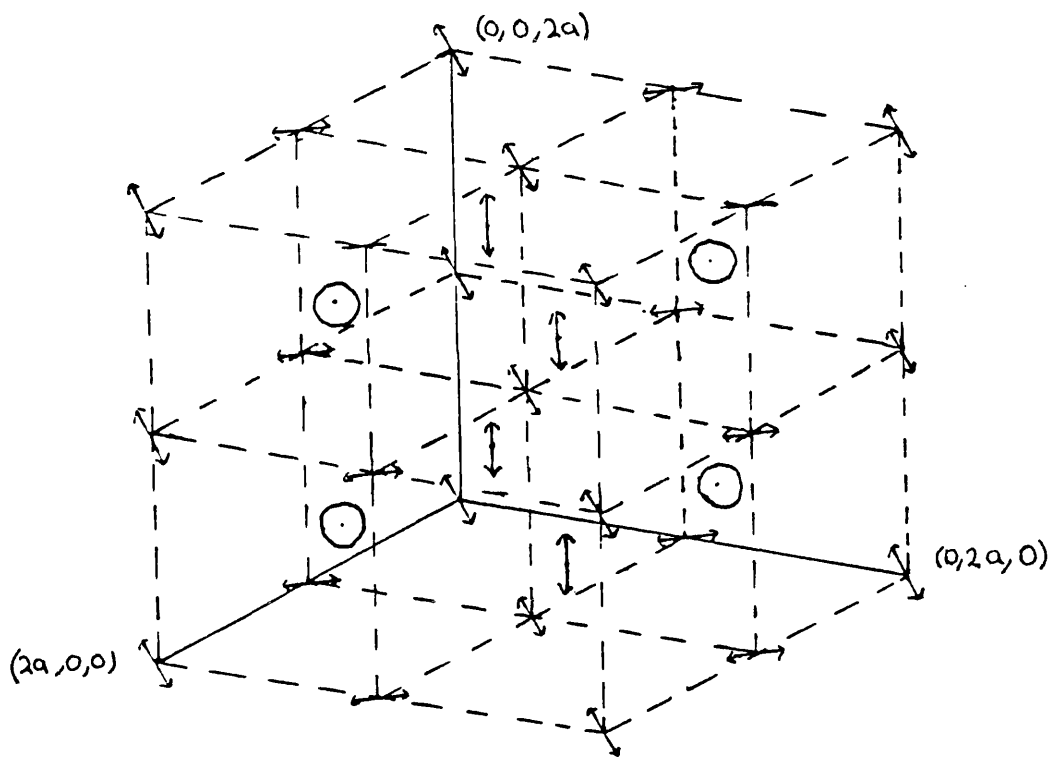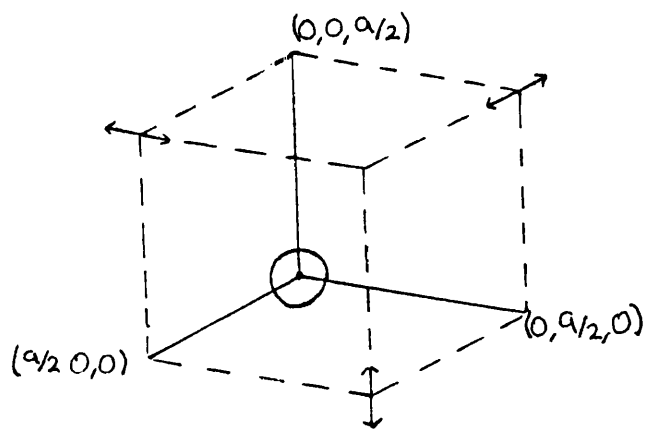
Figures (3.1.3a) and (3.1.3b): (a)-Non-frustrated arrangement of four skyrmions in a representative cell of the fcc lattice. (b)- Non-frustrated arrangement of hedgehogs within the bcc array. The figure shows eight adjacent bcc cubes.

From this unique arrangement of four hedgehogs we can generate the full fcc lattice. A lattice translation by a, along the $(x, y$ or $z)$ axes, will not involve an iso-rotation and thus, this fcc cube generates the full fcc array by a trivial lattice translation along the lines parallel to the coordinate axes. This four skyrmion arrangement within a representative cubic cell, shown in Figure (3.1.3a), forms an octant quadrant of the full fcc cube. This arrangement was proposed both by us [10] and independently [11][12].

Finally it was discovered that a bcc array of optimally orientated hedgehogs could be constructed [10] and this arrangement is indicated in Figure (3.1.3b). Here we have indicated the orientations of the hedgehogs located at the points of the eight neighbouring bcc cubes. Focusing on the unrotated hedgehog, located at the point $(3a/2, a/2, 3a/2)$ at the centre of a bcc cube and where a is the length of the bcc cube, we see that its eight nearest neighbours at the vertices of this cube, are alternately iso-rotated about the $(\hat{\tilde{x}} + \hat{\tilde{y}})\sqrt{2}$ and $(\hat{\tilde{x}} - \hat{\tilde{y}})\sqrt{2}$ axes by an angle π. Thus, the pion field of the hedgehog at the centre of this cube, which points radially outwards from its centre, matches smoothly those of the eight rotated hedgehogs at the vertices. The neighbouring bcc cube, in the x or y direction, will have the same relative orientation of hedgehogs. However, this lattice translation involves an overall iso-rotation about the z axis, by an angle π.

This bcc arrangement is related to the fcc arrangement shown in Figure (3.1.3a) by an expansion of $\sqrt{2}$ of the bcc lattice along one of its coordinate

axes. To see that this is indeed the case, the Figure (3.1.4a) indicates the orientations of the twelve nearest neighbours of an unrotated hedgehog within the fcc array. Here, the coordinate axes are those we chose to describe the fcc arrangement. Now consider the unrotated hedgehog at the point $(3a/2, a/2, 3a/2)$ within the bcc lattice, Figure (3.1.3b). In Figure (3.1.4b) we have depicted this hedgehog's eight nearest neighbours lying in the $x = y$ and $x = -y$ planes in the bcc coordinates. We have also indicated the positions and orientations of the four next nearest neighbours lying within the plane parallel to the (x, y) plane located at $z = 3a/2$, each of which is iso-rotated about the z axis by an angle π. On expanding this bcc arrangement by a factor $\sqrt{2}$ along the z axis and performing a trivial global spatial rotation about the z axis through an angle $\pi/4$, we find that the resulting arrangement is identical to the fcc arrangement depicted in Figure (3.1.4a).

In this discussion of the various lattice arrangements of skyrmions, we have denoted each lattice arrangement, according to the name given to the array of points at which the skyrmions are located. Taking the primitive cell of this particular array, we can generate the whole skyrmion crystal by combining lattice translations with iso-rotations. However, alternatively, we can construct the true primitive spatial lattice for each of these crystals, for which a simple lattice translation would not involve an iso-rotation.

These spatial lattices simply correspond to the elementary cells of the crystal, which when repeated will produce the full lattice and not require iso-rotations.
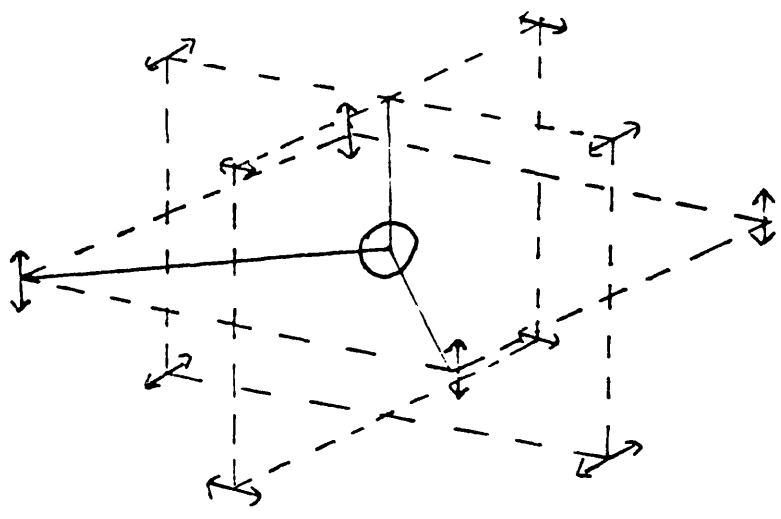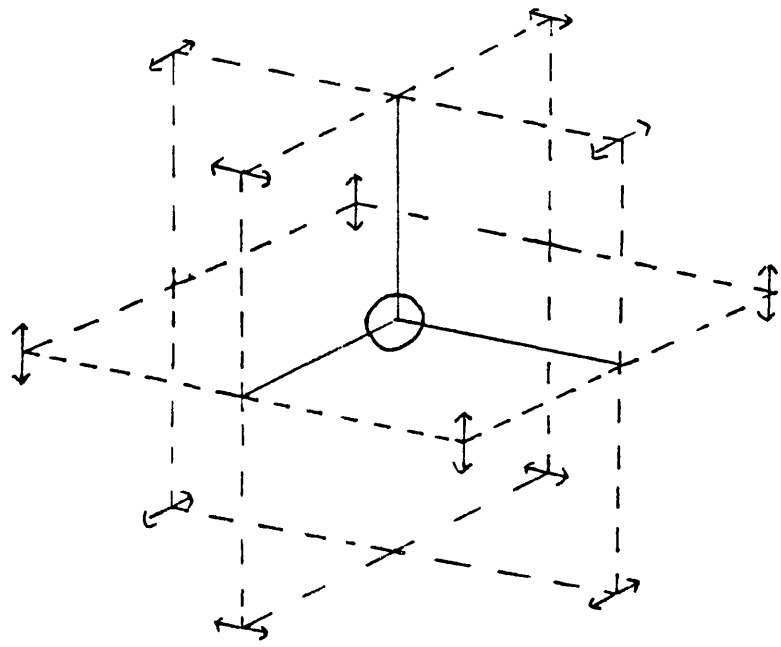
Figures (3.1.4a) and (3.1.4b): (a)-Twelve nearest neighbours of an unrotated hedgehog within the fcc array. (b) Eight nearest neighbours and the four next nearest neighbours within the (x, y) plane, of an unrotated hedgehog within the bcc array.

Hence, it is simple to deduce, that for Klebanov's arrangement, the primitive space lattice vectors are $a(\hat{\bar{x}} + \hat{\bar{y}} - \hat{\bar{z}})$, $a(\hat{\bar{x}} - \hat{\bar{y}} + \hat{\bar{z}})$ and $a(-\hat{\bar{x}} + \hat{\bar{y}} + \hat{\bar{z}})$. Hence, the true primitive cell of the Klebanov simple cubic arrangement corresponds to that of a bcc crystal.

For the Jackson cubic lattice, with its rectangular symmetry, the spatial skyrmionic structure gives the primitive lattice vectors to be $a(\hat{\bar{x}} + \hat{\bar{y}})$, $a(\hat{\bar{x}} - \hat{\bar{y}})$ and $2a\hat{\bar{z}}$ and these correspond to the primitive cell of a distorted cubic crystal.

For the fcc lattice, the spatial structure of skyrmionic matter gives the primitive lattice vectors to be $a\hat{\bar{x}}$, $a\hat{\bar{y}}$ and $a\hat{\bar{z}}$ and this corresponds to a cubic lattice.

Finally, the bcc lattice has a spatial skyrmionic structure for which the primitive lattice vectors are $a(\hat{\bar{x}} + \hat{\bar{y}})$, $a(\hat{\bar{x}} - \hat{\bar{y}})$ and $a\hat{\bar{z}}$ and which corresponds to the primitive cell of a distorted cubic crystal.

In the following sections, we shall describe the numerical investigations that have so far been undertaken for a lattice of skyrmions corresponding to these four arrangements. For all these lattices, the requirement of nearest neighbour non-frustration results in a smooth pionic field arrangement of the full crystalline field configuration. These numerical studies have investigated the effects of reducing the lattice spacing a.

At low densities a crystalline array of skyrmions will consist of an infinite product of spherically symmetric skyrmions, centred on well separated points and with their pion fields mutually iso-rotated. Klebanov's choice of a simple cubic array of skyrmions, was guided mainly by symmetry and optimising asymptotic

nearest neighbour attraction between the neighbouring skyrmions.

We shall now outline, historically, the developments that have taken place within this field. As we have seen, Klebanov proposed that the classical ground state configuration should possess cubic symmetry and in the asymptotic separation limit, have neighbouring spherical skyrmions relatively iso-rotated, so as to maximise their tensor force of attraction. In the low density limit, the configuration will be well described as a product of spherical hedgehogs, with a periodic relative iso-rotation of the pion fields of neighbouring hedgehogs. This periodicity, results in a set of twisted boundary conditions describing the full symmetry of Klebanov's simple cubic array. These boundary conditions were imposed in order to allow exact numerical minimal energy configurations to be found over a wide range of densities.

A further numerical study of this cubic arrangement, by Wurst et al [13], revealed that as the baryon density was increased, there was a phase transition from a phase of isolated skyrmions, to a condensed phase in which the energy density was more uniformly distributed. It was later realised [9] that this phase was characterised by the mean value of the σ field, $< \sigma >$, rigorously vanishing. These two phases of skyrmionic matter were subsequently seen to be analogous to the two forms of matter which exist in the simple $S^3_{phy}(L)$ model and to a realisation of the nature of this delocalising phase transition.

Goldhaber et al [14] identified that the phase transition and the vanishing of $< \sigma >$ observed in the flat space arrays in the condensed phase, were accompanied

by the appearance of an additional symmetry in the crystalline field configuration. Moreover, they deduced that in the condensed phases the skyrmion array can be described as an array of half skyrmions, a half skyrmion being a skyrmion field configuration which has a baryon number of a half. This follows as a direct consequence of the additional translation symmetry, which the condensed field configuration possesses at high densities. In Section 3.3, we shall describe in detail the nature of the twisted boundary conditions which describe this additional symmetry and the manner in which it is realised within crystalline skyrmionic matter at high densities.

The analogue of the alternate spin-isospin symmetry of dense neutron matter proposed by Smith et al and resulting from the long range tensor force of attraction between neutrons, was not completely realised in Klebanov's cubic arrangement. The analogue of this symmetry for skyrmions, was subsequently proposed by Jackson et al [9] for the classical ground state configuration of crystalline skyrmion matter. Their investigations indicated that the rectangular arrangement depicted in Figure (3.1.2c), was indeed preferable to Klebanov's choice over almost the entire density range. Moreover, they found a phase transition to exist and also that the condensed phase was again characterized by $< \sigma > = 0$ and the appearance of an additional half skyrmion symmetry in the field.

Though long range forces clearly dictate the optimal array at low densities, the strong repulsion between skyrmions would indicate that a close packed array could be energetically favoured at high densities. In particular, our fcc arrange-

ment in Figure (3.1.3a), would enable the long range forces to be effective and at the same time avoid too close an approach. We shall see later, that the results of our numerical investigations of the fcc lattice [10], reveal that this is indeed the case. At high densities the fcc array, which also undergoes a phase transition to a condensed phase of half skyrmions, has a minimum energy which is just 3.8% above the lower bound. Thus, this arrangement has been shown to be the most likely candidate for the classical ground configuration of crystalline skyrmionic matter. Cook et al [15] have even proposed an fcc lattice arrangement as a candidate for a nuclei. Kugler et al [12] performed variational calculations for this fcc array, of the minimal energy configuration, composed of an array of half skyrmions.

In the remainder of this chapter we shall review the results obtained for the various arrays which have been investigated and compare these to the results for the fcc and the bcc arrays and a series of arrays with interpolating symmetries that we also have investigated. We shall also present the results of our numerical calculations for these lattice arrangements and draw our conclusions, mentioning the most interesting, recent developments which have since taken place.

3.2 Skyrmion Arrays At Low Densities

At low densities a skyrmion crystal will be composed of isolated, distinct, well separated spherical skyrmions centred on the points of a lattice. Thus, at low

densities the static skyrmion field can be approximately represented as an infinite product of hedgehogs, $U_h(\vec{x})$ (2.1.22), of the form,

$$U(\vec{x}) = \prod_i A_i U_H(\vec{x} - \vec{R_i}) A_i^+, \qquad (3.2.1)$$

with A_i determining the orientation of the skyrmion centred at the lattice site R_i. This ansatz will be valid in the large separation limit

$$\mid \vec{R_i} - \vec{R_j} \mid \gg 1/ef_\pi. \qquad (3.2.2)$$

At the points of the lattice, the field $U(\vec{x})$ will have the value -1, though throughout most of space, the field in the low density limit will have a value close to its trivial vacuum value of 1. These regions within the crystal, where the skyrmion field $U(\vec{x})$ is close to its trivial vacuum value, separate those regions containing localised baryon density and thus, at low densities these regions fill most of space. Hence, this uncondensed phase of skyrmionic matter will be characterised by the $< \sigma >$ being close to unity.

Asymptotically, the optimal lattice and relative orientation of the skyrmions within the lattice, will be determined by the tensor potential between neighbouring skyrmions as given in equation (2.2.4). In the zero pion mass limit, this potential has a $1/ \mid \vec{R_i} - \vec{R_j} \mid^3$ asymptotic behaviour and is maximally attractive for a non-frustrated arrangement of the hedgehog skyrmion's pion fields. Thus, in order to optimize the asymptotic binding energy at low density, we require nearest neighbours to be relatively iso-rotated about an axis perpendicular to their line of centre by angle by π. However, as we have seen in the previous

section, there exist many differing lattices, with various relative orientations of skyrmions, which satisfy this requirement. To differentiate these structures, there are other factors which we expect to be important in determining the optimal arrangement. Thus, the number of nearest neighbours and the interactions between more distant neighbours, should be important and as the density is increased, the effectiveness of the packing arrangement will also become increasingly significant in determining the optimal skyrmion array.

The skyrmionic arrays so for considered, are such that the skyrmionic field configuration within neighbouring representative cells, satisfies a set of twisted boundary conditions. Thus, fields within all cells of the crystal, are related to the field within a representative cell by the lattice translation expressed as a set of twisted boundary conditions. Each of these cells is mapped by the field onto $SU(2)$ once and thus contributes 1 to the baryon number of the skyrmionic crystal.

The boundary conditions which determine the fields within a representative cell and hence the lattice translations relating the fields within different cells, are deduced from the picture of an array of localised spherical hedgehogs at low densities described in the previous section. These boundary conditions are enforced as the density of the crystalline matter is increased.

To compare these lattices, we can evaluate the asymptotic binding energy by summing the tensor potential (2.2.4), of a single representative skyrmion, over a large number of neighbouring skyrmions and for differing lattices compare them

at the same baryon density.

For each infinite array of skyrmionic matter so far investigated, we shall now present, in detail, the boundary condition which follows from the picture of a low density array of relatively rotated $B = 1$ hedgehogs described in the previous section.

1. The Klebanov [6] cubic lattice depicted in Figure (3.1.2b), asymptotically has spherical skyrmions centred on the point of a simple cubic lattice. A translation by a lattice spacing a, in the x direction, involves iso-rotation about the z axis cyclicly and by an angle π. The resulting twisted boundary conditions are best expressed in terms of the unitary matrix fields

$$U = (\sigma + i\vec{\tau} \cdot \vec{\pi})/f_{\pi}. \qquad (3.2.3)$$

Klebanov's twisted boundary conditions are then given by

$$
\begin{aligned}
U(x + a, y, z) &= \tau_z U(x, y, z) \tau_z, \\
U(x, y + a, z) &= \tau_x U(x, y, z) \tau_x, \\
U(x, y, z + a) &= \tau_y U(x, y, z) \tau_y, \qquad (3.2.4)
\end{aligned}
$$

on the points of the lattice $U(\vec{x}) = -1$ and these points correspond to the centres of the spherical skyrmions. It follows from expression (3.2.4) and from the fact that the points at the body centres of the cubic lattices are the points which are furthest from the regions of localised baryon density, that $U(\vec{x}) = 1$ at the body centres of the cubic lattice. Hence, these ± 1

points form two intersecting cubic lattices and taken together, form a bcc lattice. There exists an alternative lattice arrangement, which is degenerate in energy with this lattice and this corresponds to the other possible cyclic ordering in equation (3.2.4).

The lattice arrangement (3.2.4) results in no nearest neighbour frustration. A representative skyrmion has it's six nearest neighbours maximally attractive. However, its twelve second nearest neighbours are repulsive at large separations. Its third and fourth neighbours interactions give zero attraction, as these are unrotated relative to a representative skyrmion.

2. The Jackson and Verbaarschot [9] cubic lattice, depicted in Figure (3.1.2c), consists of alternate layers parallel to the (x, y) planes, one layer with skyrmions alternately unrotated and iso-rotated about the z axis by an angle π, and the next layer with skyrmions alternately iso-rotated about the x and y axes by an angle π. This leads to the boundary conditions

$$U(x + a, y, z) = U(x, y + a, z) = \tau_z U(x, y, z)\tau_z,$$

$$U(x, y, z + a) = \tau_y U(x, y, z)\tau_y. \qquad (3.2.5)$$

For this rectangular arrangement of skyrmions on a cubic lattice within the (x, y) plane, the $U(\vec{x}) = -1$ points form a pattern of squares. It is natural to require that $U(\vec{x}) = +1$, at the centres of these squares and at the centres of the squares in the successive planes parallel to the (x, y) plane.

The corresponding asymptotic arrangement of localised spherical skyrmions has a two-fold advantage over Klebanov's rather arbitrary choice of lattice arrangement. These are;

(a) For a given representative skyrmion all six nearest neighbours are still maximally attractive in the asymptotic limit. However, the twelve next nearest neighbours in the $(x, y), (x, z)$ and (y, z) planes, give differing tensor interactions, with an overall net attraction. The third and fourth next nearest neighbours interactions are once more both zero. This rectangular symmetry gives a net gain in asymptotic attraction over Klebanov's full cubic symmetry arrangement.

(b) Although a skyrmion is a classical baryon and as such spin is not a relevant quantum number, Klebanov was able to show how the average value of the spin and isospin changes in moving from cell to cell within a skyrmion crystal. For Klebanov's lattice, a representative cell is cubic and can be chosen such that it has a skyrmion at its centre and $U(\vec{x}) = +1$ at its six vertices.

To ensure electrical neutrality, a skyrmion crystal should, upon quantization, have its iso-spin exited so as to correspond to an array of neutrons. In order to achieve this, Klebanov employed a semi-classical quantization technique, quantizing the single collective iso-rotational zero mode of the crystal. This collective coordinate rotates the whole crystal globally in iso-

76

space. It is inappropriate to collectively quantize the individual iso-spin rotational modes of the skyrmions in the array in this manner, even at low densities, since these skyrmions are stuck together and these rotations are not zero modes. Promoting this overall iso-spin rotational collective coordinate to a dynamical variable we have,

$$U(t,\vec{r}) = A(t)U_c(\vec{r})A^+(t), \qquad (3.2.6)$$

where $U_c(\vec{x})$ is the static crystalline minimal energy skyrmion field. For a general skyrmion field, $U(\vec{x})$, the iso-spin is given by the integral of the iso-vector current density,

$$I^k = i\lambda_I^{jk}(U)Tr(\dot{A}A^+\tau_j), \qquad (3.2.7)$$

where $\lambda_I^{kj}(U)$ is the tensor of inertia of iso-space, which for both Klebanov's cubic [6] and the rectangular array of Jackson et al [16], has been shown to be a multiple of the identity. $\dot{A}$ denotes the derivative of $A(t)$ with respect to time.

Similarly, the angular momentum is given by

$$J^k = \int d^3x \varepsilon^{ijk}T_{0i} = i\lambda_S^{jk}Tr(\dot{A}^+A\tau_j), \qquad (3.2.8)$$

where $T_{\mu\nu}$ is the energy momentum tensor and $\lambda_S^{kj}(U)$ is the tensor of inertia in real space, which has also been shown to be proportional to the identity for both of these simple cubic lattices.

Klebanov was thus able to deduce from (3.2.7) and (3.2.8) that

$$i\vec{I} \cdot \vec{\tau} \sim \dot{A}A^+,$$

$$i\vec{S} \cdot \vec{\tau} \sim \dot{A}^+A. \qquad (3.2.9)$$

Thus, on moving from one cell to the next, the field configuration (3.2.6) changes by,

$$U \mapsto BUB^+, \qquad or\ equivalently \quad A(t) \mapsto A(t)B, \qquad (3.2.10)$$

where $B = i\tau_k$. Hence we see, that on moving from one cell to the next we have,

$$\dot{A}A^+ \mapsto \dot{A}A^+,$$

$$\dot{A}^+A \mapsto B^+\dot{A}^+AB, \qquad (3.2.11)$$

and that $\vec{I}$ remains the same in all cells, while $\vec{S}$ flips. Choosing $\vec{S} = \hat{\vec{z}}s_z$, we have that for Klebanov's arrangement, as defined by equation (3.2.4), s_z changes sign as we move from cell to cell in the y and z directions and remains the same as we move in the x direction. The resulting spin configuration does not correspond to that discovered by Smith et al [7]. The rectangular arrangement of Jackson et al defined by equation (3.2.5), does however have the additional merit, that the average spin arrangement within the cells does correspond to the spin arrangement of Smith et al, with alternate (x,y) planes having spins in the $+z$ and $-z$ directions. For the rectangular arrangement, a lattice displacement of a in the x or y directions,

78

leaves s_z unchanged, while a displacement in the z-direction changes its sign. Thus, the arrangement of Jackson et al is in closer analogy to the arrangement predicted, by Smith et al, to exist in dense neutron matter.

We noted in the previous section, that there exists an infinite number of lattices which generalise the Jackson et al rectangular arrangement. These arrangements correspond to hedgehogs within the alternate layers parallel to the (x, y) plane, iso-rotating about the z axis by an angle θ, relative to those hedgehogs within the intermediate planes.

This would correspond to generalising the Jackson et al boundary condition, (3.2.5), by making the replacement, $\tau_y \mapsto (\tau_x \sin \theta/2 + \tau_y \cos \theta/2)$. This generalised lattice arrangement satisfies the condition of nearest neighbours, being non-frustrated for all values of θ. However, this generalisation has to date not been investigated and its appearance seems not to have been noticed by Jackson et al.

It would be of particular relevance here, to compare numerically, the energy of the field configuration satisfying this generalised twisted boundary condition. We can also compare these lattices asymptotically, by considering the tensor interaction of a representative hedgehog skyrmion with neighbouring skyrmions. We find that the net contribution to the tensor potential, of all successive numbers of nearest neighbours, is independent of the angle θ. This startling result suggests that this 'global planar' iso-

rotation through an angle θ, is a true zero mode of the Jackson crystalline arrangement.

However, this asymptotic result may not hold at finite separations. Here, we would have to perform a numerical calculation in order to see whether or not this is a true zero mode. However, the existence of a zero mode would provide us with an alternative collective coordinate, which could be semi-classically quantized. Presumably, this would lead to different possible interpretations to Klebanov's interpretation of a skyrmion crystal corresponding to a neutron crystal. Finally, it would be expected that at high densities, this generalised symmetry would be present in the condensed phase of skyrmionic matter.

3. The fcc array depicted in Figure (3.1.3a), for which we shall later present numerical results, will have a more efficient close packed structure and thus would be expected to lead to a greater binding energy than these cubic lattices at high densities, when the localised spherical skyrmion fields are increasingly forced to distort. The fcc array has the skyrmions at the corners of the fcc cube unrotated and those on the faces iso-rotated about the normal to the corresponding face by an angle π and this leads to the following set of twisted boundary conditions,

$$U(x + a/2, y + a/2, z) = \tau_z U(x, y, z) \tau_z,$$

$$U(x + a/2, y, z + a/2) = \tau_y U(x, y, z) \tau_y,$$

$$U(x, y + a/2, z + a/2) \;=\; \tau_x U(x, y, z) \tau_x. \qquad (3.2.12)$$

This arrangement has all twelve nearest neighbours asymptotically maximally attractive, but the six next nearest have zero attraction. Thus, a significant asymptotic binding energy results.

A particularly representative cell was depicted in Figure (3.1.3a) of the fcc crystal and is a cubic octant of the full fcc cube. The points where $U(\vec{x}) = -1$, lie at four of the vertices of this representative cell and taken together form the vertices of a tetrahedron inscribed within the cell. At the remaining four vertices the skyrmion field has a value 1 and these vertices also lie at the vertices of a similar tetrahedron. The field $U(\vec{x})$ maps this cell onto $SU(2)$ and hence, within a representative cell, the field contributes $B = 1$ to the crystalline skyrmions field's total winding number B.

4. The bcc array that we shall consider is depicted in Figure (3.1.3b) and can be obtained from the fcc lattice described above, by contracting the z axis by a factor $\sqrt{2}$, the fcc nearest neighbours in the (x, y) plane now becoming the corners of the bcc cube and the skyrmions on the centres of the (x, z) and (y, z) faces becoming the ones at the centre of the bcc cube. Alternatively, expressed in terms of the bcc variables we have the twisted boundary conditions;

$$U\left(x \pm a, y, z\right) = U\left(x, y \pm a, z\right) = \tau_z U\left(x, y, z\right)\tau_z, \qquad (3.2.13)$$

$$U(x \pm a/2, y + a/2, z + a/2) = \left(\tau_y \mp \tau_x\right)U(x, y, z)\left(\tau_y \mp \tau_x\right)/2.$$

The eight nearest and four of the six next nearest neighbours are maximally attractive, and the remaining two neighbours produce no long range attraction. Hence this arrangement also leads to high asymptotic binding energy.

We can take a representative cell of this bcc array to be that cell which results when the cubic fcc representative cell is contracted along the z-axis by a factor of $\sqrt{2}$. This representative bcc cell is thus a square based prism.

Quantitatively we can compare the binding energies of these lattices by summing the asymptotic tensor interaction, (2.2.4), of a representative skyrmion, with its nearest and next nearest neighbours, as well as over a large number of neighbours at the same baryon density. The resulting asymptotic potentials are given in Table (3.2.1).

Table 3.2.1

$L^3 \times (Potential)$	Klebanov	Jackson	fcc	bcc
near neighbours	-949	-1640	-2075	-1995
many neighbours	-931	-1485	-1593	-1634

The asymptotic potentials from equation (2.2.4) for a single skyrmion divided by the skyrmion density. Near neighbours includes nearest neighbours and next nearest and many neighbours include about 160 for Klebanov [6] and Jackson [9] arrays and all neighbours within a distance of $20a$ for fcc and bcc type arrays. $L = (\text{skyrmion density})^{-1/3}$.

The contribution of distant skyrmions, is of course only meaningful in the

zero pion mass limit, which is the case considered here. Table (3.2.1) shows that the bcc array is most bound, while the fcc and Jackson and Verbaarschot arrangements are next and about equal. As expected Klebanov's array is the least bound array asymptotically.

5. Since the fcc and bcc arrays, (3.2.12) and (3.2.13), are smoothly related by a simple contraction in the z direction by factor $\sqrt{2}$, it is both natural and of interest to consider the rectangular interpolating lattices which are formed as the contraction factor is smoothly varied. Hence, we consider a regular array which interpolates between fcc and bcc, by changing the unit aspect ratio of the fcc cube of side a into a rectangular region of aspect ratio r^3 with lattice displacements in the x and y directions of ra and lattice displacements in the z directions of a/r^2. Otherwise, the boundary conditions of equation (3.2.12) are unaltered.

We define $p = r - 1/r$ to measure the deviation from fcc symmetry ($p = 0$). Hence, $p = 0.23$ ($r^3 = \sqrt{2}$) describes a bcc array. $p \gg 1$ describes separate one dimensional columns of closely packed and relatively unrotated skyrmions, while $p \ll -1$ describes separate planes of square arrays of skyrmions, within which first, third and successively odd numbered nearest neighbours are maximally attractive and the remaining even numbered nearest neighbours are relatively unrotated, with zero attraction.

Performing the sums of the asymptotic interaction in (2.2.4), over nearest and

83

next nearest neighbours as well as over a large number of neighbours at varying values of p, gives the binding energies shown in Table (3.2.2).

Table 3.2.2

$L^3 \times$(Potential)

p	-0.3	-0.2	-0.1	0.0	0.1	0.2	0.3	0.6	2.0
many	-1776	-1663	-1614	-1593	-1604	-1614	-1651	-1697	-1619

The asymptotic potentials from equation (2.2.4) for a single skyrmion divided by the skyrmion density. Many neighbours, is all the neighbours within a distance of $20a$, fcc corresponds to $(p = 0.0)$, bcc to $(p = 0.23)$. $L = $ (skyrmion density)$^{-1/3}$.

The dependence on p, of this asymptotic formula, indicates that the fcc binding energy is a local maximum, dropping away indefinitely for negative p since the separated planes contain alternating unrotated and optimally orientated skyrmions. For large positive values of p, the limit of separate columns of skyrmions which are non-interacting, the potential is zero and so there is a minimum in the asymptotic energy near $p = 1.3$. But these arguments fail as soon as the short range repulsion comes into play.

Since the fcc array is close packed, it is quite likely to have a lower energy than the others at high density. Furthermore, the limits $p \to \pm\infty$, of the asymptotic formula at fixed density, are unphysical, since at some value of p the effect of

the repulsive cores of the nearby skyrmions can no longer be neglected. This indicates the existence of another minimum at negative p and a major change in the minimum at positive p.

Thus, we see that by varying the value of p we are able to investigate the behaviour of the fcc array at high densities to bulk deformations, which may be useful in the study of heavy ion collisions.

3.3 The High Density Phase Of Skyrmionic Matter

While at low densities a skyrmion crystal can be pictured as being composed of weakly interacting individual spherical skyrmions, centred on the points of a lattice, this will not be a reasonable picture at high densities. At high densities the fields of the individual skyrmions will undergo considerable deformation and can no longer be said to be weakly interacting.

This is in direct analogy with the situation which arises for the $B = 2$ skyrmion configuration [17]. At large separations, the configuration consists of two distinct, spherical skyrmions, weakly interacting and orientated relatively so as to optimize their tensor attraction. At small separations the individual skyrmions completely loose their identity. A particular discrete reflection symmetry of the field configuration at large separation, becomes, at small separations, a continuous axial symmetry [18].

For a crystal at low densities, with large regions of trivial vacuum surrounding

the localised skyrmions, $< \sigma >$ is close to 1. As the density increases, this value decreases to zero as the size of the trivial vacuum region is reduced. For all the arrays described in the previous section this behaviour of $< \sigma >$ has been demonstrated numerically [13][9] [10] and beyond some critical density it as been found that a condensed phase, characterized by its value being rigorously zero, is energetically preferred. Thus, the value of $< \sigma >$ has been used as an order parameter to identify the differing phases and the exact critical density beyond which the condensed phase of skyrmionic matter is energetically preferred. The vanishing of $< \sigma >$ and hence the formation of the condensed phase, is associated with the field configuration attaining an additional exact half skyrmion symmetry at high densities and we shall describe this symmetry in this section.

There is an analogous behaviour for a skyrmion on $S^3_{phy}(L)$ [5], with a second order phase transition at a value of $L = \sqrt{2}$ from the low density phase, consisting of a hedgehog localised at a pole with $< \sigma >$ close to unity, to the high density delocalised phase, consisting of a trivial map skyrmion with $< \sigma >= 0$. Here the vanishing of $< \sigma >$ is a trivial consequence of the restoration of $O(4)$ symmetry at high densities.

Goldhaber and Manton [14] proposed that at high densities, the condensed phase of a crystalline array of skyrmions could be pictured as being composed of an array of half skyrmions centred on the $U(\vec{x}) = \pm 1$ points of the original low density array.

A simple picture of a half skyrmion is provided by considering a spherically

86

symmetric hedgehog field in flat space, with its profile function $f(r)$ satisfying the boundary conditions $f(r = 0) = \pi$ at the centre of the hedgehog, and $f(r = r_0) = \pi/2$ on a spherical surface of radius r_0. The field is taken to be undefined outside of this spherical boundary. This half skyrmion has $B = 1/2$ and its energy is bounded from below by $6\pi^2 f_\pi/2e$. Goldhaber and Manton found that a half skyrmion has an energy of $1.015 \times (6\pi^2 f_\pi/2e)$ at an optimal value of the radius $r_0 = 2.09 Fm$. The profile function of this solution was observed to be approximately linear.

The closeness of a half skyrmion's energy to the energy bound and the linearity of the profile function are consequences of the half skyrmion boundary condition at $r = r_0$. Since this half skyrmion resides within a finite volume, $4\pi r_0^3/3$, it is not required to stretch over the whole of space and hence it does not have the usual tail behaviour, required for the physical $B = 1$ skyrmion in order for it to have a finite energy. A second type of half skyrmion, degenerate in energy and with the same value of r_0, can be obtained by a trivial modification of the half skyrmion boundary conditions corresponding to the transformation $f(r) \mapsto f(r) - \pi/2$ and this also has $B = 1/2$. At the centre of the first type of half skyrmion $U(\vec{x}) = -1$, while at the centre of the second type, the field as a value 1 and on the spherical boundary surface the σ field vanishes for both. The first type of half skyrmion has its pion field pointing radially outwards, while the second type has its pion field pointing radially inwards. The skyrmion field is not defined outside of the spherical boundary at r_0 and these half skyrmions

exist within a 'physical space' of finite volume.

In order to understand the reasoning behind this proposed half skyrmion picture of dense skyrmionic matter, it is instructive to consider the effect that an increase of the baryon density of a skyrmion array has on its field configuration, $U(\vec{x})$.

At low baryon densities, the field's baryon density is localised in spherical regions of space about the lattice points with $U(\vec{x}) = -1$. These points are well separated at low densities and in the intermediate regions of space, the field $U(\vec{x})$ has a value close to unity and thus $< \sigma >$ also has a value close to unity. As the average baryon density of the array is increased, the size of these $U(\vec{x}) \sim 1$ regions decrease and hence, so does $< \sigma >$. However, since the winding number of the skyrmion field will be conserved at all densities, the number of connected regions of space in which $U(\vec{x}) = -1$ and $U(\vec{x}) = +1$ must be conserved and also, there must be the same number of $U \pm 1$ regions. Thus, as the density is increased, the regions of $U(\vec{x}) \sim +1$ will reduce to points, with $U(\vec{x}) = +1$. In response to a reduction in the size of the $U(\vec{x}) \sim +1$ regions of space, the field $U(\vec{x})$, within the regions of space with localised baryon density, will deform in a manner which is consistent with the particular symmetry of the array. At some critical density the skyrmion array undergoes a delocalising phase transition, to a condensed phase of skyrmionic matter. This phase of skyrmionic matter has the field's baryon density about the $U(\vec{x}) = \pm 1$ points, identical and $< \sigma >= 0$. The delocalising nature of this phase transition corresponds to the fact that there

are now no regions of zero baryon density separating the $U(\vec{x}) = -1$ points and thus, the field's overall baryon density is spread more evenly over the whole of space.

The additional symmetry of the baryon density and the vanishing of $< \sigma >$ in the condensed phase, is due to the field $U(\vec{x})$ attaining an additional translational symmetry, which relates to the fields about the $U(\vec{x}) = \pm 1$ points. That is to say, a representative cell of the array in the uncondensed phase, can be taken to contain a $U(\vec{x}) = +1$, or a $U(\vec{x}) = -1$ point and moreover, that within one of these cells the field's baryon number is $1/2$. Thus we see, that within a condensed array of skyrmionic matter, representative cells exist which contain half skyrmions.

We have seen that as the density of an array is increased beyond the phase transition density, the identification of individual skyrmions on the lattice points, possible in the uncondensed phase, is no longer possible in the condensed phase of half skyrmions. Its is also not possible to identify which were the neighbouring half skyrmions which formed the original skyrmions in the uncondensed phase.

Within the condensed half skyrmion array, there exist continuous multiply connected $< \sigma >= 0$ surfaces which divide the field into two disconnected regions. Thus, the regions with $\sigma < 0$ will contain iso-rotated half skyrmions, which are distorted versions of the spherical half skyrmions which have their pion fields pointing radially outwards and the region with $\sigma > 0$ will contain iso-rotated, distorted versions of the second type of half skyrmion. These distor-

89

tions occur because the $\sigma = 0$ boundary surfaces are not spherical and the half skyrmion boundary conditions cannot be completely attained within a crystal, since touching balls will not fill space. Moreover, since the regions with $\sigma = 0$, which would exist if spherical half skyrmions formed the full lattice, have a finite energy density, unlike trivial vacuum regions, these half skyrmions must distort to fill all of space.

A reasonable picture of the half skyrmion lattice arrangement, is however, obtained by placing spherical half skyrmions centred on the $U(\vec{x}) = \pm 1$ points within the Wigner-Seitz cells of the lattice, so that neighbouring half skyrmions are non-frustrated. The true crystalline array will then be obtained by distorting the shapes of the spherical $\sigma = 0$ surfaces, of neighbouring half skyrmions, so that they meet smoothly and fill the whole of space. The distortion of the half skyrmion boundary conditions, will require both a radial distortion and an internal twist of the half skyrmion field. One expects the distortion will however, not be too large and will produce little change of the half skyrmion field near its centre. This picture suggest that a condensed skyrmion array will have an energy per unit baryon, which is bounded from below and which is a factor 1.015 above the lower bound (1.1.21). With this picture it also seems reasonable to predict that the minimal energy configuration would be attained when the volume of the half skyrmion lattices Wigner-Seitz cell is equal to $4\pi r_0^3/3$, so as to reduce the extent of the field deformations required for the half skyrmions to fill space.

For all of the lattice arrangements described is Section 2, the existence of a

phase transition to a condensed phase of half skyrmions possessing an additional half skyrmion symmetry at high densities, has been numerically demonstrated. We shall now describe these additional symmetries.

1. For Klebanov's cubic arrangement the $U(\vec{x}) = -1$ points lie on the points of a simple cubic lattice, while the $U(\vec{x}) = +1$ points are at the body centres of this cubic lattice. Thus, these two sets of points form two intersecting simple cubic lattices and taken together form a bcc array. Hence, the condensed phase, which exists at high densities, consists of a bcc array of half skyrmions. The additional half skyrmion symmetry of this array, which relates the $U(\vec{x}) = 1$ and $U(\vec{x}) = -1$ points, is expressed as

$$
\begin{aligned}
\sigma(x,y,z) &= -\sigma(a/2 - z, a/2 - y, a/2 - x), \\
\pi_x(x,y,z) &= \pi_y(a/2 - z, a/2 - y, a/2 - x), \\
\pi_y(x,y,z) &= \pi_x(a/2 - z, a/2 - y, a/2 - x), \\
\pi_z(x,y,z) &= \pi_z(a/2 - z, a/2 - y, a/2 - x),
\end{aligned}
\qquad (3.3.1)
$$

and cyclicly. The boundary conditions express the effect of a lattice translation and relate the fields of both types of half skyrmion within neighbouring cells.

At the $U(\vec{x}) = +1$ points, at the body centre of the cubic representative cell, there sits a half skyrmion of the type which has its pion field pointing radially inwards. Manton and Goldhaber [14] showed that these boundary conditions result in the half skyrmion at the body centre being iso-rotated

91

about the line passing through the points $(a/2, a/4, 0)$ and $(0, a/4, a/2)$, by an angle π. Examination of Figure (3.1.2b), shows that the resulting pion field arrangement of this half skyrmion to its eight nearest neighbours at the vertices of the cube, is relatively non-frustrated. Thus, at high densities, the bcc array of this half skyrmion, has neighbouring half skyrmion pion fields meeting smoothly.

2. The Jackson and Verbaarschot array has the field's $U(\vec{x}) = -1$ points centered on the points of the simple cubic lattice. The $U(\vec{x}) = +1$ points are located within the planes parallel to the (x,y) planes at the centres of the squares formed by the $U(\vec{x}) = -1$ points. Thus, in the condensed phase one type of half skyrmion will be centred on the original cubic lattice points and the other type of half skyrmion will be centred on a cubic lattice which is related to the original lattice by a lattice translation $(a/2, a/2, 0)$. The additional half skyrmion symmetry is given by,

$$
\begin{aligned}
\sigma(x, y, z) &= \sigma(y, x, z), \\
\sigma(x, y, z) &= -\sigma(a/2 - x, a/2 - y, z), \\
\vec{\pi}(x, y, z) &= \vec{\pi}(a/2 - x, a/2 - y, z), \quad\quad (3.3.2)
\end{aligned}
$$

and cyclicly. Jackson et al [9] noted that the reflection symmetry of the sigma field, about the plane $x = y$, was not present in the pion fields. These symmetries, (3.3.2), show that at the point $(a/2, a/2, 0)$, (see Figure (3.1.1c)), there is a $U(\vec{x}) = +1$ type half skyrmion, which has been

92

iso-rotated about a line parallel to the line $x = y$, $z = 0$ by an angle π, in order to attain a non-frustrated pion field arrangement within a square plaquette. However, the absence of the reflection symmetry about the $x = y$ plane, seems to be due to the particular choice of the twisted boundary condition Jackson et al imposed in their numerical investigations. Had they considered instead, the boundary condition (3.2.5), that is , the generalised boundary condition in which τ_y is replaced by $\tau_x \sin\theta + \tau_y \cos\theta$, then presumably, for $\theta = \pi/4$, their numerical results would have revealed that the pionic fields were reflection symmetric about the $x = y$ plane. This expectation can easily be understood, by noting that when $\theta = \pi/4$, the low density arrangement of the pion field is such that the plane $x = y$ is either parallel or perpendicular to all of the axes about which the pion fields of the hedgehogs are iso-rotated, by an angle π.

3. The fcc array has $U(\vec{x}) = -1$ at the lattice points and these and the $U(\vec{x}) = 1$ points, form two intersecting fcc lattices. When taken together these form a simple cubic lattice of $U(\vec{x}) \pm 1$ and so in the condensed phase there exists a simple cubic array of half skyrmions. The additional half skyrmion symmetry at high densities can be expressed as;

$$\sigma(x, y, z) \;=\; -\sigma(x + a/2, y, z),$$

$$\vec{\pi}(x, y, z) \;=\; -\vec{\pi}(x + a/2, y, z), \qquad (3.3.3)$$

and cyclicly. This symmetry of the condensed half skyrmion array can also

93

be pictured in terms of the condensed array being composed of alternating $U(\vec{x}) = \pm 1$ half skyrmions.

In order to clarify matters we shall briefly describe the effect that increasing the density has on this fcc array. At low densities the skyrmions are localised about four of the vertices of the representative cube of the fcc array, as indicated in Figure (3.1.3c). Each skyrmion has a spherical $\sigma = 0$ surface separating its inner half skyrmion, $\sigma < 0$, from its outer half $\sigma > 0$. The $\sigma < 0$ regions fill most of space and connect neighbouring skyrmions. As the density increases, the inner half skyrmions increasingly fill more of space and in response, the field deforms such that the $\sigma = 0$ surface becomes more cubical. Beyond the phase transition in the half skyrmion condensed phase, the $\sigma = 0$ surfaces become perfect cubes, with sides $a/2$ which touch along the edges, leaving the $\sigma > 0$ regions divided up in to exactly similar cubes. This half skyrmion arrangement is depicted in Figure (3.3.1). Here we have indicated the axis of rotation about which the pion fields of the half skyrmions are rotated through an angle π. The inward pointing arrows signify that the half skyrmion has $U(\vec{x}) = +1$ at the lattice point and its pion field arrangement is obtained from a spherical half skyrmion, with its pion field pointing radially inwards by an iso-rotation of angle π, about the axis indicated. The open and solid circles indicate an unrotated half skyrmion of the $U(\vec{x}) = -1$ and $U(\vec{x}) = +1$ types respectively. The $\sigma = 0$ surfaces are the orthogonal planes, with either x, y or z equal to $a/2$
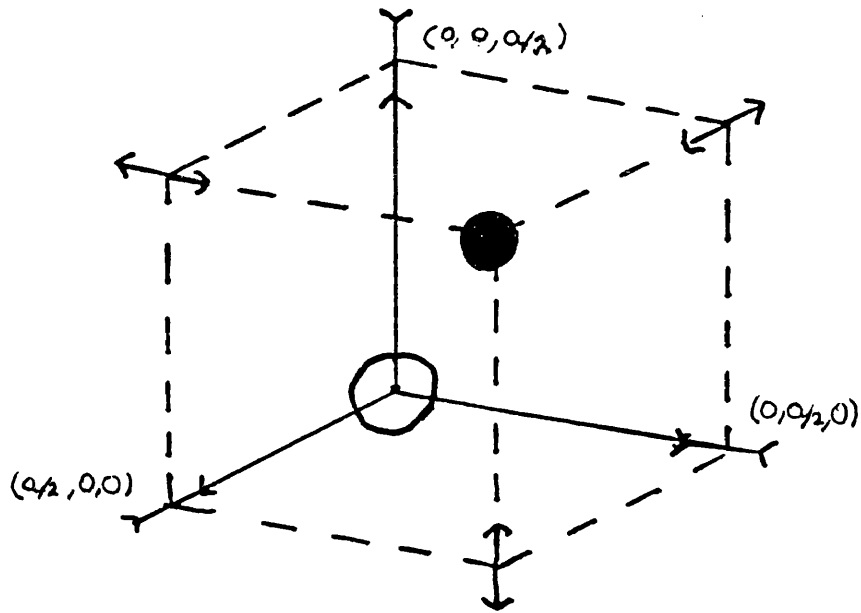
94

Figure (3.3.1): A non-frustrated arrangement of eight half skyrmions at the vertices of a representative fcc cube. The inward pointing array indicates a $U(\vec{x}) = +1$ type half skyrmion which is iso-rotated about the direction of the arrow by an angle π and the full circle denotes an unrotated $U(\vec{x}) = +1$ half skyrmion.

or $3a/4$. For this arrangement all neighbouring half skyrmions have pion fields which are relatively non-frustrated, as is indicated in Figure (3.3.2). This shows the flow of the pion field within the (x, y) plane at $z = 0$ of the fcc representative cell.

The figure clearly shows, that in the condensed phase the pion fields of either type of half skyrmion are identical and also the manner in which these fields meet smoothly on the $\sigma = 0$ surfaces. The dashed line indicates the positions of these $\sigma = 0$ surfaces within the representative cell and each square represents a cross-section at $z = 0$, through the octant of one of the cubes which contains half a skyrmion.

This symmetry also enables us to perform our numerical calculations in the condensed half skyrmion phase, within a octant of the representative cell of the fcc array, Figure (3.3.1), since the pion fields within each $\sigma < 0$ and $\sigma > 0$ cube are related by expression (3.3.3). We shall later detail the manner in which these numerical studies were performed.

Both the bcc and the interpolating lattices, which result as p varies, possess the same symmetry as fcc, with a trivial change in the lattice spacings in one direction as compared to the others. Thus, the variation of p generalises the cubic array of half skyrmions at $p = 0$, to a rectangular array of half skyrmions.
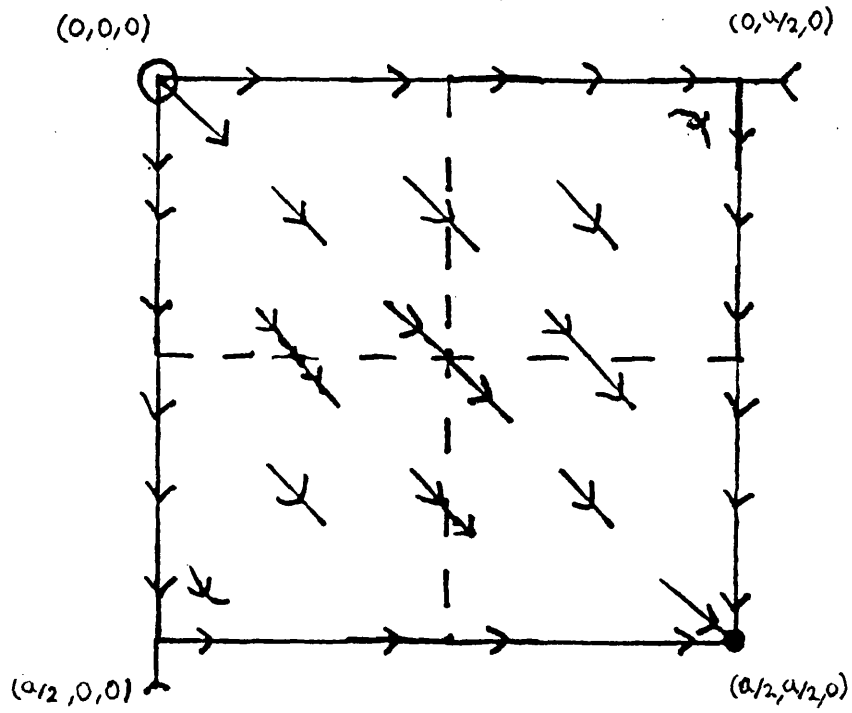
Figure (3.3.2): The iso-vector pion field arrangements in the $z = 0$ plane, within the half skyrmion cube depicted in Figure (3.3.1).

3.4 Numerical Calculations

In this section we shall outline the numerical procedure we adopted for the study

of the fcc, bcc and interpolating lattice. This procedure was the same as the one

employed by Jackson et al [9] and has the advantage over Klebanov's procedure

of increasing the rate of convergence by a factor of two.

Numerical calculations of the minimum energy of the Skyrme Lagrangian, as

a function of a, have been carried out for the fcc and bcc configurations and for

a range of crystal arrays interpolating between them with $-0.35 < p < 0.32$.

The calculation procedure employed, involved solving a discretised form of

Hamilton's Equations. Introducing the canonical momentum

$$\Pi_k = \frac{\delta L}{\delta \partial_t \phi_k}, \qquad (3.4.1)$$

where L is given by equation (2.1.17) and the field ϕ_k satisfies the constraint

$\phi^a \phi^a = f_\pi^2$, the Hamiltonian Equations read

$$\dot{\phi}_k = A_{kl}^{-1} \Pi_l,$$

$$\dot{\Pi}_k = \partial_t (B_{kl} \partial_i \phi_l) + \lambda \phi_l, \qquad (3.4.2)$$

where,

$$A_{kl} = (1/4 + \{\partial_t \phi_m\}^2) \delta_{kl} - \partial_i \phi_k \partial_i \phi_l,$$

$$B_k l = (1/4 + \{\partial_\mu \phi_m\}^2) \delta_{kl} - \partial_\mu \phi_k \partial_\mu \phi_l. \qquad (3.4.3)$$

The Roman indices run from 1 to 3 (spatial coordinates) and the Greek indices

run from 0 to 3 (space-time coordinates). The Lagrange multiplier, λ, has been

introduced to enforce the field constraint. Here we have introduced the dimensionless units via the transformation $x_\mu \mapsto x_\mu / 2ef_\pi$.

In order to obtain static, minimal energy configurations we treat the time variable as a 'pseudo time' variable and use a field relaxation technique that ensures as we advance in 'pseudo time' steps Δt, we always move down hill in energy. We perform the minimisation of the energy in a single octant of the face centered cube for the dilute phase and in an octant of the half skyrmion cube in the condensed phase. That is, an octant of the fcc representative cell depicted in Figure (3.3.1). Exactly the same procedure was used for the bcc and intermediate cases, by trivially changing the aspect ratio of the cube into a rectangular region, with lattice displacements in the x and y or z directions becoming ra or a/r^2 respectively, but otherwise keeping the same boundary conditions.

As an initial field configuration we employed hedgehog fields smoothed at the boundaries of the cell. We assume that across the plane connecting the centres of the skyrmion, the pion fields are reflection symmetric.

The mesh size was typically 18^3 mesh points to the octant of the cube in the dilute phase and the same number, or fewer points in the octant of the half skyrmion cube in the condensed phase, providing substantially greater accuracy. Convergence was assumed, when the extrapolated energy did not vary significantly over several hundred iterations, during which the baryon number was stable to 0.01%. Converged non-condensed phase solutions always had a baryon density greater than 0.96 and condensed phase solutions a baryon density greater

than 0.99.

The results so obtained for the field energies and values of $<\sigma>$ were extrapolated to an infinite number of iterations, as in [9], where this error was shown to be exponential. Then the energies were extrapolated to zero mesh size. This was easy in the condensed phase, where the energy and baryon density are spread fairly uniformly in space so that the energy varies linearly with $1/n^2$, where n^3 is the number of mesh points; but in the dilute phase the number of points covering each skyrmion reduces as the size of the cube increases and the extrapolation is less clean. The baryon density also reflects this feature, so the deviation of the numerical calculation of the baryon number B from 1, is also a measure of errors due to finite mesh size and this provided an alternative extrapolation procedure. The value of $1 - B$ is proportional to $1/n^2$ for large n in the condensed phase, but the slope varies with a. The extrapolations to zero mesh size was therefore performed by linear extrapolation of the energy with respect to $1 - B$, the slope determined by varying n for some typical cases.

This procedure is very accurate for the condensed phase, leading to errors of a fraction of an MeV, but in the dilute phase typical errors are two MeV. To ensure continuity at the second order phase transition points the energies in the dilute phase were adjusted (within their errors) to agree with the more accurate values determined with the condensed phase boundary conditions.

The rate of convergence of the energy, as in [9], was observed to be about two times as fast as that for $<\sigma>$. In order to determine the location of the

phase transition point accurately, much use was made of the value of the order parameter $< \sigma >$. By following the variation of $< \sigma >$ as the lattice spacing was reduced, we accurately determined lattice spacing at which $< \sigma >$ vanishes. However, in order to provide reliable values of $< \sigma >$, it was necessary to obtain well converged solutions in the condensed phase. Thus, within the condensed phase we devoted a considerable amount of computer time to obtaining well converged solutions. Indeed, without reliable values of $< \sigma >$, the second order nature of the phase transition would not have been established.

The numerical calculation was performed using a Cray computer and involved considerably more C.P.U. time than those which had previously been performed with cubic arrays of skyrmions. This was because a whole series of differing lattices, generated by varying the aspect ratio of the fcc cube, were considered. As a result, this involved obtaining about sixty converged solutions within each phase, about twelve times as much data as was required by Jackson et al [9] for their calculation with a rectangular skyrmionic lattice.

Moreover, unlike the previous calculations, we obtained reliable extrapolation to zero mesh size for all our data at differing values of a. This involved establishing how the energy varied as the number of lattice points was varied and also required well converged data. Jackson et al on the other hand, only performed the extrapolation for the minimum energy condensed configuration at high densities.

Finally, as we shall detail in the next section, we also investigated the effects

of including a pion mass term, (see (2.1.5)), which explicitly breaks Chiral Symmetry and for which we obtained a considerable number of fcc ($p = 0$) converged solutions.

3.5 <u>Numerical Results</u>

The solutions show some very general features which hold for all values of the aspect ratio p so far investigated. Consider first the fcc array, $p = 0$. At low density the skyrmions are well localised around their lattice positions $(0, 0, 0)$, $(0, a/2, a/2)$, $(a/2, 0, a/2)$, $(a/2, a/2, 0)$, each with a nearly spherical surface $\sigma = 0$ separating the inner half skyrmion, $\sigma < 0$, from the outer half, $\sigma > 0$. This latter region extends to neighbouring skyrmions, is connected and fills most of space. The space average $< \sigma >$ of the σ field is thus close to 1, while $< \vec{\pi} > = 0$ due to the cubic symmetry.

As the density is increased the energy per skyrmion drops smoothly, as does $< \sigma >$. The skyrmions spread out a little and the $\sigma = 0$ surfaces get more cubical. Then a second order phase transition is reached, the energy still dropping smoothly, but the $\sigma = 0$ surfaces now become perfect cubes of side $a/2$, which touch along the edges leaving the $\sigma > 0$ region divided up into exactly similar cubes. The $\sigma = 0$ surfaces are orthogonal planes with either x, y or z equal to $a/4$ or $3a/4$. The half skyrmions $\sigma < 0$ and $\sigma > 0$ now have identical $\vec{\pi}$ distributions, but there is no longer a unique way of associating any $\sigma < 0$ half skyrmion with

a corresponding $\sigma > 0$ half skyrmion. If the density were to be decreased from this symmetrical phase, the skyrmion density could either re-concentrate around the original points where $\sigma = -1$, or alternatively on the points where $\sigma = 1$.

Above the phase transition, $a = a_c$, we find $< \sigma > \sim (a - a_c)^2$, (see Figure (3.5.1)). This is the signature of such a second order phase transition and the linear plot of $< \sigma >^2$ against a, also shown in Figure (3.5.1), provides the most accurate determination of a_c .

The extra symmetry acquired at the phase transition is that given by equation (3.3.3). Exactly the same second order phase transition, with corresponding scaling of x, y and z coordinates, occurs for all values of p in the range $-0.35 < p < 0.32$, and probably for all p. The bcc array seems in no way a special case.

A similar second order phase transition was observed for the rectangular array by Jackson et al [9], who also claim that Klebanov's cubic arrangement undergoes a first order phase transition.

As the density of skyrmions is further increased beyond the phase transition density the energy continues to fall until it reaches a minimum, which for the fcc symmetry is only 3.8% above the theoretical lower bound, a figure which agrees with the result of Kugler and Shtrikman [12]. It then rises rapidly. These results are illustrated in Figure (3.5.2) where the energy is plotted against $L = \rho^{-1/3}$, where ρ is the skyrmion density, for the fcc and bcc array, and the Klebanov array for comparison. The modified cubic of Jackson and Verbaarschot [9] has not been plotted as it lies just above the bcc curve and has the same shape. The
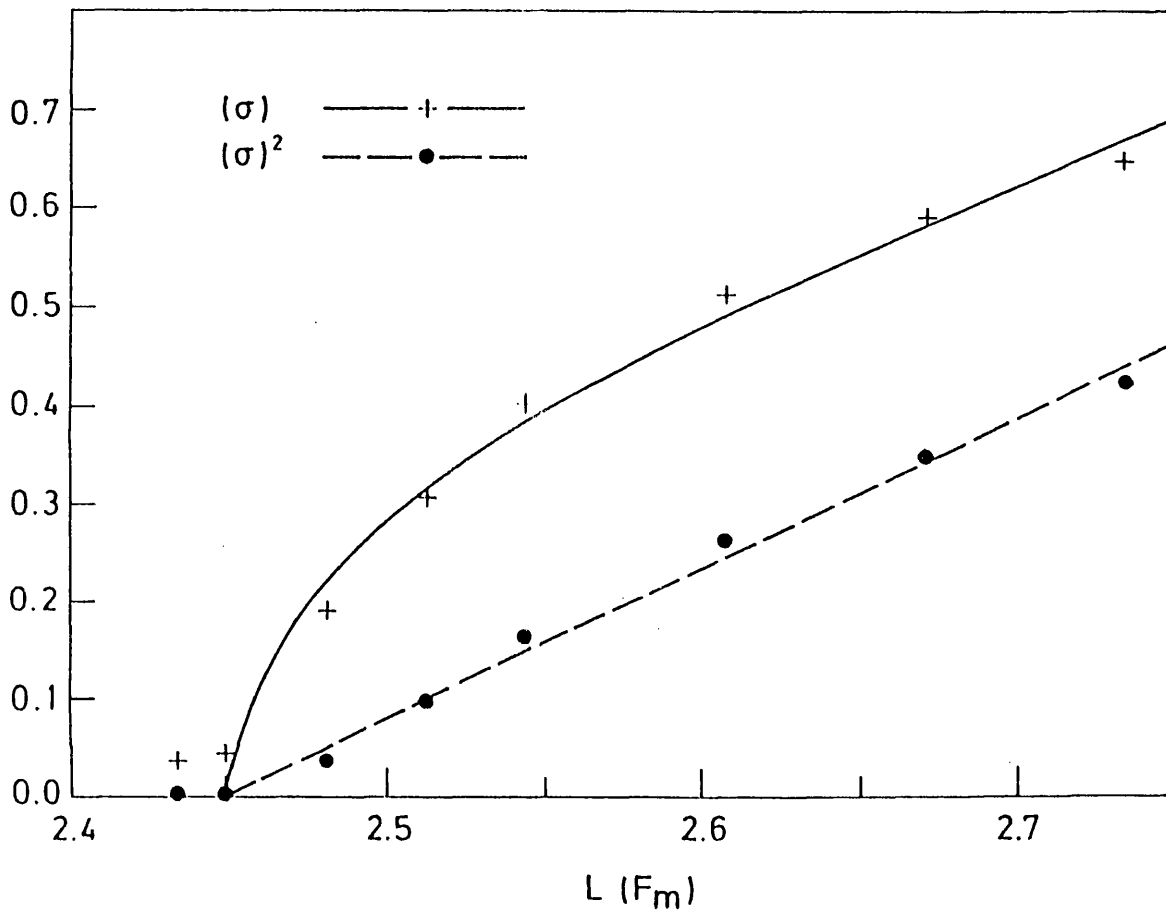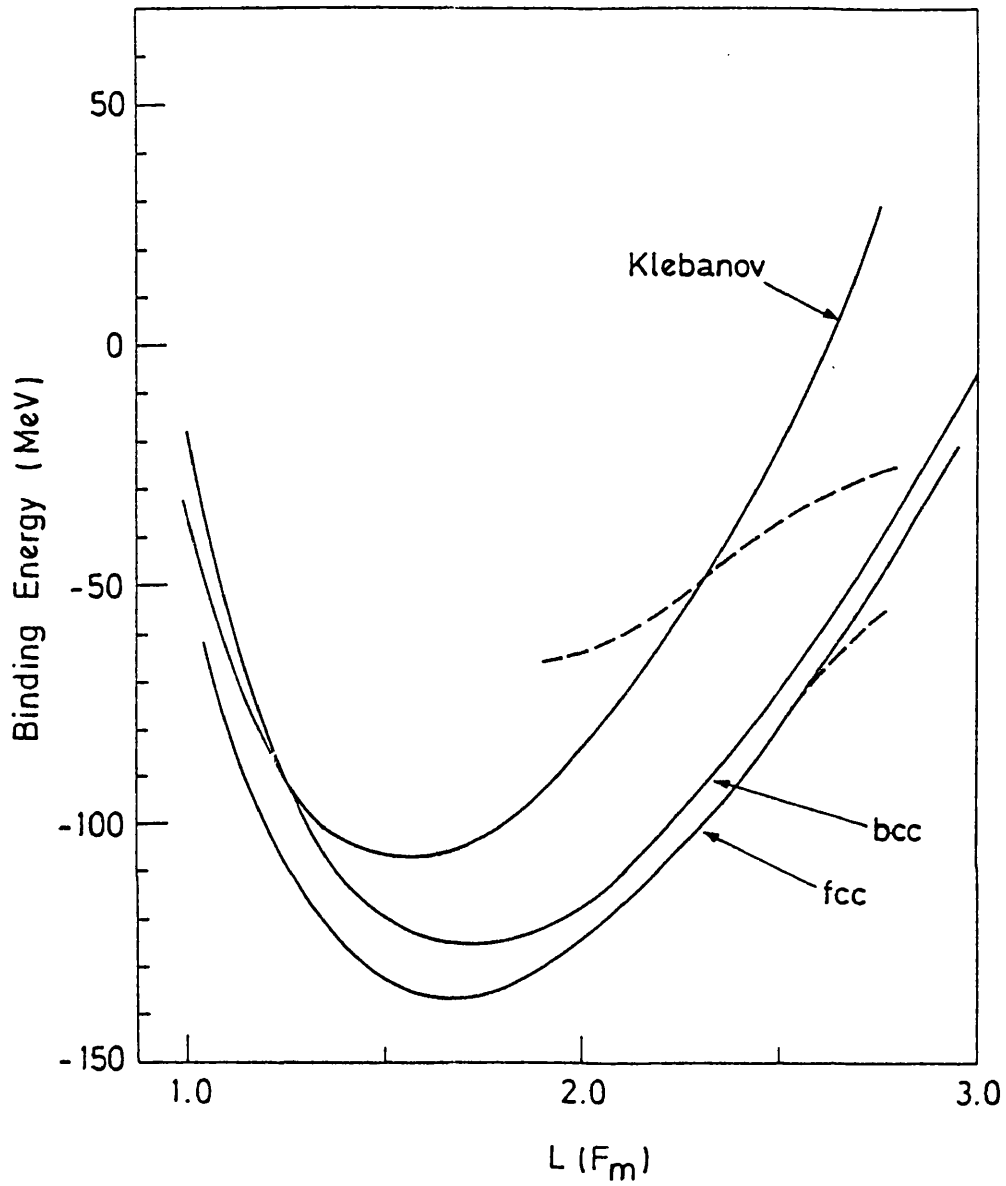
Figure (3.5.1): Plots of $< \sigma >$ and $< \sigma >^2$ versus L with $L = (density)^{-1/3}$.

Figure (3.5.2): Plots of energy versus $L = (density)^{-1/3}$; fcc array, bcc array and Klebanov's cubic array. The curve for the Jackson cubic array has not been plotted as it lies just above the bcc array. Solid lines have half skyrmion symmetry and dashed do not.

uncondensed phase is shown branching smoothly from the condensed phase, for both the fcc and bcc arrays. In terms of the parameters used by Klebanov [6], and Jackson and Verbaarschot [9] $f_\pi = 64.5\text{MeV}$ and $e = 5.45$, the minimum energy is 727.4MeV at $L = L_0 = 1.666\text{Fm}$ and the fcc phase transition occurs at 779.5MeV and $L = L_c = 2.45\text{Fm}$. The minima and also the phase transition occur at nearly the same density in the fcc, bcc and alternative cubic [9] arrays. This is clearly visible in Figure (3.5.3) where constant energy contours, (solid lines), have been plotted in the (L, p) plane. Also shown is the line of critical points, (dashed line), and the line of minima in L at constant p, (dot-dashed line). The critical points occur at an almost constant density with hardly any dependence on p. Furthermore, near the critical density, the equal energy contours are almost parallel to the p axis so that Skyrme matter is hard to decompress but very easy to deform, in fact rather like jelly. This feature persists nearly to the minimum. The circular contours in Figure (3.5.3) are deceptive, since $p = 0.23$ corresponds to a factor 1.4 in aspect ratio, while the same contour can be reached by increasing L by 18%.

Near the minimum we might expect that small changes in L and p would produce predominantly, a stretching of the fields in the appropriate directions without essentially changing their shape. The two components of energy e_2 and e_4 quadratic and quartic in derivatives, would then scale as:

$$e_2 = \frac{E_0}{6}\left(\frac{2}{r^2} + r^4\right)\frac{L}{L_0} = \frac{E_0}{2}\left((1 + p^2) + \frac{p^3}{3} + \cdots\right)\frac{L}{L_0} \qquad (3.5.1)$$
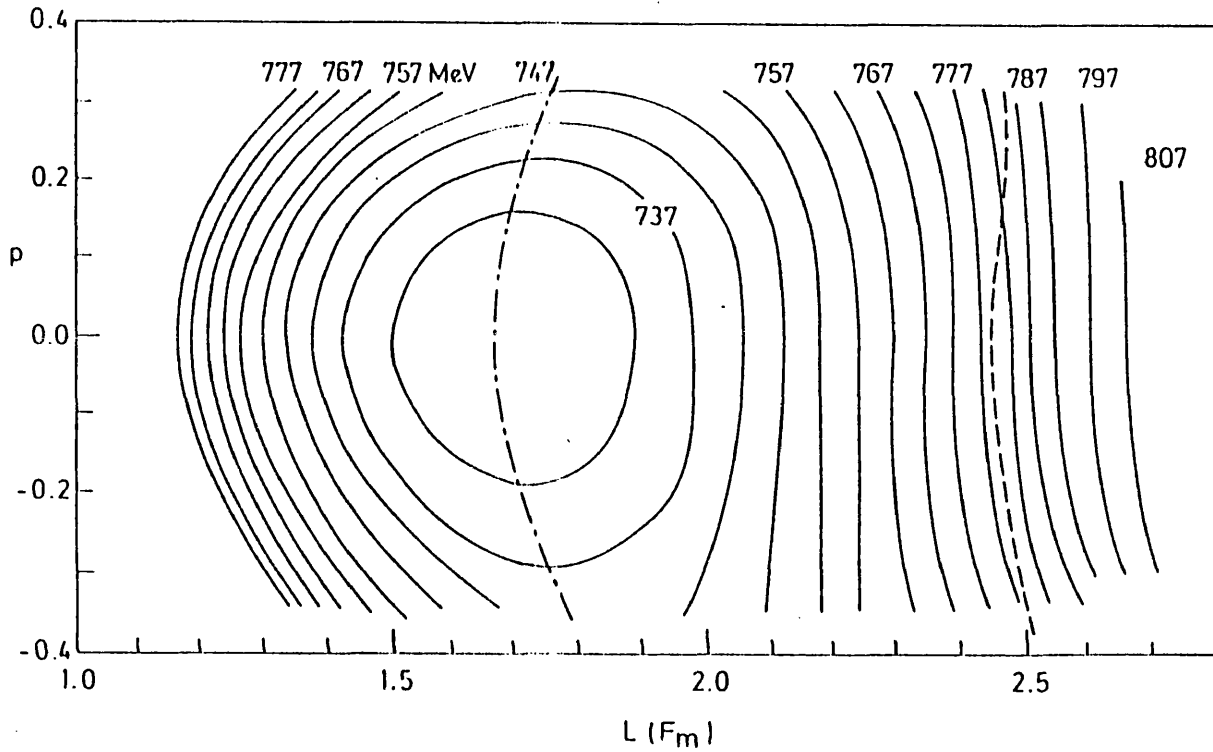
Figure (3.5.3): Contour plots of equal energy in the (L, p) plane where $L = (density)^{-1/3}$ and p measures the deviation from fcc symmetry (see text). Also shown are the curves for minimum energy with respect to L at fixed p and of the phase transition points separating the condensed half skyrmion phase from the dilute phase.

$$e_4 = \frac{E_0}{6}(\frac{1}{r^4} + 2r^2)\frac{L_0}{L} = \frac{E_0}{2}((1 + p^2) - \frac{p^3}{3} + \cdots)\frac{L_0}{L}. \qquad (3.5.2)$$

From fcc symmetry, both e_2 and e_4 are separately stationary with respect to p at $p = 0$. The total energy E is a minimum E_0 when $L = L_0$ and $e_2 = e_4 = E_0/2$. But the numerical solutions do not support such a simple scaling. For $p = 0$ there is only a small correction, a better approximation being

$$E_{p=0}(L) = \frac{E_0}{2}((\frac{L}{L_0} + \frac{L_0}{L})(1 - \epsilon) + 2\epsilon) \qquad (3.5.3)$$

with $\epsilon = 0.0515$. However, the dependence on p is more interesting. e_4 does indeed have a minimum at $p = 0$, with roughly the expected coefficient for p^2, though it falls more slowly with L, but e_2 has a maximum rather than a minimum, with a negative coefficient for p^2 which increases linearly with L. At L_0 the p^2 contribution of e_2 to E is negative and smaller than the positive e_4 contribution, but it increases with L until it gets larger, so that the curvature of E in p varies smoothly from a positive value at L_0 through zero at a critical density corresponding to $L = L_d = 2.43\mathrm{Fm}$, to negative curvature above this second critical point.

There are therefore at least two independent soft modes which go negative at L_c and L_d, the mode which breaks the half skyrmion symmetry but keeps fcc symmetry and the mode which breaks fcc symmetry but maintains the half skyrmion symmetry. Though L_c and L_d are very close, they appear not to be equal, but the two phase transitions may none the less be related and since the second is triply degenerate, there may be a whole class of modes which go

negative at this critical density, signalling perhaps a solid-liquid phase transition.

The above picture explains the salient features of Figure (3.5.3), the near independence of both the critical point L_c and the energy on p near the critical density. It enables us to express the energy as a smooth function of L, p and $<\sigma>$ such that for each L and p, minimising with respect to $<\sigma>$ gives the calculated energies and values of $<\sigma>$. The phase transition which breaks the half skyrmion symmetry then arises from $E(L, p, <\sigma> = 0)$, changing from minimum to maximum in $<\sigma>$ as L increases through L_c, and similarly fcc symmetry is broken at L_d as $E(L, p = 0, <\sigma>)$ changes from a minimum to a maximum in p. From symmetry, the energy must be an even function of $<\sigma>$ and for small $<\sigma>$ it may be parameterised in terms of $<\sigma>^2$ and $<\sigma>^4$ as:

$$E(L, p, <\sigma>) = E_{p=0}(L) \quad + \quad E_0[\alpha(L)p^2 + \beta(L)p^3 + \gamma(L)p^4 + \delta(L)p^5 + \cdots]$$

$$+ \quad E_0[q(L) <\sigma>^2 + v(L) <\sigma>^4] \qquad (3.5.4)$$

where the coefficients are given by

$$\alpha(L) = 0.649 - 0.487\frac{L}{L_0} + 0.089\frac{L_0}{L}$$

$$\beta(L) = 0.300 + 0.006\frac{L}{L_0} - 0.119\frac{L_0}{L}$$

$$\gamma(L) = -1.64 + 0.78\frac{L}{L_0} + 0.71\frac{L_0}{L}$$

$$\delta(L) = 0.53 - 0.55\frac{L}{L_0}$$

$$q(L) = (1 - \frac{L}{L_c})(0.430 + 0.243\frac{L_c}{L})$$

$$v = 0.0218(\frac{L}{L_c} + 3.00\frac{L_c}{L}). \qquad (3.5.5)$$

The first four coefficients are known rather accurately, since they can be calculated from solutions for the condensed half skyrmion phase and are chosen to fit the p dependence of the energy right through the region $L_0 < L < 2.8$ for $-0.35 < p < 0.35$, but the last two coefficients describe the start of the dilute phase and would be less accurately determined from solutions in the dilute phase. But here also one can use the solutions in the condensed phase to determine $q(L)$ and $v(L)$ below L_c, by including a pion mass term

$$E_m = (m_\pi f_\pi)^2 (1 - < \sigma >) L^3 \qquad (3.5.6)$$

for each skyrmion, to drive the solutions away from $< \sigma >= 0$ and half skyrmion symmetry, the pion mass acting like a chemical potential for $< \sigma >$. This enables us to determine the coefficients in (3.3.5) much more accurately.

The first factor in $q(L)$ was chosen to change sign at the critical length $L = L_c = 2.45$, a point which is best determined from the extrapolation of $< \sigma >^2$ in Figure (3.5.1), and the magnitudes and forms of $q(L)$ and $v(L)$ are then adjusted to fit the values of $< \sigma >$ as a function of L, which arise from including the pion term above, for various values of m_π. These predict results consistent with the values of $< \sigma >$ in Figure (3.5.1) and the difference in energy between the condensed and dilute phases above L_c from Figure (3.5.2). We have not included $p^2 < \sigma >^2$ terms in E, though there is a small effect, nor have we included the slight p dependence of L_c in the parameterisation. The coefficient $\alpha(L)$ changes sign at $L = L_d = 2.43$ and the coefficient $\gamma(L)$ also changes sign at nearly the

same L. Thus, for fixed L, $L < L_d$ and small $|p|$, the energy has a minimum at $p = 0$ and a maximum for $p < 0$ which merge at $L = L_d$, the maximum is at $p = -0.175$ for $L = 2.25$ and at $p = -0.46$ for $L = 2.0$. For L just above L_d there is a maximum at $p = 0$ and a minimum at positive p, at a distance from $p = 0$ which depends mostly on the p^3 coefficient $\beta(L)$ and which merges with the maximum at L_d. There is presumably another minimum at larger negative p for $L > 2$, which is outside the range of the present calculation and does not show up in Figure (3.5.3).

It is hard to calculate the field distributions for densities lower than those shown in Figures (3.5.2) and (3.5.3), or for large $|p|$, but the asymptotic form of the energy arising from equation (2.2.4) (see Table 3.2.2) predicts a maximum for fcc symmetry, $p = 0$, with energy falling continuously for negative p. Due to short range repulsion one would expect that there would be a minimum for fixed density at some negative p, but, as shown above, this is beyond the range of our calculations. For positive p, the minimum which appears in the asymptotic formula starts at the phase transition L_d at $p = 0$, and moves to larger p as L increases. But there is really no good reason to believe that at low densities the cubic or rectangular structures studied so far should be minima. It is worth noting that the ratios $L_c/L_0 = 1.47$ and $L_d/L_0 = 1.46$ are only 4% and 3% above the critical ratio of $\sqrt{2}$ which Manton [5] derived for skyrmions on S_3 where the lower bound can be achieved exactly. Since the energy for the fcc in R_3 is only 3.8% above the lower bound, Manton's argument can be modified in an

approximate way to explain why L_c differs by only a few percent from $\sqrt{2}L_0$, but the argument for L_d lying so close is less clear. We shall present arguments in the next chapter which explain the closeness of L_d and L_c, by considering deformations in the shape of $S^3_{phy}(L)$.

Finally, as we have already indicated, we expect the energy of the half skyrmion to be 'bounded' from below by the energy per unit baryon number of a hedgehog-like half skyrmion. Such a half skyrmion is contained within a sphere of radius r_0. Manton and Goldhaber [14] determined the optimal value of r_0 to be $0.77Fm$ and this corresponds to the value of $L_0 = 1.571$ in our crystalline variables. The energy of this half skyrmion per unit baryon number is just 1.015% above the lower bound.

Figure (3.5.2), indicates that this value of L_0, for a half skyrmion, is close to those values of L_0 at which the minimum of the energy is attained for all the condensed skyrmion arrays so far considered. Indeed, the values of L_0 for the Klebanov array of $1.548Fm$ and for the fcc array of $1.666Fm$, are within a few percent of this value.

Manton and Goldhaber observed that it is plausible that the distortions of a spherical half skyrmion, required for it to fit in to a Wigner-Seitz cell of a half skyrmion lattice, will raise the energy least if the volumes of the Wigner-Seitz cell and of the spherical half skyrmion are the same. In this case , this will minimise the distortions which are necessary for a spherical half skyrmion to fill the Wigner-Seitz cell. Thus, the close proximity of these values seems

to justify this idea. We note finally, that the minimum energy of all the lattice arrangements is indeed bounded by the 'half skyrmion lower bound', with the fcc array just 1.023% above this bound. Thus, presumably the distortions involved in the spherical half skyrmion filling the Wigner-Seitz cubic cell of the fcc lattice are small.

3.6. Approximate Parameterised Variational Forms

The distribution of the σ and $\vec{\pi}$ fields at the minimum are extremely well approximated by the formulae

$$\sigma = \cos(\xi)\cos(\eta)\cos(\varsigma)$$

$$\pi_x = \sin(\xi)\sqrt{1 - \frac{1}{2}\sin^2(\eta) - \frac{1}{2}\sin^2(\varsigma) + \frac{1}{3}\sin^2(\eta)\sin^2(\varsigma)} \qquad (3.6.1)$$

and cyclicly for π_y and π_z, where $\xi = 2\pi x/a$, $\eta = 2\pi y/a$ and $\varsigma = 2\pi z/a$. This formula is a three dimensional analogue of the exact two dimensional solution for the Non-Linear Sigma Model, described in [19] in terms of the Jacobi elliptic functions sn and cn which replace sines and cosines.

This formula for the σ field clearly indicates, through its functional separability of the x, y, z dependencies, that there are $\sigma = 0$ cubic surfaces within this condensed half skyrmion field configuration. Moreover, this form has proved useful in picturing the symmetries possessed by the pion fields which we discussed in Section 3.3.

113

An extension of formula (3.6.2), including variational parameters which modify the arguments ξ, η, ς by

$$\xi \;\mapsto\; \xi + \bar{\alpha} \sin \frac{2\pi x}{a_x},$$

$$\eta \;\mapsto\; \eta + \bar{\alpha} \sin \frac{2\pi y}{a_y},$$

$$\varsigma \;\mapsto\; \varsigma + \bar{\beta} \sin \frac{2\pi z}{a_z}, \qquad\qquad (3.6.2)$$

and similarly the factors $\frac{1}{2}$ and $\frac{1}{3}$ can be found to fit the whole range of densities and deformations considered here for the half-skyrmion condensed phase [20].

On $S^3_{phy}(L)$, we noted in Chapter 2, that in the uncondensed phase, a finite conformal transformations of the trivial map gives the correct bifurcation point and has a finite energy in the flat space limit, as L tends to infinity. However, in this limit the energy of the finite conformal map differs from that of the true flat space skyrmion by a small but significant amount. In the next chapter we construct this map explicitly. Weiss et al [21] considered a simple one parameter generalisation of the finite conformal map and were able to accurately reproduce the energy of the skyrmion on $S^3_{phy}(L)$ for all values of L.

It was thus suggested [21] that a finite conformal mapping of the half skyrmion fields in the condensed phase, might provide a reasonable description of the uncondensed phase solutions and the bifurcation point. A finite conformal mapping of the σ and $\vec{\pi}$ fields is given by,

$$\tilde{\sigma} \;=\; \frac{(\lambda^2 - 1) + (\lambda^2 + 1)\sigma}{(\lambda^2 + 1) + (\lambda^2 - 1)\sigma},$$

$$\tilde{\pi}_i \;=\; \frac{2\lambda \pi_i}{(\lambda^2 + 1) + (\lambda^2 - 1)\sigma}. \qquad\qquad (3.6.3)$$

For this transformation, the matrix K_{ij} (see equation (2.3.2)) becomes,

$$\tilde{K}_{ij} = \frac{\tilde{\pi}'^2}{\tilde{\pi}'^2} K_{ij}. \qquad (3.6.4)$$

For values of λ greater than 1 and with the σ and $\vec{\pi}$ fields give by equations (3.6.3) and (3.6.4), the skyrmions localises about the $\sigma = 1$ points . For values of λ in the range $0 \leq \lambda \leq 1$ the skyrmions tend to localise about the $\sigma = -1$ points, corresponding to the lattice sites of the fcc crystal. The energies of configurations with λ greater than one are related to those with $1 > \lambda > 0$ by the transformation $\lambda \mapsto 1/\lambda$.

The value $\lambda = 1$ is an extremum of the energy and corresponds to the fields having the half skyrmion symmetry of equation (3.3.3). The energy of this variational form was found numerically to be a minimum for $\lambda = 1$ up to a value of $L_c = 2.58 Fm$ and beyond this a bifurcation in the energy occurs, with the $\lambda = 1$ form becoming a maximum of energy. These results are in reasonable agreement with the exact numerical results we have presented.

This demonstrates that the modes of instability which result in the delocalising phase transition for the fcc array are predominantly the infinitesimal conformal modes which transform the field variables. A full variational calculation with the parametric forms (3.6.2) and the generalisation including the variation parameter λ for the uncondensed phase however, still fails to accurately reproduce the exact results. The major discrepancy once more occurs in the asymptotic limit. By analogy with their $S^3_{phy}(L)$ generalisation of the finite

conformal map, they extended their variational form such that λ became a two parameter function of position. This modified variation form, with the correct asymptotic inverse cubed dependance of the energy on the separation distance, they claimed to be completely consistent with our numerical results [21].

3.7 <u>Conclusion</u>

There are several rather general conclusions to be drawn from all these detailed calculations. The salient feature is that there is a robust phase transition as the density is increased from a system of isolated skyrmions with no strongly preferred symmetry, to a regular lattice of half skyrmions. The transition is in general second order and the condensed system has lowest energy with fcc symmetry. The phase transition and condensed phase look remarkably similar to Manton's solution [5] on a 3-sphere. The energy minimum occurs at a density of $0.217Fm^{-3}$ and the phase transition at $0.068Fm^{-3}$. These should not be compared directly to nuclear matter density $0.17Fm^{-3}$. The Klebanov[6] choice of parameters sets energy and length scales determined by f_π, which is set at the unrealistic value of 64.5Mev. Also skyrmionic matter contains both nucleons and Δ and the latter have not been projected out. At high density this may be a reasonable approximation, but not at low densities. Furthermore, the present calculations contain only potential terms and no kinetic energy contributions. The effects of including these to one loop order can be crudely estimated from

the work of Zahed et al. [22] for a single skyrmion on R_3 and Generalis and Williams [23] for S_3. One loop contributions appear to lower the skyrmion mass by about 20% in the dilute phase or near the phase transition, with most of the contribution occurring effectively in the e_4 term rather than in e_2. Even larger corrections may occur near the minimum energy of the condensed phase. Such changes in the relative strength of e_4 and e_2 would increase the above densities by a significant factor, to bring them more in line with predictions for nuclear matter.

In most of the above calculations we have concentrated on the zero pion mass case, using a finite pion mass only to explore the energy surface as a function of $< \sigma >$. This seems a good procedure for several reasons. Our main interest is to explore the effects of the transition to half skyrmion symmetry and the pion term destroys this symmetry explicitly. The pion mass is important for well separated skyrmions, because over large regions of space (far from the center of the skyrmions), it is the dominant term in the action. But in our dense system this occurs nowhere and so the pion and σ distributions will not be altered by much. There is also the question of whether it is correct to use the free field values of the pion mass and f_π in such dense systems. According to Forkel et al.[24], the half-skyrmion transition corresponds to chiral symmetry restoration and they argue one should consider that the f_π in equation (3.5.6) really corresponds to $< \sigma >$ and would thus give no contribution in the condensed phase. The mass term in (3.5.6) ensures that skyrmions will prefer to concentrate around points

with $\sigma = -1$ rather than $\sigma = +1$. The dominant effect of the pion mass on the energy is to introduce a term proportional to the volume occupied by the the skyrmion; this shifts the minimum, decreasing L_0 by 2.2% and increasing its energy by 42MeV; it also slightly increases the energy difference between the bcc and fcc minima. The pion mass term always leads to a non-zero $< \sigma >$. For $L < L_c$, $< \sigma >$ is small and dominated by the balance between the $< \sigma >$ term in E_m and the $< \sigma >^2$ term in (3.5.4), it is proportional to $m_\pi^2/q(L)$ and so gets larger as L approaches L_c. At the minimum $< \sigma > = 0.12$. Near L_c the quartic term in $< \sigma >$ in (3.5.4) becomes important and this has the effect of smoothing the abrupt increase of $< \sigma >$, which occurs at the phase transition as seen in (3.5.1). Above L_c, again the shift in $< \sigma >$ is dominantly proportional to m_π^2, but involves both $q(L)$ and $v(L)$. Essentially, in view of the smallness of the pion mass, it merely leads to a smooth transition from the low to the high density phase. Of course, $< \sigma >$ will never be rigorously equal to zero and in a strict sense there will be no phase transition for non-zero pion mass. Similar conclusions hold on S_3[25].

Finally, we note that Kugler et al [12] proposed that for values of $L > L_0$, crystalline skyrmionic matter undergoes a phase separation rather than expanding to fill the increased size of the lattice. Thus, for $L > L_0$, skyrmionic matter would be composed of a region in which the baryon density was that of the lattice at $L = L_0$ and a region of trivial vacuum with zero baryon density and zero energy density. Thus, beyond L_0 the energy of skyrmionic matter would be

118

constant and equal to the minimum value.

However, since no kinetic effects have so far been considered, it seems unreasonable at this stage to ignore the branch of the curve, which at low baryon densities will correspond to a well separated array of $B = 1$ hedgehogs. It would seem reasonable that this branch of the curve may represent some transient form of skyrmionic matter.

References

[1] A.D.Jackson and M.Rho, Phys. Rev. Lett. 51 (1983) 751

[2] A.Jackson and A.D.Jackson, Nucl. Phys. A457 (1986) 687

[3] E.Braaten and L.Carson, Phys. Rev. D56 (1986) 1897

[4] E.Braaten, S.Townsend and L.Carson, 'Novel Structures of Static
Multisoliton Solutions in the Skyrme Model'
Uni. of Minnesota preprint (1984)

[5] N.S.Manton, Commun. Math. Phys. 111 (1987) 469

[6] I.Klebanov, Nucl. Phys. B262 (1985) 133

[7] R.A.Smith and V.J.Pandharipande, Nucl. Phys. A237 (1975) 407

[8] T.H.R.Skyrme, Nucl. Phys 31 (1962) 556

[9] A.D.Jackson and J.J.M.Verbaarschot, Nucl. Phys. A484 (1988) 419

[10] L.Castillejo, P.S.J.Jones, A.D.Jackson, J.J.Verbaarschot and A.Jackson,
Nucl.Phys. A501 (1989) 801

[11] D.I.Dyakonov and A.D.Mirlin, preprint 1327,
Leningrad Nuclear Physics Institute (1987)

[12] M.Kugler and S.Shtrikman, Phys. Lett. B208 (1988) 491

[13] G.E.Brown, A.D.Jackson and E.Wurst, Nucl. Phys. A468 (1985) 450

[14] A.S.Goldhaber and N.S.Manton, Phys. Lett. B198 (1987) 231

[15] N.D.Cook and V.Dallacasa, Phys. Rev. C35 (1987) 1883

[16] T.S.Walhout, Nucl. Phys. A484 (1988) 397

[17] J.J.Verbaarschot, T.S.Walhout, J.Wambach and H.W.Wyld
Nucl. Phys. A468 (1987) 520

[18] V.B.Kopeliovich and B.E.Stern, J.E.T.P. Lett. 45 (1987) 203
N.S.Manton, Phys. Lett. B192 (1987) 177
J.J.Verbaarschot, Phys. Lett. B195 (1987) 235

[19] A.D.Jackson, J.J.M.Verbaarschot, I.Zahed and L.Castillejo,
Stony Brook preprint.

[20] A.D.Jackson and C.Weiss, private communication.

[21] A.D.Jackson, C.Weiss, A.Wirzba and A.Lande, "Accurate Variational
Forms for Multi-Skyrmion Configurations" Stony Brook preprint (1988)

[22] I.Zahed, A.Wirzba and U.-G.Meissner, Phys. Rev. D33 (1986) 830

[23] S.Generalis and G.Williams, Nucl. Phys. A484 (1988) 620,

[24] H.Forkel, A.D.Jackson, M.Rho, C.Weiss and A.Wirzba,
"Chiral Symmetry Restoration and the Skyrme Model"
Stony Brook preprint (1989)

[25] A.Wirzba, private communication and Skyrmion Workshop, Nordita, (1988)

CHAPTER 4

SKYRMIONIC MATTER ON A CLOSED SURFACE
OF VARYING CURVATURE

4.1 A Geometrical Picture Of Skyrmions

We have seen that the properties of flat space arrays of skyrmions bear a striking similarity to those of a single skyrmion on a $S^3_{phy}(L)$. In particular, we have noted that both systems undergo a phase transition as the density of skyrmionic matter is increased from a localised phase, in which $< \sigma >$ is close to one, to a delocalised phase, where $< \sigma >$ is rigorously zero. The vanishing of $< \sigma >$ follows trivially on $S^3_{phy}(L)$ from the full $O(4)$ symmetry of the trivial map and for flat space arrays is a consequence of the additional half skyrmion symmetry at high densities. Moreover, it has been shown that on $S^3_{phy}(L)$ this phase transition is of second order and associated with the disappearance of zero modes at high densities. The disappearance of these three Goldstone modes and the vanishing of $< \sigma >^2 + < \pi >^2$ at high densities, has led to the interpretation of this phase transition as representing the restoration of chiral symmetry at high densities [1]. However, in flat space this interpretation is less clear, as the additional, discrete half skyrmion symmetries are not associated with the disappearance of

the Goldstone modes.

Thus, there is a somewhat non-trivial relation between these two dense skyrmionic systems, yet the gross features of both are very similar. This has been interpreted as the curvature of $S^3_{phy}(L)$ simulating the interaction of the skyrmions in the dense crystalline environment.

Hence, we are led to investigate further the role of curvature on $S^3_{phy}(L)$, by considering different shapes of physical space which have a locally varying curvature. Moreover, if we restrict ourselves to closed surfaces which are continuously deformable into $S^3_{phy}(L)$, we can investigate the role of deformation in the shape of this sphere. It is to be expected that this will be related to the bulk deformation of crystalline arrays, numerically studied for fcc crystalline matter [2] and that it will also have an analogous density L_d, beyond which the trivial skyrmion on $S^3_{phy}(L)$ is unstable with respect to shape deformation and that this density will be in close proximity to that of L_c.

In order to develop such a generalised shape analysis, it is instructive to understand the geometric nature of the Skyrme Model. Such a geometrical picture is to be expected, since the skyrmions stability is topological. Manton [3] has shown that such a geometric picture does indeed exist, which we shall review briefly.

The existence of such a picture might be expected from the outset, since the stationary solutions of the Non-Linear Sigma Model's energy functional defines harmonic maps and these have a definite differential geometric interpretation.

The Skyrme Model's energy functional can thus be interpreted as a natural extension of the functional generating harmonic maps and this extension has been shown to have a firm differential geometric interpretation, as demonstrated by Loss [4]. Also the Skyrme energy functional, as pointed out by Manton [3], is very similar to the models used in certain non-linear elasticity theories [5].

A skyrmion on a generalised three dimensional physical space, M^3_{phy}, is a non-trivial mapping of M^3_{phy} onto S^3_{iso}. From the outset we take physical space to be Riemanian, orientatable and connected. Thus, a skyrmion is a mapping ϕ, such that

$$\phi : (M^3_{phy}, g) \mapsto (S^3_I, \tau), \qquad (4.1.1)$$

where g and τ are the metrics on M^3_{phy} and S^3_{iso} respectively.

These two metrics express the local geometric lengths of both spaces. The mapping ϕ, deforms M^3_{phy} in to S^3_{iso} and thus changes these lengths. Hence, the natural geometric quantity measuring the extent of this deformation is constructed from the metrics in expression (4.1.1).

The mapping induces a new metric on M^3_{phy}, which is the pull back of the metric τ, written as

$$K = \phi^* \tau, \qquad (4.1.2)$$

which is globally defined on M^3_{phy} as a consequence of the mappings non-triviality. This symmetric pull back metric, in a natural, local coordinate system, (x^i), on

M^3_{phy} is given by

$$K_{ij} = \partial_i \phi^a \partial_i \phi^b \tau_{ab}, \qquad i = 1, 2, 3 \qquad (4.1.3)$$

where $\phi^a (a = 1$ to 3) are the three local coordinate representatives of the mapping ϕ.

A measure of the extent of the deformation induced by the mapping, is given by comparing the pull back metric with the metric of physical space. Thus, we define the deformation matrix as

$$D = g^{-1} K. \qquad (4.1.4)$$

This is a three by three matrix, formed by multiplying the inverse metric with the pull back metric in some local coordinate system on M^3_{phy}. However, this deformation matrix is not a coordinate independent quantity. Since we are interested in invariants which express the geometric deformation induced by the skyrmions, we consider the invariants of D, which can be constructed from its three eigenvalues which we shall write as λ_1^2, λ_2^2, λ_3^2.

We note that if these all have a unit value, then the mapping ϕ is an isometry of M^3_{phy} onto S^3_{iso}. In this case the mapping produces no deformation. Also, the deviations of these eigenvalues from unity, measure the extent of the deformation.

The invariants of D, (4.1.4), are the permutation symmetric functions of its three eigenvalues and the three characteristic invariants are

$$TrD = \lambda_1^2 + \lambda_2^2 + \lambda_3^2,$$

126

$$1/2\{TrD^2 - (TrD)^2\} \quad = \quad \lambda_1^2\lambda_2^2 + \lambda_1^2\lambda_3^2 + \lambda_2^2\lambda_3^2, \qquad (4.1.5)$$

$$\det D \quad = \quad \lambda_1^2\lambda_2^2\lambda_3^2,$$

where we have taken local coordinate systems on M_{phy}^3 and S_{iso}^3, in which D is diagonal, that is, normal coordinate systems on both spaces.

The Skyrme energy functional is constructed from the first two of these invariants. The first invariant term gives

$$e_2 = \int_{M_{phy}^3} \sqrt{g}(\lambda_1^2 + \lambda_2^2 + \lambda_3^2) \qquad (4.1.6)$$

and is simply the Non-Linear σ-Model energy functional. Similarly, the second invariant gives the Skyrme energy functional;

$$e_4 = \int_{M_{phy}^3} \sqrt{g}(\lambda_1^2\lambda_2^2 + \lambda_1^2\lambda_3^2 + \lambda_2^2\lambda_3^2). \qquad (4.1.7)$$

In this chapter we shall always use Manton's dimensionless unit [3], defined in Chapter 2.

We can give a geometrical interpretation of these two expressions in terms of the effect ϕ has on a set of orthonormal frame vectors over M_{phy}^3. The first invariant measures how the sum of the squared lengths of the orthonormal frame vector on physical space, changes under the map ϕ.

The second invariant measures how the sums of the squared lengths of the three cyclicly permutated cross-products of pairs of these orthonormal frame vectors on physical space, change under the mapping. Thus, it measures the changes of local areas produced by the mapping.

The third invariant is not considered here. However, it has been used as an alternative to the Skyrme Term for stabilising solitonic configurations [6]. Since this term scales like inverse length cubed, it will prevent the collapse of finite energy solutions. The invariant measures how the squared length of the cross-product of the orthonormal set of frame vectors changes under the mapping ϕ. It thus measures how the mapping changes the local volumes.

Hence, the Skyrme energy functional has a natural geometric interpretation. Moreover, deviations of the energy from the topological bound measure the deviation of the deformation matrix from unity. This is revealed by re-expressing the energy functional as

$$E = e_2 + e_4$$

$$= \int_{M^3_{phy}} \sqrt{g}\{(\lambda_1 - \lambda_2\lambda_3)^2 + (\lambda_2 - \lambda_1\lambda_3)^2 + (\lambda_3 - \lambda_1\lambda_2)^2\}$$
$$+ 6\int_{M^3_{phy}} \sqrt{g}\lambda_1\lambda_2\lambda_3. \qquad (4.1.8)$$

The last term has a topological interpretation. It is simply the integral of $\sqrt{D}$, which is the Jacobian factor of mapping ϕ and transforms the measure on M^3_{phy} to that on S^3_{iso}. Since both spaces are orientatable, the square roots of D and of the Jacobian factor can be defined consistently. The value of the integral will simply be equal to the volume of S^3_{iso}, which is $2\pi^2$ multiplied by the mapping's winding number B. The other terms are manifestly positive and hence we can

128

see the energy is indeed bounded from below by

$$E \geq 12\pi^2 \mid B \mid .\qquad(4.1.9)$$

Moreover, this bound will only be saturated if $\lambda_1 = \lambda_2 = \lambda_3 = 1$. That is, when ϕ is an isometry of M_{phy}^3 to S_{iso}^3. Thus, it can be seen that the energy function measures the deviation of the eigenvalues of D from unity. Clearly the identity map for S_{phy}^3 is an isometry and hence it saturates the bound.

When M_{phy}^3 is flat physical space, R^3, Manton et al [7] showed that the bound cannot be saturated since no isometry exists. The usual $B = 1$ hedgehog on compactified R^3, which is a minimiser of the energy functional, has an energy $1.23 \times 12\pi^2$. The deviation of its energy from the bound is a reflection of the differing curvature of R^3 and S_{iso}^3.

Manton, using this eigenvalue formulation, further showed that the stability properties of the trivial map on $S_{phy}^3(L)$ can be deduced by considering the effect of varying the map. Since we shall generalise this technique to incorporate shape deformation, we shall only briefly review his techniques and his conclusions here.

For the trivial map of $S_{phy}^3(L)$ onto $S_{iso}^3(1)$ the eigenvalues of the deformation matrix are given by:

$$\lambda_1^2 = \lambda_2^2 = \lambda_3^2 = \frac{1}{L^2},\qquad(4.1.10)$$

taking the metric's components g_{ij} to be dimensionful. Under a small change of the map these eigenvalues change and we express the new eigenvalues as

$$\lambda_i = \frac{1}{L}(1 + \delta_i), \qquad i = 1, 2, 3 \qquad(4.1.11)$$

129

where δ_i are small dimensionless quantities varying over M_{phy}^3. The resulting energy can be expressed to second order as:

$$E^{(2)} = 12\pi^2(L + \frac{1}{L}) + \frac{2}{L^2}\int \sqrt{g}(1 + \frac{2}{L^2})I_1 + \frac{1}{L^2}\int \sqrt{g}(1 + \frac{2}{L^2})I_2$$
$$+ \frac{4}{L^2}\int \sqrt{g}I_3. \qquad (4.1.12)$$

Here, we have for convenience, introduced the infinitesimal functions;

$$I_1 = \delta_1 + \delta_2 + \delta_3, \qquad (4.1.13)$$

which is a first order quantity and

$$I_2 = \delta_1^2 + \delta_2^2 + \delta_3^2 \qquad (4.1.14)$$

and

$$I_3 = \delta_1\delta_2 + \delta_1\delta_3 + \delta_2\delta_3, \qquad (4.1.15)$$

which are of second order.

Since the winding number of a map is a topological invariant, we require that it remain unchanged under variations of the mapping. Thus, to second order we have the constraint that the change in baryon number be of third order. The winding number expressed in terms of the eigenvalues of the deformation matrix takes the form:

$$B = \frac{1}{(2\pi^2)}\int \sqrt{g}\lambda_1\lambda_2\lambda_3, \qquad (4.1.16)$$

and for the identity mapping gives $B = 1$. Thus, substituting the expression (4.1.11), for the deformed eigenvalues (4.1.11), in to (4.1.16), the expression for

130

the baryon number, leads to the constraint

$$\int \sqrt{g} I_1 = -\int \sqrt{g} I_3 + 0(\delta^3). \qquad (4.1.17)$$

Imposing this constraint, the expression for the energy to second order (4.1.12), has the form

$$E^{(2)} = 12\pi^2(L + \frac{1}{L}) + \frac{1}{L^2}\int \sqrt{g}(1 + \frac{2}{L^2})I_2 - 2\int \sqrt{g} I_3. \qquad (4.1.18)$$

There is no first order term in this expression and hence we see that the trivial map is a stationary point of the energy functional. Moreover, the second order term is positive definite for $L < \sqrt{2}$ and negative definite for $L > \sqrt{2}$. Thus, the identity map is a local minimum up to $L = \sqrt{2}$ and beyond it is a local maximum. At the point $L = \sqrt{2}$, the path of steepest descent is observed to be achieved when $\delta_1 = \delta_2 = \delta_3$. This corresponds to an infinitesimal local conformal transformation. Hence the trivial map is unstable against such a transformation at values of $L = \sqrt{2}$ and undergoes a second order phase transition at the corresponding density.

This observation was further strengthened by the complete calculation of the mode spectra [8] with the trivial map background. The complete solution of this second order variation problem, reveals that the infinitesimal conformal modes have eigenvalues that go from positive to negative as the value of L is increased beyond $\sqrt{2}$.

For large values of L beyond $\sqrt{2}$, Manton [3] considered a finite conformal map as an ansatz. This will incorporate the infinitesimal mapping and is the

analogue of the finite conformal transformation (3.6.4), considered by Jackson et al [10] and discussed in the previous chapter. This takes the general hedgehog form and in the polar coordinate systems, (μ, θ, ϕ) on $S^3_{phy}(L)$ and $(\tilde{\mu}, \tilde{\theta}, \tilde{\phi})$ on S^3_{iso},

$$
\begin{aligned}
\tilde{\mu} &= 2\tan^{-1}(\alpha \tan \frac{\mu}{2}), \\
\tilde{\theta} &= \theta, \\
\tilde{\phi} &= \phi.
\end{aligned}
\tag{4.1.19}
$$

For $\alpha = 1$ this reduces to the trivial map. For $\alpha > 1$ the mapping produces a localisation of the skyrmion about the north pole $\mu = 0$, while for $0 < \alpha < 1$ it produces localisation centred on the south pole $\mu = \pi$. These two configurations are related by the transformation $\alpha \mapsto 1/\alpha$. Minimising the energy of this conformal map with respect to α, shows for $L < \sqrt{2}$ there is only one physical solution, $\alpha = 1$, the trivial map. For $L > \sqrt{2}$ there are three stationary values of α, two of which have identical energies for values of α and $1/\alpha$ and are minima, while the third $\alpha = 1$ is a maxima. Thus, we have a phase transition of the standard 'pitchfork' type. For infinite L the trivial map has infinite energy, as seen by equation (2.3.11), while the two others have finite limits with energy $\sqrt{2} \times 12\pi^2$. Thus, in the flat space limit their energy is seen to be close to that of the flat space hedgehog. The baryon density of the solutions is observed to be localised in a region $\mu \sim 1/L$ for large L. The exact solution is very similar in the flat space limit, having an energy consistent with that of the flat space

132

skyrmion and of the general hedgehog form with the two degenerate solutions localised about opposite poles and being related by the transformation:

$$f(\mu) \mapsto \pi - f(\pi - \mu).$$

(4.1.20)

4.2 Varying The Metric Of $S^3_{phy}(L)$

We shall now consider the effect of allowing both the map and shape of physical space to vary in order to investigate the stability of the minimal energy trivial map solution on $S^3_{phy}(L)$ as a function of its average baryon density. Of course, we have in mind the analogous 'minimal' energy fcc array's instability with respect to bulk deformation above L_d, as described in the previous chapter. Due to the complexity of finding the soft modes of deformation for this crystal and as the conformal instabilities are common to both systems, we hope to reveal another such 'universal' instability.

As the Skyrme energy functional contains no term directly measuring the shape of physical space, the minimisation problem involving variation of the shape of physical space may be a pathological one. The inclusion of additional geometrical physical space terms, such as a curvature term, might well overcome these difficulties. However, we have no physical basis for such an addition and so we shall for the moment consider only small variations about the sphere which, as we shall see, we can make sense of and return to the difficulties the more

general minimisation problem poses at a later date.

We can consider small deformations of the shape of physical space and assume these leave the manifold M^3_{phy} smooth. Such small deformations can be encoded in a corresponding infinitesimal changes of the metric, g, on M^3_{phy}. These will then lead to corresponding, infinitesimal changes in the eigenvalues of the deformation matrix D and the $\sqrt{g}$ factor in the measure. We can represent these changes in the eigenvalues due to such a shape deformation and those due to variation of the map, by their effect on the deformation matrix's eigenvalues. We express these in the form:

$$\lambda_i \mapsto \lambda_i \frac{(1 + \delta_i)}{(1 + \varepsilon_i)}, \qquad i = 1, 2, 3 \qquad (4.2.1)$$

where ε and δ are small quantities defined on M^3_{phy}, corresponding to the shape and map deformation respectively.The change in the measure on M^3_{phy} is encoded in the change in the $\sqrt{g}$ factor and we express this as:

$$\sqrt{g} \mapsto \sqrt{g}(1 + \varepsilon_1)(1 + \varepsilon_2)(1 + \varepsilon_3), \qquad (4.2.2)$$

Thus, for fluctuations about the identity map on $S^3_{phy}(L)$, we express the new eigenvalues as:

$$\lambda_i = \frac{1}{L} \frac{(1 + \delta_i)}{(1 + \varepsilon_i)}. \qquad i = 1, 2, 3 \qquad (4.2.3)$$

On substituting expression (4.2.2) and (4.2.3) into the energy functional (4.1.8)

134

and expanding, we have the energy to second order given by:

$$E^{(2)} = 12\pi^2(L + \frac{1}{L}) + \frac{1}{L^2} \int_{M_{phy}^3} (2I_1 + J_1 + I_2 + J_2 - J_3 - 2H_2 + 2H_3)$$

$$+ \frac{1}{L^4} \int_{M_{phy}^3} \sqrt{g} \frac{1}{L^4}(4I_1 - J_1 + 2I_2 + 2J_2 + 4I_3 - J_3 - 4H_2), \quad (4.2.4)$$

where we have used the same infinitesimal expressions as in (1.1.13) to (1.1.19) and in addition have introduced the following infinitesimal functions:

$$J_1 = \varepsilon_1 + \varepsilon_2 + \varepsilon_3,$$

$$J_2 = \varepsilon_1^2 + \varepsilon_2^2 + \varepsilon_3^2,$$

$$J_3 = \varepsilon_1\varepsilon_2 + \varepsilon_1\varepsilon_3 + \varepsilon_2\varepsilon_3, \qquad (4.2.5)$$

$$H_2 = \delta_1\varepsilon_1 + \delta_2\varepsilon_2 + \delta_3\varepsilon_3,$$

$$H_3 = \delta_1(\varepsilon_2 + \varepsilon_3) + \delta_2(\varepsilon_1 + \varepsilon_3) + \delta_3(\varepsilon_1 + \varepsilon_2).$$

On setting the infinitesimal quantities, (4.2.5), equal to zero, expression (4.2.4) reduces to the expression for the energy second to order, (4.1.12), resulting from infinitesimal fluctuations about the trivial map, as of course it should.

The winding number constraint does not change since this is a topological invariant, dependent only on the mapping and hence, we still require expression (4.1.17) to be satisfied by the δ's. However, we require a second constraint for our purposes, that the volume be constrained. This is so as to eliminate instability with respect to metric deformation which reduces the volume towards that at which the minimum occurs. Hence, we require that the volume given by

$$V = \int_{M_{phy}^3} \sqrt{g}, \qquad (4.2.6)$$

135

be fixed. Hence, requiring its variation to be of third order, this gives us the constraint:

$$\int_{M^3_{phy}} \sqrt{g}\,J_1 = -\int_{M^3_{phy}} \sqrt{g}\,J_3 + O(\delta^3). \qquad (4.2.7)$$

Imposing the two constraints (4.1.17) and (4.2.6) gives the energy to second order as:

$$E = 6\pi^2(L + \frac{1}{L}) \;+\; \frac{1}{L^2}\int \sqrt{g}(1 + \frac{2}{L^2})(\gamma_1^2 + \gamma_2^2 + \gamma_3^2)$$
$$-\; 2\int \sqrt{g}(\gamma_1\gamma_2 + \gamma_1\gamma_3 + \gamma_2\gamma_3), \qquad (4.2.8)$$

where we have introduced the new infinitesimal quantities

$$\gamma_i = \delta_i - \varepsilon_i. \qquad\qquad i = 1, 2, 3 \qquad (4.2.9)$$

This is exactly analogous to the expression (4.1.18) and thus we have similar conclusions for this class of multiple infinitesimal variation.

There is no first order term, hence the trivial map and $S^3_{phy}(L)$ are stationary against these infinitesimal multiple variations for all values of L. Moreover, this solution is a local minimum up to a volume corresponding to $L = \sqrt{2}$ and beyond this point it is an unstable extremum. The path of steepest descent at $L = \sqrt{2}$ is given by the condition

$$\gamma_1 = \gamma_2 = \gamma_3. \qquad (4.2.10)$$

This is the condition that the space, resulting from the infinitesimal deformation of the shape of $S^3_{phy}(L)$, be conformally mapped into S^3_{iso} by the infinitesimally

varied mapping. A finite version of this condition is

$$K = \Omega^2 g, \qquad\qquad (4.2.11)$$

where Ω^2 is the local conformal factor which varies over M_{phy}^3 and expresses the change in length of the orthonormal frame vectors induced by the mapping. This is indeed a direct generalisation of Manton's finite conformal mapping for a general shaped physical space, (4.1.19).

So we conclude, that on $S_{phy}^3(L)$ both the shape deformation and the delocalising phase transitions are of second order, occurring at a volume corresponding to $L = \sqrt{2}$. We also note that these generalised infinitesimal deformations can be expressed in terms of the three infinitesimal quantities γ_i and this is a consequence of the similarity in the shapes of the physical and the target spaces. Thus, to second order in the energy, we find that variations of the map and the metric are able to compensate each other and presumably are responsible for the observation that $L_d = L_c$. For flat space arrays this suggests that infinitesimal map fluctuations are unable to completely compensate for bulk deformations and hence the two phase transitions occur at different densities. However, their close proximity may be a measure of their ability to compensate for each other.

4.3 A Hedgehog On An Elliptical Three Surface

In order to illustrate the observations of the previous section, we shall now consider a specific example, generalising the shape of the sphere, $S^3_{phy(2)}$. The simplest such model would be to replace $S^3_{phy}(L)$ by a space whose shape varied through a one parameter family of metrics, with one specific value corresponding to a $S^3_{phy}(L)$. An obvious candidate space is an ellipsoid. There are two such ellipse spaces and these can be represented as embedded surfaces within R^4, satisfying

$$\frac{w^2}{a^2} + \frac{x^2}{b^2} + \frac{y^2}{b^2} + \frac{z^2}{b^2} = 1, \qquad (4.3.1)$$

or

$$\frac{w^2}{c^2} + \frac{x^2}{c^2} + \frac{y^2}{d^2} + \frac{z^2}{d^2} = 1, \qquad (4.3.2)$$

where (w, x, y, z) are Cartesian coordinates with R^4 and a, b and c, d are real constants, defining the length and width in R^4 of these elliptical surfaces. These both result in a one parameter family of metrics on M^3_{phy} for varying length to width ratios. Clearly the magnitudes of these parameters are related only to the volume, while their ratios determine the curvature of the ellipse.

In the flat space calculations we considered bulk deformations of a cube to a rectangle. Thus, as the cubic shape was changed, either in compression or expansion in the direction of one of its sides, this resulted in an asymmetry

about the cubic shape. For the second of these elliptical spaces, (4.3.2), the transformation $c \mapsto d$ and $d \mapsto c$, produces an identically shaped space and thus, the sphere condition $(c = d)$ is a unique symmetry point of this transformation. Thus, for a skyrmion on this ellipse, the result of deformation in the shape of space for $c > d$ or $c < d$, should be symmetric about $S^3_{phy}(L)$, $(c = d)$.

However, we do not expect this to be the case for the first of these ellipses, (4.3.1). The space which results for $a < b$ is of an oblate type, with an axis of symmetry about its minor axis. The ellipse which results when $a > b$ is of the prolate type, with an axis of symmetry about its major axis. Thus, the transformation $a \mapsto b$ and $b \mapsto a$ does not produce a space which is isomorphic to the original. Hence, we cannot expect for these elliptical deformations, of the ellipse (4.3.1), that the sphere will, in general, be unique. Thus we see, that the shape deformations of $S^3_{phy}(L)$ to the elliptic space (4.3.1), is in direct analogy to those shapes produced by our bulk deformations of the fcc lattice. These changed the shape of the fcc cubic cell in to a square based prismoidal cell. Thus, the results of our numerical calculations, with respect to the effects of these bulk deformations of the fcc lattice, (see Chapter 3), were in general found to be asymmetric about this cubic symmetry for varying aspect ratios of the cell.

Since the space (4.3.1) has a rotation symmetry about its major axis $(a > b)$, or its minor axis $(a < b)$, which passes through its poles, these two poles are identified as unique points of symmetry. Since the hedgehog ansatz also involves

a similar unique identification of the poles and rotation symmetry, we see that on this space the hedgehog ansatz is a sensible one, on grounds of symmetry. Thus, in the remainder of this section we shall investigate the effects, on a $B = 1$ hedgehog skyrmion, of changing the shape of physical space constrained to satisfy (4.3.1).

The shape of this ellipse is related to the ratio of the lengths a and b. For larger values of the ratio a/b, the ellipse becomes needle like and of prolate symmetry, while for small values it becomes disc like and of oblate symmetry. We choose the coordinates for this ellipse to be the 'standard' polar angles $0 \leq \theta$, $\phi \leq \pi$ and an angle $0 \leq \mu \leq \pi$, which are related to the Cartesian coordinates of R^4 by

$$w = a \cos \mu,$$

$$x = b \sin \mu \cos \theta,$$

$$y = b \sin \mu \sin \theta \cos \phi,$$

$$z = b \sin \mu \sin \theta \sin \phi, \qquad (4.3.3)$$

and thus, we see constraint (4.3.1) is satisfied. In this polar coordinate system the metric on M_{phy}^3 is diagonal, with elements:

$$\{b^2(1 - e \sin^2 \mu), b^2 \sin^2 \mu, b^2 \sin^2 \mu \sin^2 \theta\}, \qquad (4.3.4)$$

where we have retained the dimensioned length b and introduced the dimensionless eccentricity

$$e = (1 - a^2/b^2)^{1/2} \qquad (4.3.5)$$

140

which governs the shape of the ellipse. Thus we have our desired one parameter metric, (ignoring the length variable b), with the eccentricity parameter expressing changes in shape. For $e = -\infty$ we have the needle, for $e = 1$ the disc and for $e = 0$ the sphere.

For numerical representation of the data, the eccentricity parameter will be replaced by the new parameter y which takes values from plus infinity to minus infinity and corresponds to the sphere at $y = 0$. Such a symmetric variable is

$$y = \frac{a^2}{b^2} - \frac{b^2}{a^2}, \qquad (4.3.6)$$

and is related to e by

$$y = -e\frac{(2 - e)}{(1 - e)}. \qquad (4.3.7)$$

The needle corresponds to $y = +\infty$ and the disc to $y = -\infty$. This is analogous to replacing the aspect ratio r^3, by the p for the flat space arrays of interpolating symmetry, studied in Chapter 3.

The volume element on physical space is given by

$$b^3 \Delta \sin^2 \mu \sin \theta \, d\mu d\theta d\phi, \qquad (4.3.8)$$

where

$$\Delta = \left(1 - e\sin^2 \mu\right)^{1/2}. \qquad (4.3.9)$$

In order to simplify the numerical complexities of our calculation, we choose to employ the hedgehog ansatz for the skyrmion map. This seems a sensible ansatz

due to its high degree of symmetry and its consistency with the symmetries of this physical space. Moreover, for $e = 0$ this will incorporate both the trivial map and the standard hedgehog form previously employed on a $S^3_{phy}(L)$. This hedgehog mapping is given by

$$\sigma = \cos f(\mu),$$

$$\pi_x = \sin f(\mu) \cos \theta,$$

$$\pi_y = \sin f(\mu) \sin \theta \cos \phi,$$

$$\pi_z = \sin f(\mu) \sin \theta \sin \phi. \qquad (4.3.10)$$

Since we wish to consider only $B = 1$ solutions we shall impose the boundary conditions

$$f(0) = 0, \qquad\qquad f(\pi) = \pi, \qquad\qquad (4.3.11)$$

on the profile function, this ensures that the hedgehog has unit winding number B. The resulting deformation matrix for the hedgehog is diagonal and has eigenvalues:

$$\lambda_1^2 = \frac{\dot{f}^2}{b^2 \Delta^2},$$

$$\lambda_2^2 = \lambda_3^2 = \frac{\sin^2 f}{b^2 \sin^2 \mu}. \qquad (4.3.12)$$

Thus, the hedgehog's energy functional is given by:

$$E(f) = 4\pi \int_0^\pi d\mu \sin^2 \mu \Delta \{ b(\frac{\dot{f}^2}{\Delta^2} + 2\frac{\sin^2 f}{\sin^2 \mu}) + \frac{1}{b}\frac{\sin^2 f}{\sin^2 \mu}(2\frac{\dot{f}^2}{\Delta^2} + \frac{\sin^2 f}{\sin^2 \mu})\}(4.3.13)$$

where we have performed the trivial θ, ϕ integrations.

The Euler Equation following from the functional variation of (4.3.13),

142

with respect to $f(\mu)$ is:

$$(b^2 + 2\frac{\sin^2 f}{\sin^2 \mu})\ddot{f} + \{b^2(1 + e\frac{\sin^2 \mu}{\Delta^2}) + e\frac{\sin^2 f}{\Delta^2}\}\frac{\sin 2\mu}{\sin^2 \mu}\dot{f}$$

$$+ \sin 2f\dot{f}^2 - (b^2 + \frac{\sin^2 f}{\sin^2 \mu})\Delta^2\frac{\sin 2f}{\sin^2 \mu} = 0. \qquad (4.3.14)$$

This is an ordinary, second order, non-linear differential equation for $f(\mu)$ and

standard integration techniques can be applied to it to obtain a solution.

However, it should be noted that for $e = 0$, the trivial map $f(\mu) = \mu$, is a

solution, the equation reducing to that for $S^3_{phy}(L)$ given in Chapter 2, (2.3.9).

Before describing the numerical solution of this equation it is instructive to

consider a power series solution, in power of the eccentricity. Thus we choose to

take the eccentricity to be small and consider only solutions which are symmetric

about the equator.

Since $e = 0$, the trivial map is the solution of (4.3.14) and we were led to

solve this equation order by order in power of e about the trivial solution. To

second order in e we found the following symmetric solution,

$$f(\mu) = \mu + a_1 e \sin 2\mu + e^2(a_2 \cos^2 \mu + a_3 \sin^2 \mu)\sin 2\mu + 0(e^3), \qquad (4.3.15)$$

with the constants given by

$$a_1 = \frac{4 + 3b^2}{8(3 + b^2)},$$

$$a_2 = \frac{(-10 - 15b^2 - 5b^4 + 224a_1 - 408a_1^2 + 146a_1b^2 + 20a_1b^4 - 64a_1^2b^2 + 40a_1^2b^4)}{8(33 + 26b^2 + 5b^4)},$$

$$a_3 = \frac{(-16 - 23b^2 - 7b^4 + 200a_1 - 72a_1^2 + 126a_1b^2 + 16a_1b^4 + 24a_1^2b^4)}{8(33 + 26b^2 + 5b^4)}. \qquad (4.3.16)$$

143

This solution has the symmetry

$$f(\mu) = \pi - f(\pi - \mu), \qquad (4.3.17)$$

characterising the symmetric phase. We can now calculate this solution's energy in power of e, as a function of b and on substitution in (4.3.13), expanding and integrating we have:

$$E^{(2)} = \frac{2\pi^2}{b}[3(b^2 + 1) + \frac{3e}{8}(-b^2 + 1) \qquad (4.3.18)$$
$$+ \frac{e^2}{64}\{b^2(5 - 96a_1 + 128a_1^2) + 25 - 128a_1 + 384a_1^2\}] + O(e^3).$$

This energy does not depend on the parameters a_2 and a_3, in expression (4.3.15) for $f(\mu)$, since first order fluctuations in the eigenvalues of the deformation matrix completely account for the second order variation of the energy for a solution to the Euler Equation (4.3.14).

In order to compare like with like, we need to eliminate the variable b in favour of the variable L measuring the volume of space and hence the average baryonic density. Thus, we introduce the new variable

$$L = (\frac{V}{2\pi^2})^{1/3}, \qquad (4.3.19)$$

where the volume, V, of physical space is given by;

$$V = 4\pi b^3 \int_0^\pi d\mu \sin^2 \mu \Delta \qquad (4.3.20)$$

and hence L will be a function of both b and e. Expanding the right hand side of expression (4.3.19) in powers of e, gives to second order the result,

$$L = b\{1 - \frac{e}{8} - \frac{e^2}{24} + O(e^3)\}. \qquad (4.3.21)$$

144

Using this relation we eliminate b in favour of L, in expression (4.3.18), for the energy and obtain to second order in the eccentricity e,

$$E^{(2)} = 2\pi^2[3(L + \frac{1}{L}) + \frac{5}{64}e^2\{\frac{(2 - L^2)(L^2 + 1)}{(L^2 + 3)}\} + 0(e^3)]. \qquad (4.3.22)$$

Thus, as expected, we see $L_d = \sqrt{2}$, since the second order term is observed to change from being positive to negative on increasing the value of L beyond $\sqrt{2}$. Hence, the $S^3_{phy}(L)$ shape $(e = 0)$, is stable against these elliptical deformations up to a value of $L = \sqrt{2}$, beyond this value it is unstable to the deformations. However, we have not revealed the expected asymmetry for positive and negative values of e as this will be a higher order effect. We shall here continue this expansion to reveal this asymmetric behaviour and our numerical results will clearly demonstrate this.

Finally we have shown, again as expected, that at $L = \sqrt{2}$ the steepest path of descent corresponds to a local infinitesimal conformal transformation. To reveal this we shall construct a generalisation of Manton's finite conformal map on $S^3_{phy}(L)$, (4.1.19).

For a finite local conformal map we have the condition (4.2.11), which translates here to the condition that,

$$\lambda_1^2 = \lambda_2^2 = \lambda_3^2 \qquad (4.3.23)$$

and leads to the following first order differential equation for $f(\mu)$:

$$\frac{\dot{f}^2}{\sin^2 f} = \frac{\Delta^2}{\sin^2 \mu}. \qquad (4.3.24)$$

145

This can be trivially integrated to give the following solution,

$$f(\mu) = 2\tan^{-1}\{\alpha(\frac{\Delta - \cos\mu}{\Delta + \cos\mu})^{1/2}(\frac{\Delta + k\cos\mu}{\Delta - k\cos\mu})^{k/2}\}, \qquad (4.3.25)$$

where $k = \sqrt{e}$ is pure imaginary for e negative and α an integration constant. It is easy to show that $f(\mu)$ is a real valued function for $e < 0$, by re-expressing (4.3.25) as,

$$f(\mu) = 2\tan^{-1}[\alpha(\frac{\Delta - \cos\mu}{\Delta + \cos\mu})^{1/2}\exp\{-\sqrt{-e}\tan^{-1}(\frac{\sqrt{-e}\cos\mu}{\Delta})\}]. \qquad (4.3.26)$$

This solution, $f(\mu)$ to (4.3.24), satisfies the boundary conditions (4.3.11). Here α is simply the conformal parameter and for a sphere $e = 0$, expressions (4.3.25) and (4.3.26) reduce to Manton's expression (4.1.19). For values of $\alpha \neq 1$ the symmetry

$$f(\mu) = \pi - f(\pi - \mu), \qquad (4.3.27)$$

is broken. Thus for $\alpha = 1$, $f(\mu)$ has the symmetry of equation (4.3.27) and is observed to be a particular generalisation of the trivial map on the three sphere to an ellipse

For $\alpha = 1$, expanding this solution to second order in e we obtain

$$f(\mu) = \mu + \frac{e}{4}\sin^2\mu + e^2(\frac{5}{48}\cos^2\mu + \frac{3}{48}\sin^2\mu) + O(e^3). \qquad (4.3.28)$$

We can now compare this to the exact second order solution, (4.3.15), which at the value of $L = \sqrt{2}$ gives:

$$f(\mu) = \mu + \frac{e}{4}\sin^2 2\mu + e^2\sin 2\mu(\frac{17}{280}\cos^2\mu + \frac{19}{210}\sin^2\mu) + O(e^3). \qquad (4.3.29)$$

146

Thus, we see these expressions agree to first order and that at $L = \sqrt{2}$ the true solution is conformal to first order. However, to second order there is a slight discrepancy, reflecting the non-exactness of the finite conformal map ansatz. For α not to equal one, the energy of this conformal mapping is degenerate with respect to α and $1/\alpha$, corresponding to the skyrmion localising on either pole of the ellipse. Thus, this is indeed the analogue of the $S^3_{phy}(L)$ conformal mapping.

4.4 Numerical Results For A Hedgehog On An Ellipsoid

We obtain numerical solutions to the Euler Equation (4.3.13), within a range of volumes corresponding to values of L in the range 0.8 and 1.6 and eccentricities in the range 0.9 to -0.9. These values e, have corresponding values of y about -10 to 10 respectively, which appears to be the most interesting region of values of y.

The profile function for a $B = 1$ solution to the Euler Equation, will have at the end points the behaviour,

$$f \sim \alpha\mu, \qquad \mu \sim 0$$

$$f \sim \pi - \beta(\pi - \mu), \qquad \mu \sim \pi \qquad (4.4.1)$$

where α and β are positive constants, dependent on e and L and determining the slope of f at the respective end points. The Euler Equation can be integrated inwards from 0 to $\pi/2$ and from π to $\pi/2$ and by varying α and β, the matching

147

conditions for f and $\dot{f}$ at $\pi/2$ can be satisfied to give smooth numerical solutions. In general α and β can have different values, however, in the symmetric phase the solutions have the symmetry of equation (4.3.27) and α and β are trivially equal. In arranging α and β to satisfy the matching condition at $\pi/2$, a standard Newton-Raphson minimisation technique was used. For this local minimisation technique a 2×2 matrix, formed from calculating the derivatives of the miss-match in f and $\dot{f}$ at $\pi/2$ with respect to α and β, must be inverted. In the symmetric phase there is only one solution, while in the non-symmetric phase three solutions exist. Thus, as one might expect, the determinant of this 2×2 matrix is zero at the phase transition density. Thus, determining the variation in the value of this determinant as e and L vary, enables us to determine simply and accurately the phase transition points L_c, for given eccentricities.

Symmetric phase solutions can also be obtained by integrating the Euler Equation from only one end point to $\pi/2$, where the condition $f(\pi/2) = \pi/2$ must be met as a trivial consequence of the solution's symmetry, (4.3.27). This symmetry was often imposed in order to increase the efficiency of our integration techniques in the symmetric phase.

In general, for increasing values of the magnitude of the eccentricity, the difficulty in obtaining solutions over the full region 0 to π increases. Since at large eccentricities the curvature of physical space is high in certain regions and low in other regions, the profile function varies rapidly in response to these local variations in curvature. In the case where e is both large and negative, that is,

148

where the curvature of the 'needle' is sharpest at the end points, these difficulties are accentuated, since the matching difference is highly sensitive to the values of α and β. These difficulties undermine the Newton-Raphson technique of minimisation, though it is unlikely that overcoming these difficulties would require a greater refinement of our integration technique, if a wider range of values of e were of interest.

The Euler Equation (4.3.14), explicitly involves b, which we eliminate in favour of L through the relation (4.3.19), in which the value of the volume, V, of physical space, is evaluated trivially by numerically integrating at different values of e. Thus, in obtaining solutions to the Euler Equation, we choose to fix the values of L and e and subsequently to eliminate the corresponding value of b from this equation, by using the relation (4.3.19).

The symmetric phase results reveal that a trivial map on $S^3_{phy}(L)$ becomes unstable to elliptical perturbation of the metric of physical space, coupled to symmetric perturbation of the map, at a value of $L = L_d = \sqrt{2}$. This is in agreement with the general second order deformation calculation of the previous section. This is clearly depicted in the contour plot Figure (4.4.1), of constant energy contours for varying values of y and L (note that in Figure (4.4.1) the energies are quoted in fractions of the lower bound, $12\pi^2$).

For L less than $\sqrt{2}$ and near $L = 1$, these contours have a positive curvature with respect to y about $y = 0$, $S^3_{phy}(L)$. As L is increased the contours flatten and the curvature about the line $y = 0$ changes sign beyond a value of
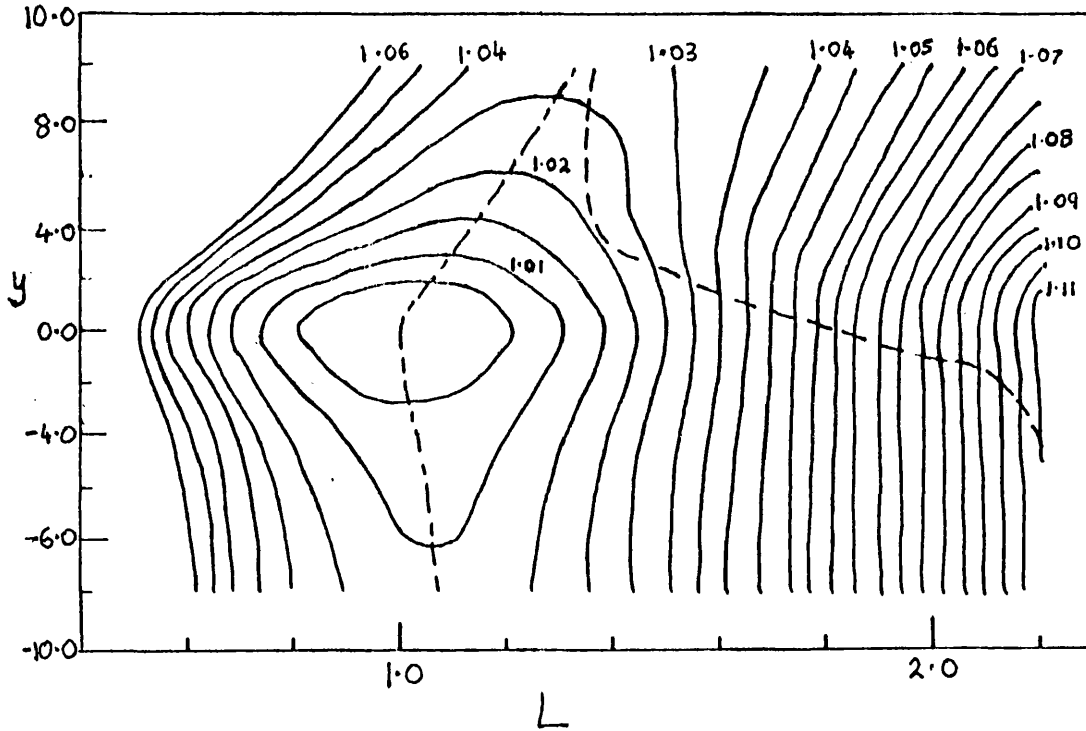
149

Figure (4.4.1): Contour plots of $(energy)/12\pi^2 = E/12\pi^2$ in the (L, y) plane where $L = (averagedensity)^{-1/3}$ and y measures deviations from S^3_{phy} (see text). Also shown is the curve of minimum energy, (dot-dashed lines), with respect to L at fixed p and the curve of phase transition points, (dashed line), separating the symmetric phase from the non-symmetric phase.

150

$L = L_d = \sqrt{2}$. Thus, the sphere is locally stable for values of L up to $\sqrt{2}$ and unstable for values beyond. For small values of $| \ y \ |$, the contours are approximately symmetric about the line $y = 0$ since infinitesimal deformations of the shape of the sphere do not differentiate the 'disc' and the 'needle' type shape deformations. This is consistent with our second order small eccentricity expansion of the energy (4.3.22) for a symmetric solution. For larger values of $| \ y \ |$ the contours become asymmetric as higher order effect becomes significant and the 'needle' type deformations of $S^3_{phy}(L)$ are energetically preferable.

The dashed line on this plot shows how the density of the symmetry breaking phase transition varies with y. This transition is found to be second order at all values of y investigated. For values of y between 3 and -2, the value of L_c varies rapidly from about $L = 1.23$ to $L = 1.58$, passing through $L = \sqrt{2}$ at the value of $y = 0$ corresponding to the sphere. Thus, we see as predicted, $L_c = L_d = \sqrt{2}$ for a skyrmion on $S^3_{phy}(L)$. For y less than -2, the value of L_c varies less rapidly, becoming seemingly independent of y at large negative values corresponding to a disc, with a value of $L_c \sim 1.6$. For y greater than 3, the dependence of L_c on y also lessens as y increases, becoming approximately independent of y beyond values of y greater than 4.5, with the value of L_c about 1.18. In general we see that the density at which the symmetry breaking phase transition occurs, decreases as y increases and thus symmetric skyrmionic matter will persist to lower densities on a disc-like space than on a needle-like space.

The dot-dashed line of Figure (4.4.1) indicates the value of L_{min} corresponding

151

to the minimum of the energy for varying values of y. The absolute minimum energy is attained at the point $L = 1$, $y = 0$ corresponding to the identity mapping on $S^3_{phy}(1)$. The values of L_{min} for large negative values of y are smaller than their corresponding positive values and the dependence of L_{min} on y appears to be fairly linear as y increases or decreases from $y = 0$. At a value of $y \sim 10$, we have that $L_{min} \sim 1.16$ and also that the L_{min} contour approaches the L_c contour, presumably merging for large values of y corresponding to the 'needle'.

For $L \leq 1$, Manton [3] has shown the trivial mapping on $S^3_{phy}(L)$ has an absolute minimum of the energy. Thus, in this region the sphere $y = 0$, at fixed L, is seen to be a minimum of the energy compared to all other values of y. This behaviour persists up to a value of $L \sim 1.25$ for the symmetric phase. This contour plot is deceptive at the minimum, a change of y by about 2 has a correspondingly equal effect on the energy, as would a change of L by 0.1 and thus of the volume by 0.001. Hence, we see that dense Skyrme Matter on an ellipse has a jelly-like behaviour, being relatively easily deformed though resistant to expansion or compression.

For values of L greater than 1.25 and values of y less than about -4, the energy becomes seemingly independent of y and the energy contours close on themselves as L increases. Thus, in this region, as dense Skyrme matter is expanded, it offers no resistance to deformation, a characteristic of our dense crystalline matter under bulk deformation. This behaviour persists up to a volume of 1.6, beyond which the symmetric Skyrme matter undergoes a second order

phase transition to a non-symmetric phase of matter.

For values of L greater than about 1.3, symmetric Skyrme matter is seen to prefer to sit on a space with y large and positive. However, in this region non-symmetric matter is energetically preferred.

Thus, the plot (4.4.1) has many of the features observed in the analogous contour plot Figure (3.5.3) for crystalline symmetric dense skyrmionic matter on flat space. Both have a jelly-like behaviour near the minimum energy density. Also, the asymmetry of the energy contours about the line $y = 0$ of $S^3_{phy}(L)$, is similar to that observed about the line $p = 0$ of the fcc array. We also see that the preferred needle-like deformations of $S^3_{phy}(L)$ are the analogue of the preferred planar deformations of the fcc crystal, while the less favourable disc-like deformations of $S^3_{phy}(L)$ are analogous to the less favourable chain-like deformations of fcc matter. However, the large gains of energy observed for the needle-like shape at volumes above 1.3 appear to be a feature of the local curvature of this shape, not present in our flat space crystalline matter results. However, this comparison of the plots is deceptive. The range of p values considered in the array calculation corresponds to values of y between 2.6 and -4.8. It is here that the similarity of the two plots is most striking, the large gains of energy for needle-like deformation lying just outside this region. Indeed, in this region, the value of L_c varies fairly linearly as is also the case for the crystalline matter plot.

In Figure (4.4.2), we show how the energy of the symmetric solutions varies with L at various fixed values of y. This plot shows clearly that for a given value
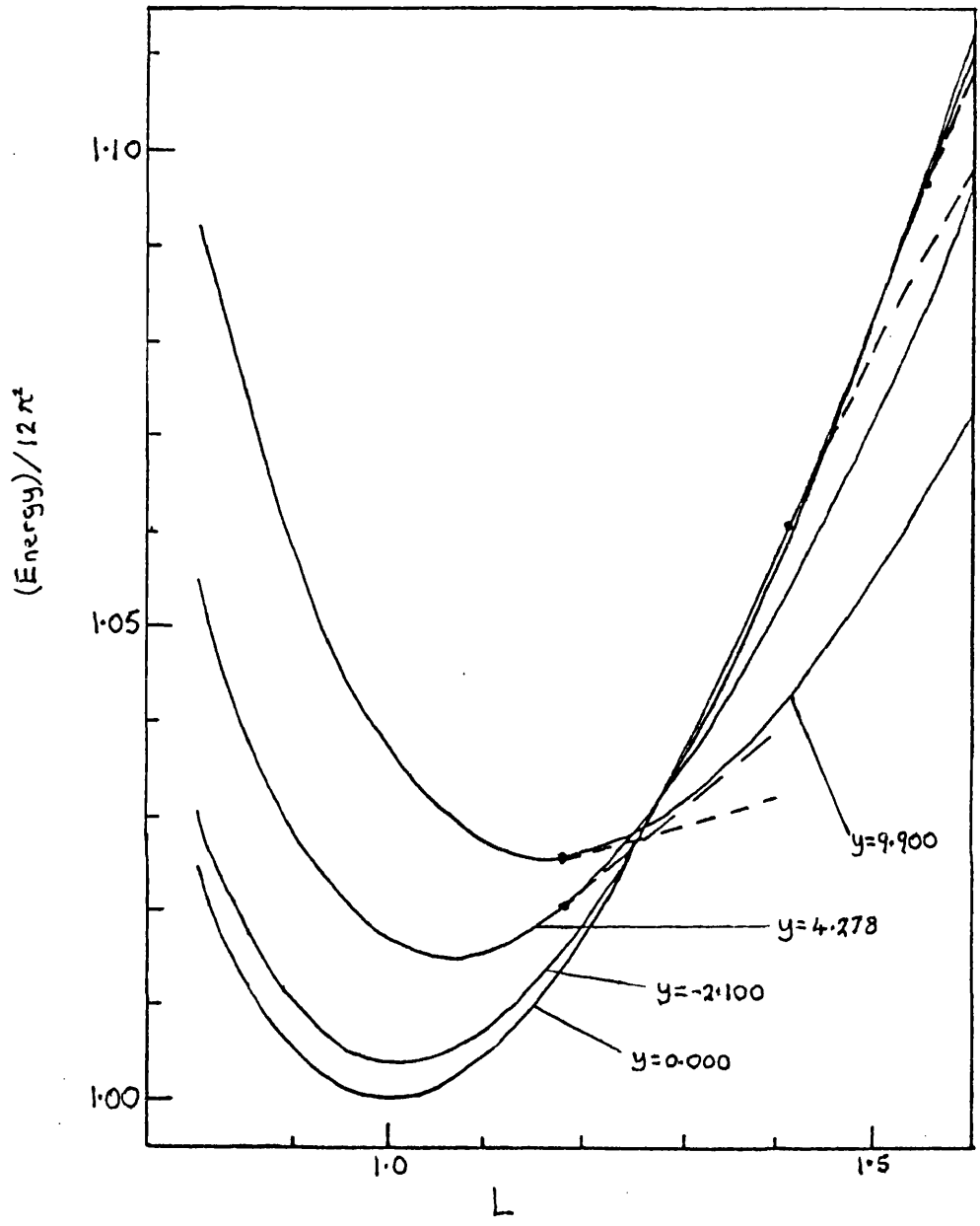
Figure (4.4.2): Plots of $(energy)/12\pi^2$ of symmetric phase, (solid lines) and non-symmetric phase, (dashed lines), versus L for various values of y. Solid dots indicate phase transition points.

of y there is a definite minimum energy at some value of $L = L_{min}$. This plot also shows that this minimum of the energy occurs at a value of $L = L_{min}$ which increases as the value of y changes from zero, corresponding to the sphere. As y increases, the $y = 4.278$ and 9.9 plots show that beyond L_{min} the energy flattens out as y becomes increasingly positive. We have also indicated the values of $L = L_c$ at which the second order phase transition occurs by a solid dot. Its second order nature is clear from the manner in which non-symmetric energy curves, (dashed lines), smoothly merge with their corresponding symmetrical energy curves at L_c, (solid lines). The value of L_c is also clearly seen to approach L_{min} as y increases, as was indicated by the contour plot (4.4.1) and moreover, this suggests that for large values of y these points will coincide, so that the energy will attain its minimum value for all volumes beyond this point and become independent of L. For negative values of y and values of L greater than about 1.25, the energy plots lie on top of each other, as suggested by the $y = 0$ and $y = -2.1$ curves. This is a reflection of the independence of the energy to changes in y for negative values of y, as was indicated in plot (4.4.1).

An alternative and revealing representation of the symmetric phase data of plot (4.4.1) is shown in Figure (4.4.3). Here contours of constant L are depicted as y is varied and corresponding values of the energy attained. The results of our numerical calculation for both the symmetric and non-symmetric phase have both been included on this plot. The symmetric data, (solid lines), for a range of values of L between 0.8 and 1.6 and the non-symmetric data, (dashed lines),
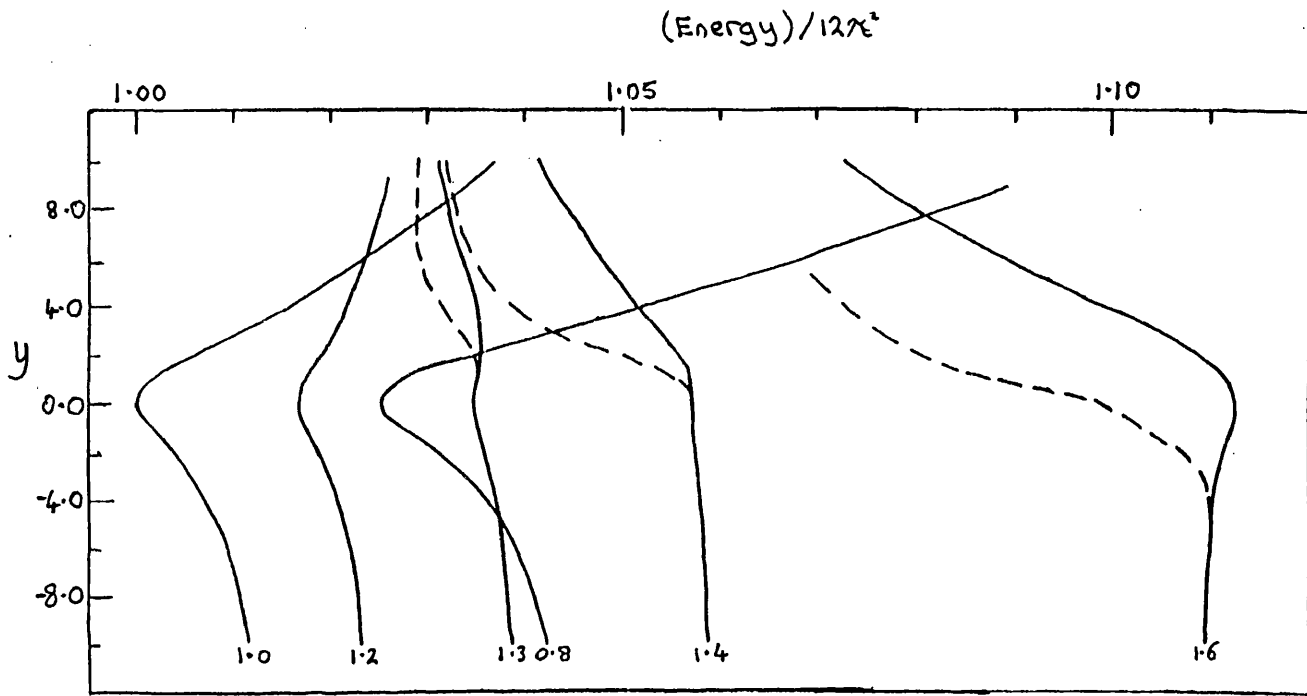
Figure (4.4.3): Contour plots of L in the $(E/12\pi^2, y)$ plane. Solid lines indicate the symmetric phase and dashed lines indicate the non-symmetric phase.

for a range of values of L between 1.2 to 1.6 are indicated,as are both, over the entire range of values of y that we numerically investigated.

The local symmetry of the symmetric phase data with respect to the line $y = 0$, corresponding to the sphere, can be clearly seen on this plot. In the symmetric phase, this clearly demonstrates that the hedgehog on a sphere cannot distinguish between positive and negative changes in the value of y about zero and thus between the prolate and oblate type elliptical shaped spaces. Moreover, we see that about the line $y = 0$, corresponding to the sphere, the curvature of the symmetric phase contours decrease in value as L increases from $L_{min} = 1$ to $L = 1.6$. At a value of $L = 1.4$, the curvature of the contour is seen to be almost zero at $y = 0$, though still positive. This indicates that the value of L at which the sphere becomes unstable to shape deformations will be slightly greater than the value of $L = 1.4$ and as we have already stated this occurs at a value of $L = L_d = \sqrt{2}$.

For the symmetric phase, with respect to non-local changes in the value of y from $y = 0$, this plot also reveals that for values of $L \sim 1.25$, the sphere $y = 0$ is no longer stable to prolate type deformation of the shape of space. This is indicated by the $L = 1.3$ contour having minimum energy at a large positive value of y which occurs outside the range of our data, and similarly for values of L beyond this value. However, for the $L = 1.2$ contour and for values of L below this, the minimal value of the energy occurs at $y = 0$.

Thus, the contour plot clearly indicates the manner in which the region of

157

local stability of the sphere, with respect to shape deformations in the symmetric phase, shrinks as L is increased from $L_{min} = 1$ to $L_c = \sqrt{2}$. For positive y values, the oblate deformations of the sphere, the constant L contours flatten as L increases from $L_{min} = 1$, until at $L = L_c = \sqrt{2}$, the sphere $y = 0$, is also unstable with respect to these types of deformation. However, there is no local instability of the sphere with respect to oblate deformations and even beyond the value of $L = L_c = \sqrt{2}$, the constant L contours remain flattish. This indicates that no great gains in energy are possible for oblate type deformations of the sphere.

The constant L contours of the non-symmetric data indicated on this plot, are clearly seen to merge smoothly with the symmetric contours at steeply increasing values of y as L increases. This smoothness clearly indicates the second order nature of the symmetry breaking phase transition. For values of L less than 1.0, symmetric contours are shown, indicating that in this region of L only the symmetric phase exists. However, at a value of $L \sim 1.25$, both phases exist and hence, all contours beyond a value of $L = 1$, have the non-symmetric phase contour breaking away at some value of y. For the $L = 1.2$ contours, the non-symmetric contour lies almost on top of the symmetric contour for values of y greater than about 4. This indicates that for values of $L \sim 1.2$ and y greater than about 4, both phases might exist with very similar energies. As the value of L increases, the contours of both phases become separable and the gain in the energy of the non-symmetric to the symmetric phase becomes significant, with

the value of y at which the symmetry breaking transition occurs decreasing. Thus, for the $L = 1.4$ contour, the break away point is seen to occur at a value of y which is close to zero but still positive. This indicates that the value of L_c for the sphere $y = 0$, is close to $L = 1.4$ and as was already indicated, actually has a value $L = L_c = \sqrt{2}$. At a value of $L = 1.6$, the phase transition occurs at a value of $y \sim -5$, when space has oblate symmetry.

For values of y beyond about 2 and values of L greater than about 1.3, the energy of both phases decreases sharply as y increases. The rather large gain in energy, for non-symmetric solutions over symmetric ones in this region, is a consequence of the local curvature of these needle-like shapes. As y is further increased, the constant volume contours of both phases converge to an energy of about $1.03 \times 12\pi^2$. For $L = 1.3$, both phases have contours which vary slowly for values of y greater than about 8 and seemingly will converge at very large y. This behaviour is a consequence of the closeness of the values of L_c and L_{min} at large values of y, indicated in Figures (4.3.1) and (4.3.2).

In order to gain a deeper understanding of these observations it is useful to study the functional dependence of the profile function $f(\mu)$ at a variety of eccentricities and densities. Many of the observations concerning the energy plots can in fact be explained as local curvature effects. Thus, to this end we introduce the local curvature of this manifold. Thus, we have for the metric g on physical space, with the diagonal components given in (4.3.4), that the Ricci curvature

tensor is diagonal with elements

$$R_{11} = -2\frac{(1-e)}{\Delta^2},$$

$$R_{22} = -2(1-e)\frac{\sin^2\mu}{\Delta^4}(1-\frac{e}{2}\sin^2\mu),$$

$$R_{33} = -2(1-e)\frac{\sin^2\mu\sin^2\theta}{\Delta^4}(1-\frac{e}{2}\sin^2\mu), \qquad (4.4.2)$$

where the (μ,θ,ϕ) coordinates are labelled $(1,2,3)$ respectively. The local curvature scalar R, obtained by contracting the Ricci tensor with the inverse metric g_{ij}, is thus given by

$$R(\mu) = -2\frac{(1-e)(3-e\sin^2\mu)}{b^2\Delta^4}, \qquad (4.4.3)$$

from which we see the local scalar curvature is a function of μ only. Setting $e = 0$ gives the scalar curvature of a $S^3_{phy}(L)$ to be $-6/L^2$, which is negative with our convention for the sign of the curvature. For $e = 1$ $(y = -\infty)$, the curvature of the ellipse is seen to be zero at all values of μ except $\pi/2$, where it is negative infinity. Thus, in this limit, space is indeed disc-like, being flat except at its rim where the curvature is $-\infty$. Setting $e = -\infty$ $(y = +\infty)$, space becomes needle-like, with the curvature being negative infinity at the poles and small at $\mu = \pi/2$, though finite.

Another useful quantity we shall now introduce for representing the skyrmion is its baryon density. This is given by

$$B^0(\mu) = \frac{1}{2\pi^2}\frac{\sin^2 f}{b^3\Delta\sin^2\mu}\dot{f}, \qquad (4.4.4)$$

which can be trivially integrated over physical space M^3_{phy}, to give one for $f(\mu)$, satisfying bounding conditions (4.3.11). This quantity also depends on μ only.

Since the identity mapping on $S^3_{phy}(1)$ saturates the lower bound, we expect that a skyrmion would prefer to sit on a region of space of constant scalar curvature -6. Thus, on a space with a local curvature which is not constant, we might predict that a skyrmion will try and sit on regions of space where the curvature is -6. Moreover, the energy of the trivial map on $S^3_{phy}(L)$, as L is decreased from $L = 1$, increases rapidly, while as L is increased it increases less rapidly. Thus, we expect a skyrmion would prefer to sit on regions of space where the curvature has its optimal value of -6 and with curvature less than, rather than higher than this value. Finally, we know as the volume of space is increased past $L = \sqrt{2}$ and the curvature of space becomes small, the skyrmion on $S^3_{phy}(L)$ prefers to localise about some point rather than be stretched over a large volume of space. Thus, it is to be expected the skyrmions will try to avoid being stretched excessively.

To illustrate this, consider the plot depicted in Figure (4.4.4) showing the variation of baryon density with μ in equation (4.4.4) for a variety of symmetric solutions at a value of $L = 1$ and for values of y between 9.9 and -9.9. The baryon density of $y = 0$ is constant at $1/2\pi^2$, showing the complete delocalisation of the identity mapping on $S^3_{phy}(1)$. As y increases, the skyrmion's baryon density begins to localise about $\mu = \pi/2$. At $y = 9.9$ it is heavily peaked about $\mu = \pi/2$ and confined to the region $\pi/4 < \mu < 3\pi/4$. Thus, on the needle-like space with $L = 1$, the skyrmion prefers to sit on the flattest region of space with zero
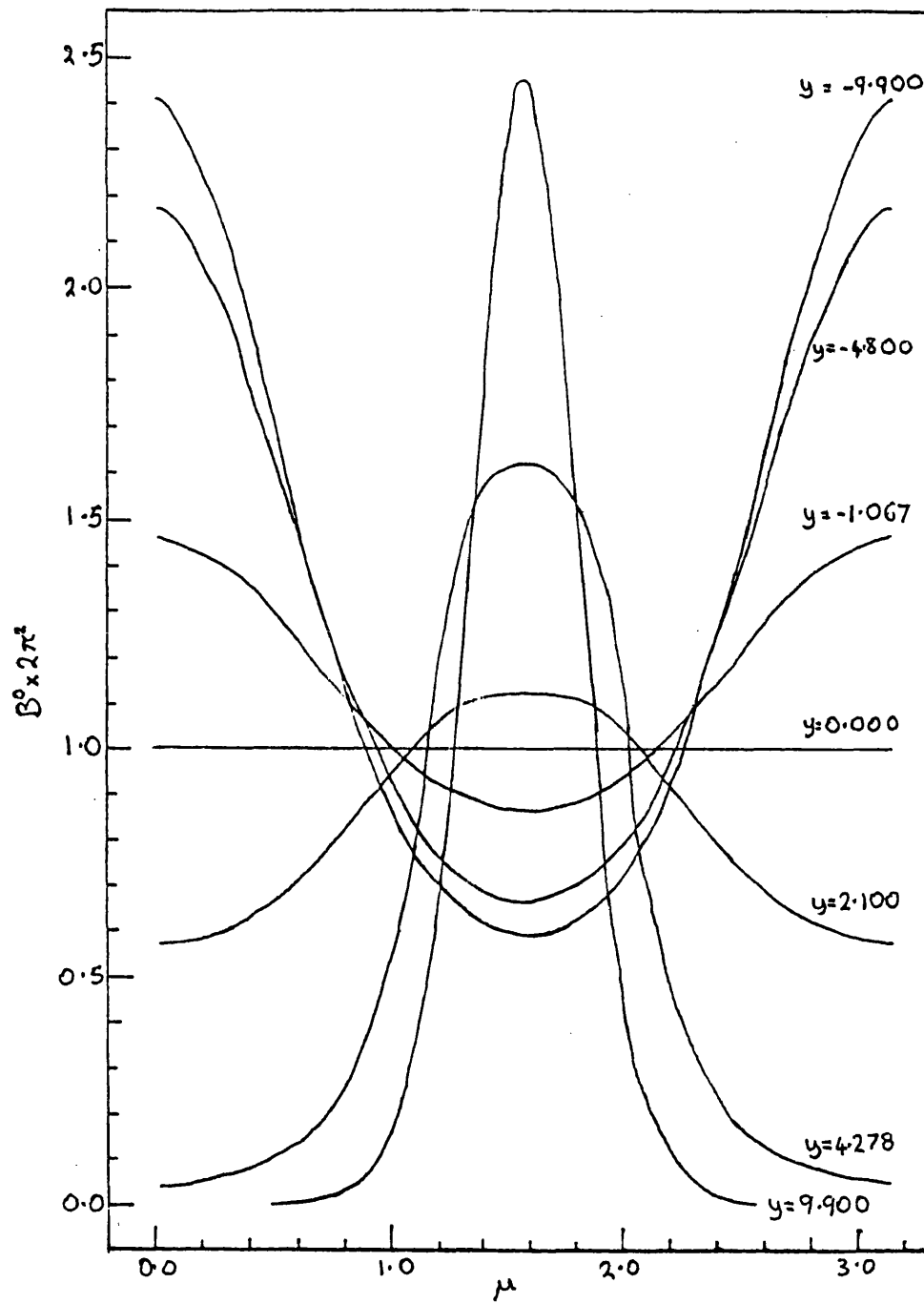
Figure (4.4.4): Plots of $(baryondensity) \times 2\pi^2 = B^0 \times 2\pi^2$ versus μ (see text) at $L = 1.0$ and varying values of y.

baryon density at its poles. As the value of y decreases, the curvature at the poles becomes less negative and the skyrmion density increases in this region, though still being peaked at the flattest $\mu = \pi/2$ value for $y > 0$. As y continues to decrease to negative values, the baryon density continues to increase at the poles and to decrease at $\mu = \pi/2$. At $y = -9.9$ the skyrmion is localised about both poles symmetrically, though this localisation is less pronounced than that about $\mu = \pi/2$ at $y = 9.9$. Thus, on a disc-like shape at $L = 1$, the skyrmion prefers to sit on the flattish poles, while on the high curved rim it has a reduced but finite baryon density. This is a consequence of the symmetric relation (4.3.17), which results in the boundary condition,

$$f(\pi/2) = \pi/2, \qquad\qquad (4.4.5)$$

and prevents a complete depletion of the baryon density on the rim at $\mu = \pi/2$. Thus, in conclusion it is as we expected, at a volume of space corresponding to $L = 1$, the skyrmions response to local variations in the curvature is marked. Also as we expected, it prefers to localise on the flattish region of space and avoids as far as possible the highly curved regions of space.

Figure (4.4.5) shows the local variation of the scalar curvature, R, at $L = 1$ for values of y corresponding to those in Figure (4.4.4). Comparing the two does indeed reveal that the baryon density, on regions of space with curvature less than the optimal -6, is greater than that on the less favourable, highly curved regions of space. Hence, for $y = 9.9$, this flattish region of space which
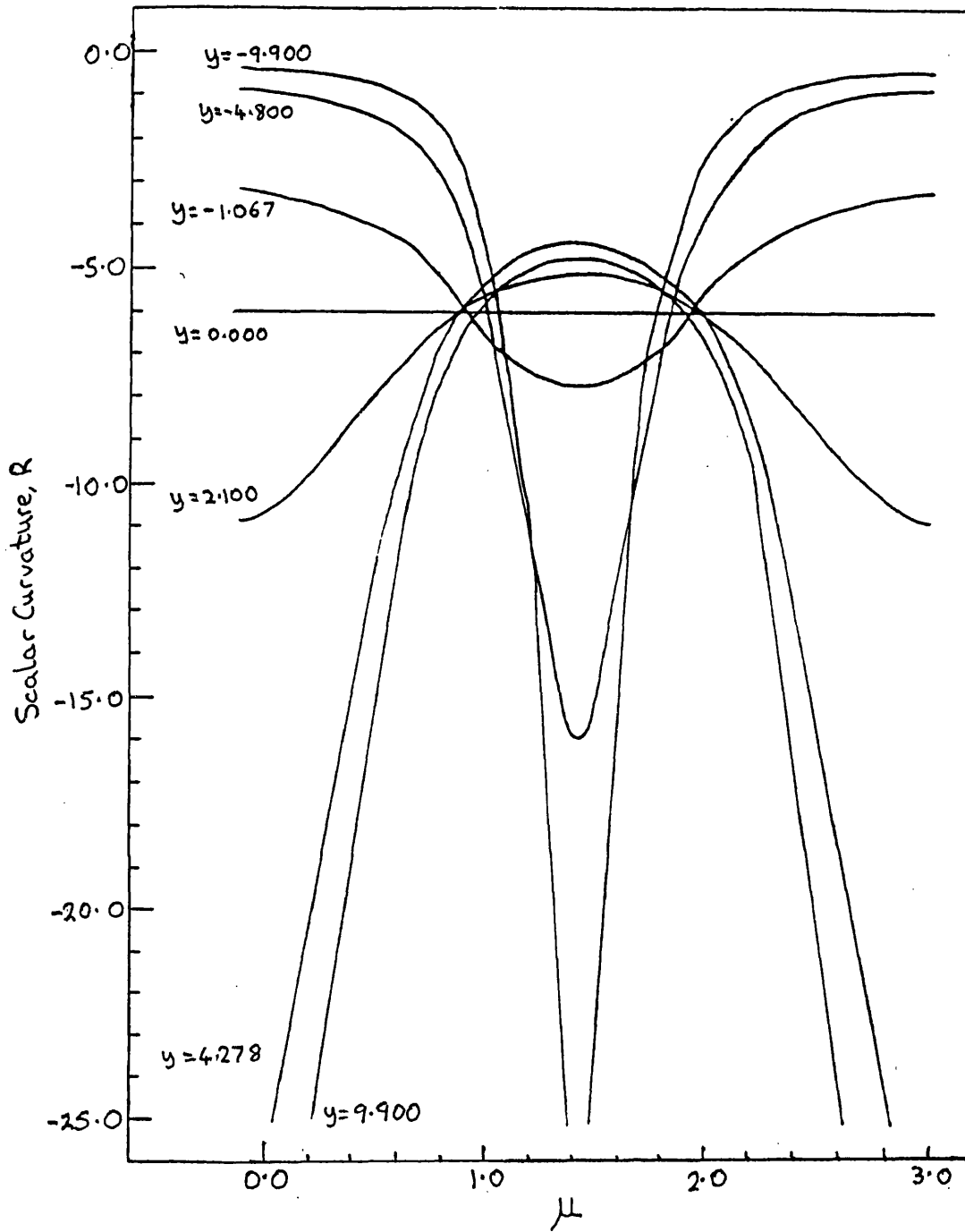
Figure (4.4.5): Plots of scalar curvature R, versus μ at $L = 1.0$ and varying values of y.

occurs in the range $1.1 < \mu < 2$, is seen to correspond to the region of space in which the baryon density resides, while outside this region the baryon density was indeed found to be zero. At $y = -9.9$, the optimal values of the curvature occur at $\mu \sim 1.21$ and $\mu \sim 1.93$ and the skyrmion is expected to sit on the two disconnected regions $0 < \mu < 1.21$ and $1.93 < \mu < \pi$, where the curvature is greater than or equal to -6. Indeed, a high proportion of its density is contained within these segments but not all, as a consequence of the boundary condition (4.4.5).

In Figure (4.4.6), we show the baryon density, (solid lines), at $L = 1.2$ at the values of $y = 9.9$, 4.278 and 0. For a direct comparison we also include on the same plot a local curvature (dashed lines) for these shapes. The second, $y = 4.278$ curve, (dot-dashed line), shows the baryon density of a non-symmetric solution.

Once again, in the symmetric phase for positive values of y, the baryon density is localised about the flattest $\mu = \pi/2$ points. At this volume, both the $y = 4.278$ and $y = 9.9$ curves show the baryon density to be almost completely localised in a region of space where the curvature is greater than -6. The increased localisation as L increases to 1.2, in the optimal $R > -6$ regions of space, reflects the increased volume of space. At a volume of 1.0 the skyrmion density for $y = 9.9$ experiences compression, being forced to sit on regions of space where the curvature was less than -6. At $L = 1.2$, this compression has been dissipated and this is reflected in its energy being close to its minimum value at this volume and
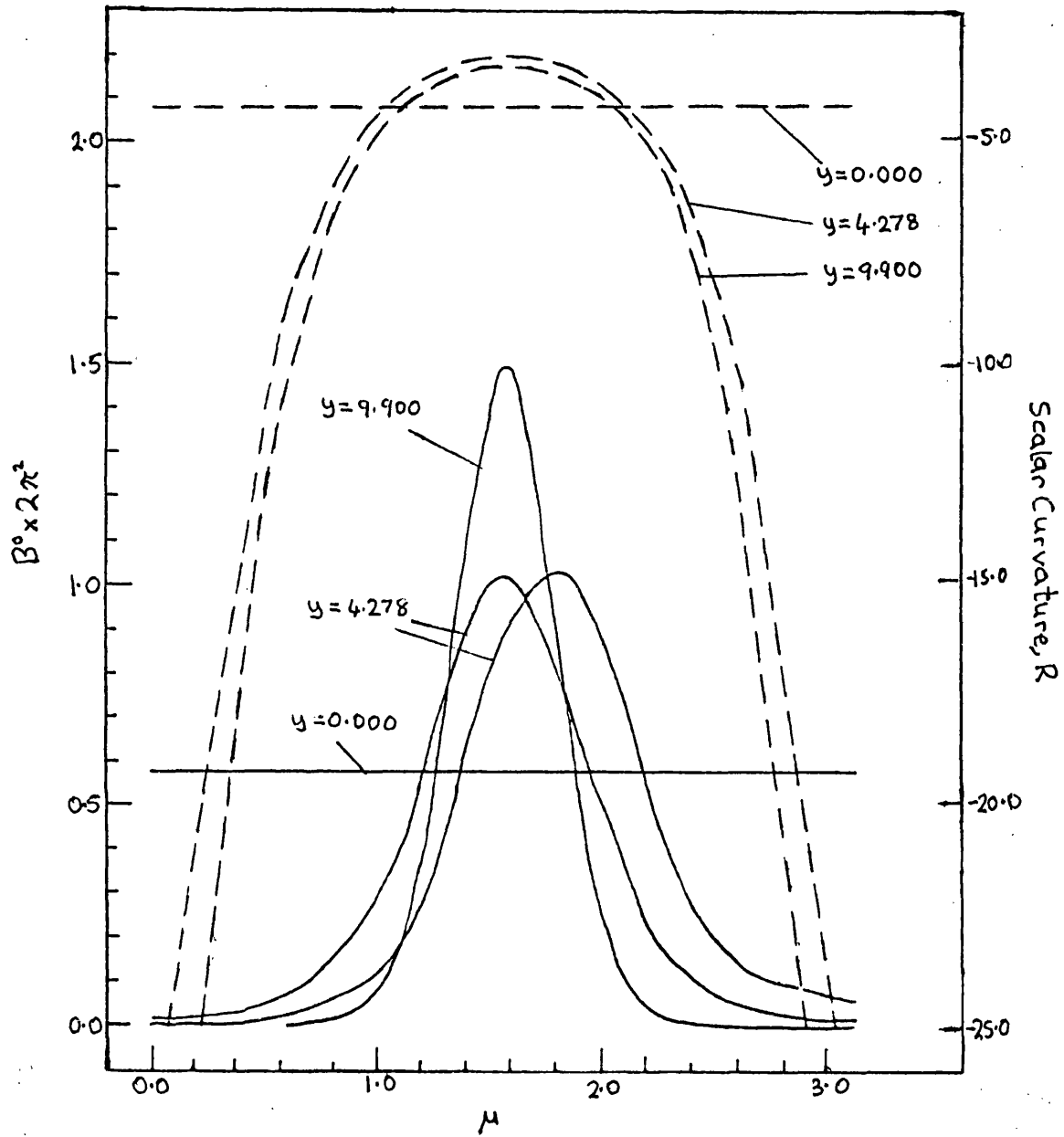
Figure (4.4.6): Plots of both $B'' \times 2\pi^2$, (solid lines) and scalar curvature R, (dashed line), versus μ (see text) at $L = 1.2$ for various values of y.

hence, the value of L being close to $L_{min} \sim 1.17$ at this value of y. The $y = 4.278$ non-symmetric density is seen to have moved towards a pole, as expected, in this case the $\mu = \pi$ pole, there of course being a corresponding solution which moves towards the $\mu = 0$ pole. However, for $L = 1.2$, the extent of pole localisation is small, the phase transition density for this value of y occurring at a value of $L = L_c = 1.18$. Moreover, we see that the localisation at the pole has been suppressed by the large negative curvature in these regions. Thus, the non-symmetric skyrmion has translated the bulk of its baryon density towards a $R = -6$ point, allowing a small but finite amount at the $\mu = \pi$ pole.

It should be clear by now that the localising-delocalising description of the phase transition, so obvious for the $S^3_{phy}(L)$, is misleading for spaces with highly varying local curvature, the symmetric phase solution also having a high degree of localisation. Thus, we choose to characterise the phase transition from symmetric to non-symmetric solutions in terms of the symmetry expression in equation (4.3.27) and whether or not a solution has this symmetry.

In Figure (4.4.7), we show the baryon density (solid lines) and curvature (dashed lines) in the non-symmetric phase at values of y between 9.9 and 0.975 and at a value of $L = 1.4$. The completely delocalised solution on $S^3_{phy}(L)$, $y = 0$, is also indicated on the plot. For comparison, in Figure (4.4.8) we show the baryon density for the symmetric phase for values of y between -9.9 and 9.9. At the value of $L = 1.4$ the curvature has been reduced substantially. For a non-symmetric skyrmion, as y increases, its density at π pole is seen to

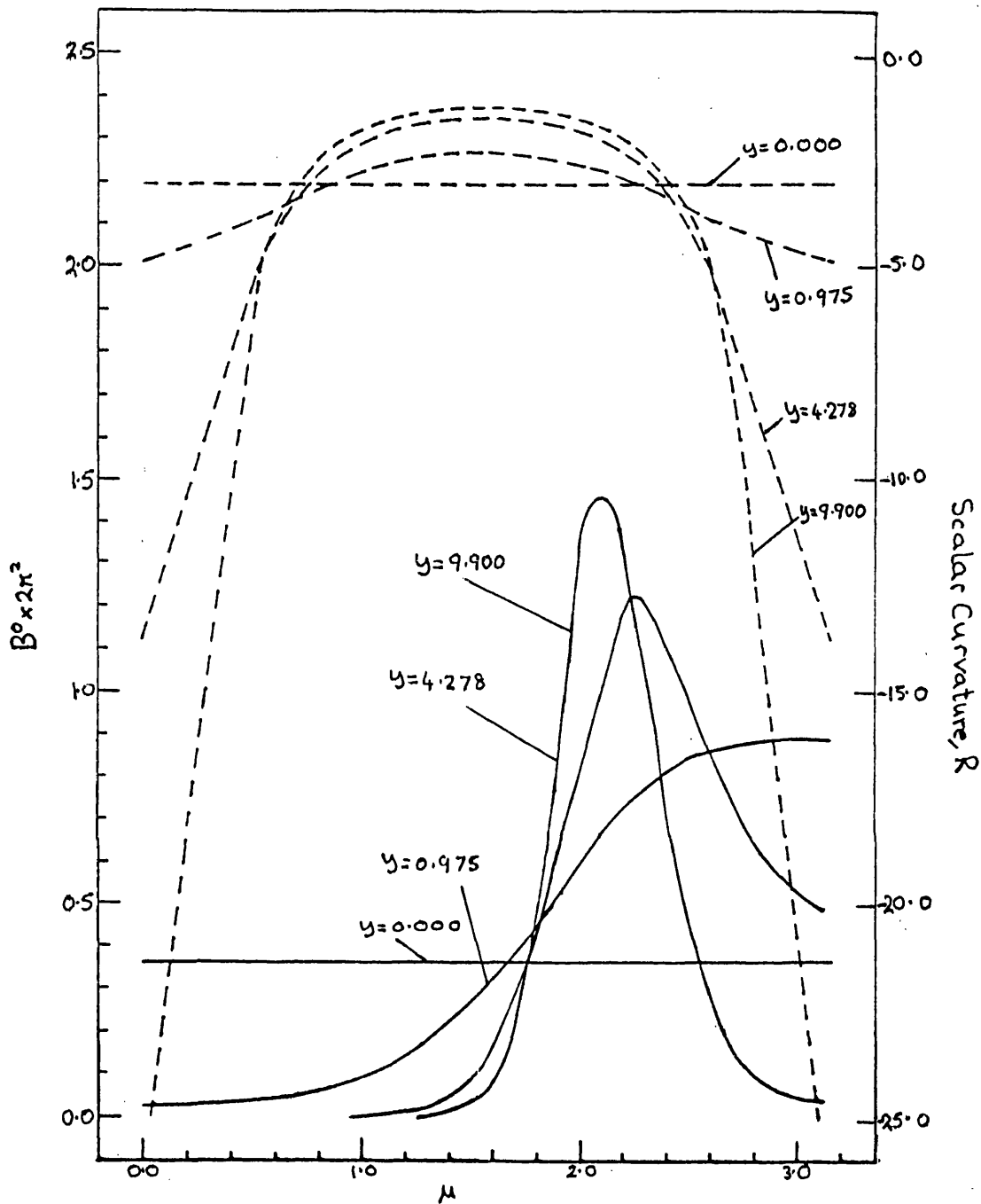**Figure (4.4.7):** Plots of both $B'' - 2\pi^2$, (solid lines), and the scalar curvature R, (dashed line), versus μ (see text) in the non-symmetric phase at $L = 1.4$ for various values of y. The symmetric phase curve at $y = 0$ is also plotted.
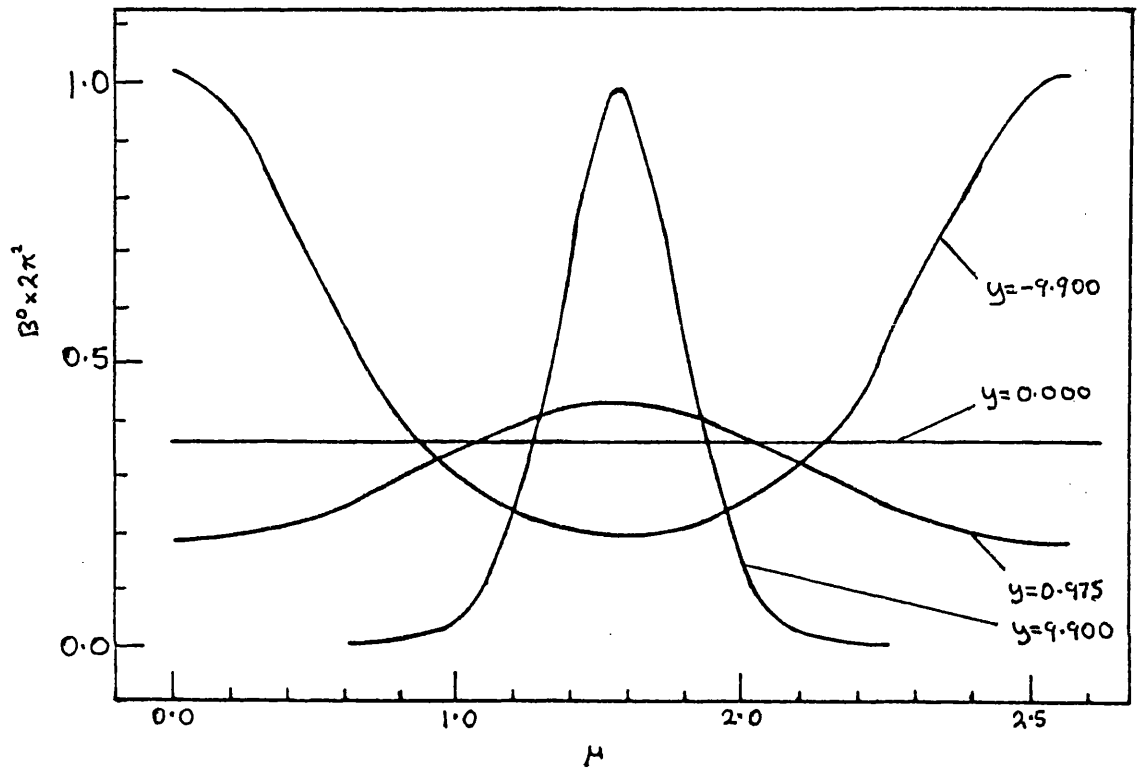
Figure (4.4.8): Plots of $B^0 \times 2\pi^2$ versus μ in the symmetric phase at $L = 1.4$ for various values of y.

deplete as the curvature decreases. Thus, at a value of $y = 0.975$ the curvature of space never reaches the optimal -6 value and the density is a maximum at the pole, where the curvature is closest to this value and well spread over the flattish lower hemisphere of space. The corresponding symmetric solution has a fairly delocalised skyrmion with a finite density over the whole of space peaked at $\mu = \pi/2$. The gain in energy in the non-symmetric phase is small, about $0.002 \times 12\pi^2$. The baryon density of the non-symmetric phase solution becomes increasingly localised at $y = 4.278$, about a point with $R = -2.4$, near the π pole. The density at the π pole is now reduced, but still high, with the optimal curvature point at $\mu = 2.61$ close to the pole. Comparison with Figure (4.4.6) shows the density has now translated towards the pole at this increased volume. At $y = -9.9$, the curvature is high at the poles and the skyrmion centres on a $\mu \sim 2.1$ point, at which $R = -1.18$ and has a finite density at the $R = -6$ point. Its highly peaked nature allows more of the skyrmion to sit on a region of space with curvature closer to the optimal -6, as opposed to the symmetric skyrmion (4.4.8), which sits entirely within the $R = -6$ points which enclose a flattish hemispherical region of space. The larger gain in energy, of about $0.009 \times 12\pi^2$, of the symmetric skyrmion, is a reflection of the symmetric skyrmion's inability to stretch from the $\mu = \pi/2$ to the optimal $\mu \sim 0.55$ and $\mu = 2.59$ points at this large volume. This stretching was not necessary at $L = 1.2$ when both phases had similar energies. The $y = -9.9$ symmetric density plot shows the skyrmion density peaked at the poles and the $R = -6$ points indicated on this curve,

showing that the skyrmion tries to deplete its density on the highly curved rim as far as possible.

The form of the symmetric profile function $f(\mu)$ (solid lines) is indicated in Figure (4.4.9) at y values of 9.9, 0.0 and -9.9 for $L = 1.4$. At $y = 9.9$ we have included the non-symmetric solution, (dashed line). We see that the slope of the profile varies considerably in response to rapid changes in curvature as μ varies at the 9.9 and -9.9 values of y. At $y = 9.9$ the slope of the symmetric solution is small at both poles and thus, the baryon density is very small in this highly curved region. About $\mu = \pi/2$ it has a large slope and hence its baryon density is localised in this region about $\mu = \pi/2$, as was seen in Figure (4.4.8). At -9.9 the reverse effect is observed, with a large slope at the poles and a reduced slope at the $\pi/2$ on the highly curved rim and hence the baryon density of Figure (4.4.8) results. At 9.9 the non-symmetric profile has a negligible slope from $\mu = 0$ to about $\mu = 1.0$ and hence its baryon density is almost zero on this highly curved region of space. The slope is now large and fairly constant in the $\mu \sim 2.1$ region and thus the baryon density is heavily peaked in this region of space. At the π pole the slope is small but finite and hence, so is the baryon density. This was seen to be the case in Figure (4.4.7). The two $y = 9.9$ curves appear to be parallel in the $f \sim \pi/2$ regions and this non-trivial effect seems to be related to the manner in which the baryon density translates in bulk from the symmetric to the non-symmetric solutions on the needle-like shape.

In Figure (4.4.10), we show plots of the non-symmetric profiles $f(\mu)$, for values

171
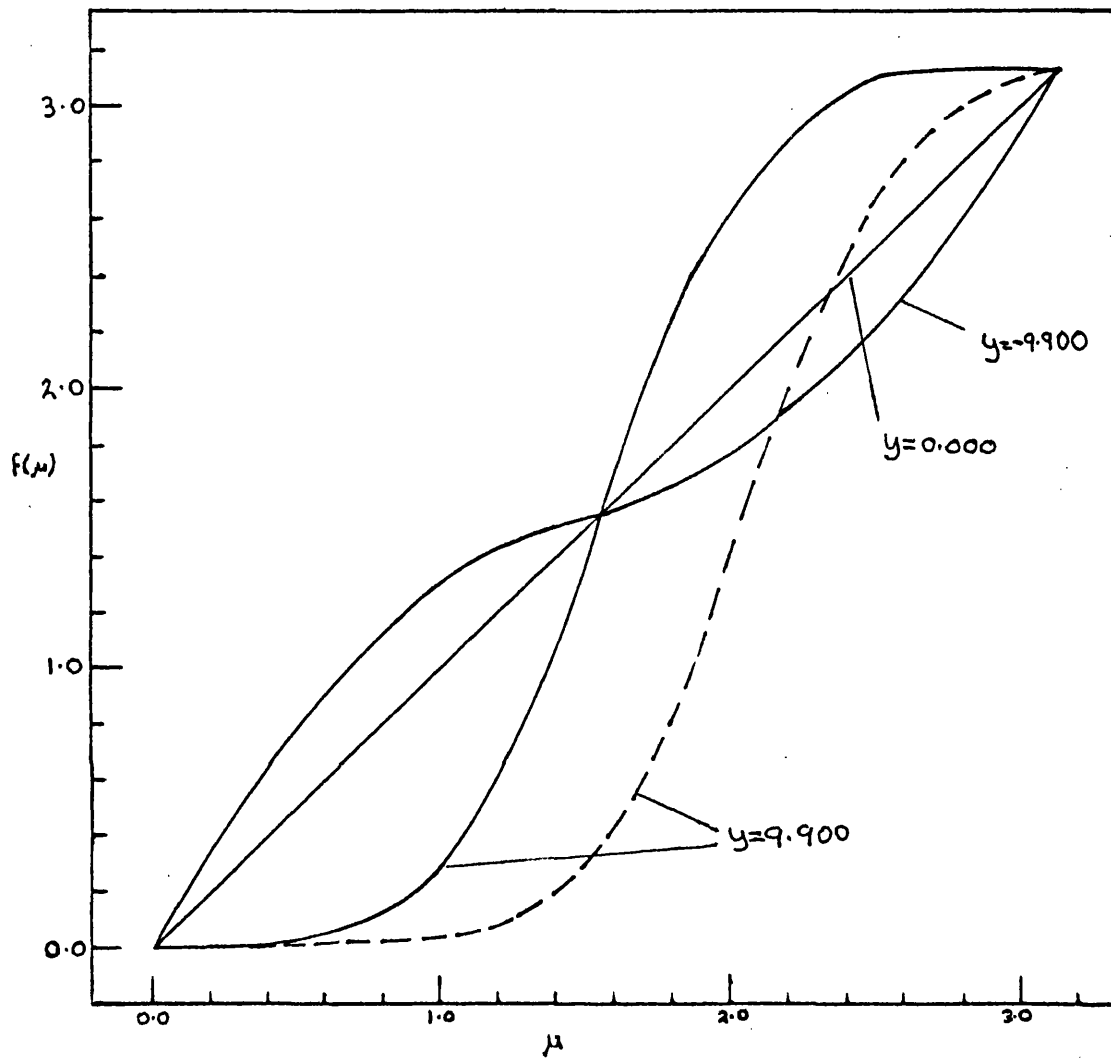
Figure (4.4.9): Plots of the profile function $f(\mu)$, versus μ (see text) at $L = 1.4$ for various values of y. Both the symmetric phase's, (solid lines) and the nonsymmetric phase's, (dashed lines), profile functions are plotted.

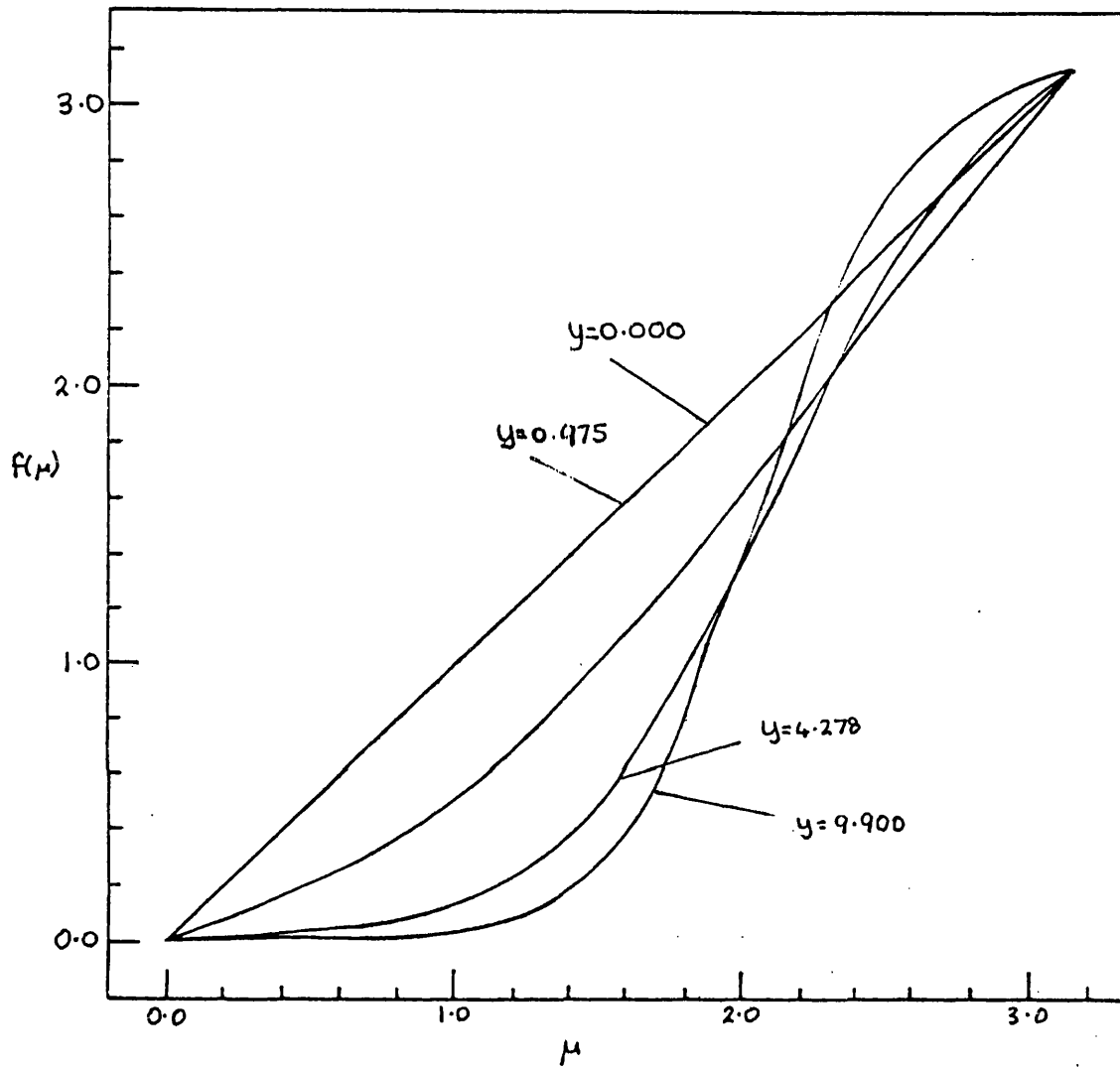**Figure (4.4.10):** Plots of the profile function $f(\mu)$ in the non-symmetric phase, versus μ at $L = 1.4$ for various values of y. The line $f(\mu)$ is also included, corresponding to the trivial mapping of S^3_{phy}, (see text).

of $y = -9.9$, 4.278 and 0.975, at a value of $L = 1.4$. Here we see clearly, that as y increases the profile 'buckles' at the π pole in order to reduce its slope there and hence its baryon density decreases as the curvature at this pole becomes large.

As L is increased beyond 1.4, local curvature effects becomes less significant as space flattens out. At large volumes the unfavourable response of a skyrmion to stretching becomes important. In the symmetric phase a skyrmion will need to stretch significantly in order to reach any regions of optimal curvature which exist. Thus, we found this phase to be significantly unfavourable for values of y greater than -4.8 at $L = 1.6$, as can be seen clearly in Figure (4.4.3).

In Figure (4.4.11) we show the non-symmetric phase (solid lines) baryon densities and curvature (dashed lines) for y values of -1.067, 0.0 and 0.975. These are heavily localised at the π pole to avoid stretching over a large region of space. For $y = 0.975$ the curvature is closest to the optimal -6 value at the poles, while at $y = -1.067$, at the poles it is furthest form its optimal value. This is reflected in the energy of the $y = 0.975$ solution, having an energy $0.017 \times 12\pi^2$ less than that at $y = -1.067$.

For values of y less than zero, the curvature of space is highest on the rim at $\mu = \pi/2$. At this volume, the curvature at this point is smaller in magnitude than -6. Thus, we would expect the density to peak about the $\mu = \pi/2$ point. However, this rim has a large diameter and would require the skyrmion to stretch significantly in order to sit there and is thus unfavourable. This resistance to stretching would however be overcome if the skyrmion were to localise about
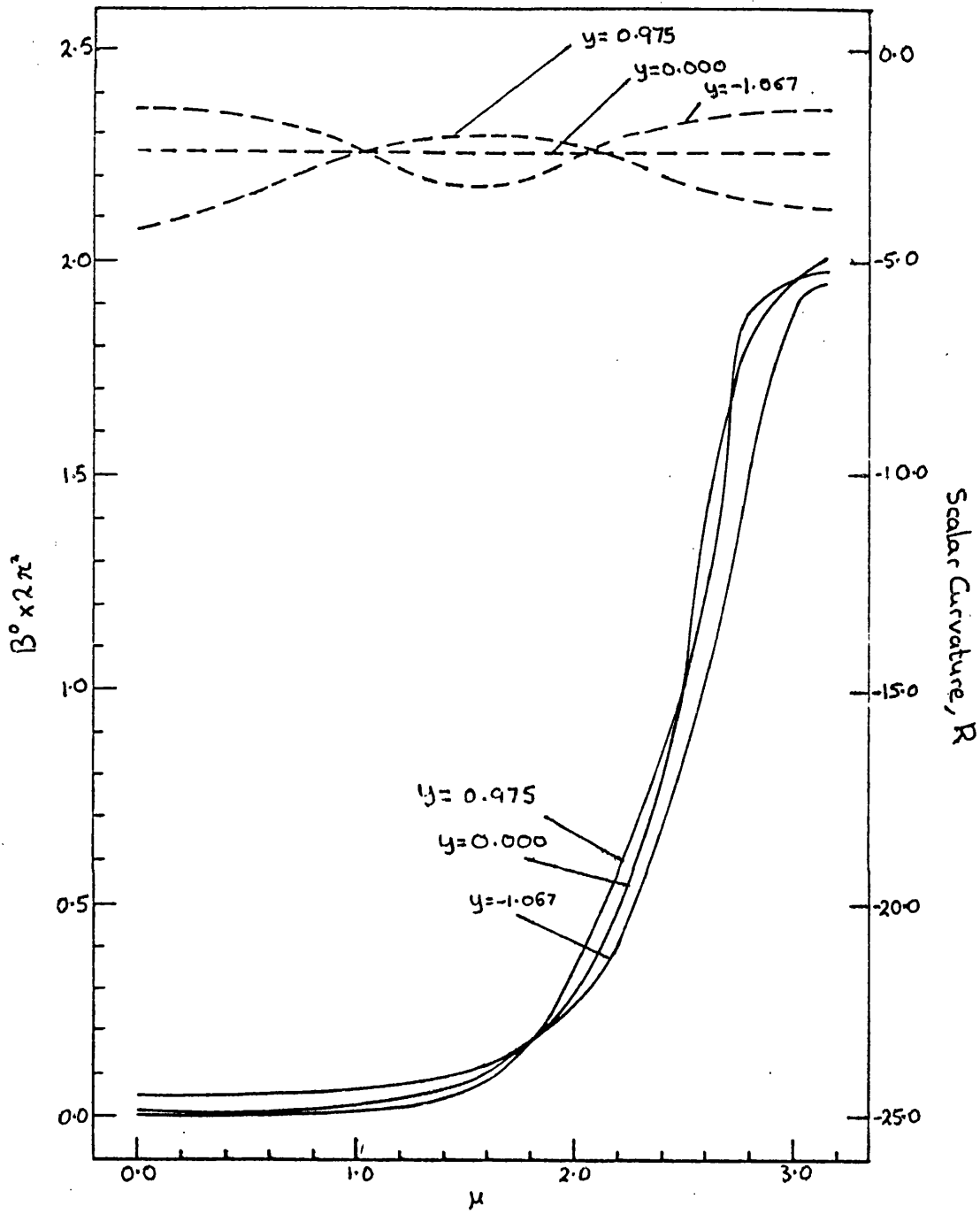
174

Figure (4.4.11): Plots of both $B^0 \times 2\pi^2$, (solid lines), and the scalar curvature R, (dashed line), versus μ (see text) in the non-symmetric phase at $L = 1.6$ for various values of y.

a point on this rim. However, by employing the hedgehog ansatz we have not allowed it to. Thus, the unfavourability of the disc-like shapes, as compared to the needle-like shapes may be a consequence of our constrained hedgehog form which only allows the skyrmion to localise about a pole in the non-symmetric phase.

Thus in conclusion, we see that the local curvature effect leads to many interesting features of dense baryonic matter on the ellipse. Indeed, in terms of the local curvature and response of a skyrmion to compression and expansion, we have been able to understand the reason for these effects.

The local curvature enhances the localisation of the skyrmion, enabling it to sit on regions of space where the curvature is closest to the optimal value -6, although avoiding unfavourable regions with curvature less than this optimal value. Our needle-type deformation of $S^3_{phy}(L)$, with the hedgehog form, is seen to enhance these effects, whereas for disc-like deformations the boundary conditions of the symmetric phase prevent complete depletion from the unfavourable regions occurring on its hemisphere, the rim. In the non-symmetric phase, the hedgehog form and also the unfavourable stretching of this hedgehog at high volumes, prevents the skyrmion from sitting on this rim when it would be favourable. Thus, the hedgehog on a 'disc' has its symmetric - non-symmetric phase transition suppressed to higher volume as large energy gains are not possible. The large gains in energy, for large positive values of y as the symmetry is broken, are reduced as y becomes very large and as the points at which the optimal curvature of -6

176

occur, they progressively move towards the $\mu = \pi/2$ points. At large enough volumes no such $R = -6$ optimal points exist, space being flatter and skyrmions localise about a pole for all values of y.

In the limit $y \mapsto -\infty$, ie. the disc, there are two competing skyrmion arrangements. In the symmetric phase two half skyrmions exist in this limit, each of which is on the flat regions of space, centred about the poles. On the rim of this disc, the symmetric boundary condition $f(\pi/2) = \pi/2$, must be satisfied. In the non-symmetric phase a localised skyrmion sits on one of these flattish regions about a pole, while on the opposite flat region, a value of $f(\mu) = 0$ or π results. Thus, in this region of space the skyrmion has its trivial vacuum value and the energy density is zero. Hence, in this limit $f(\mu)$ will satisfy the additional boundary condition $f(\pi/2) = 0$ or π, on the discs infinitely curved rim. In the infinite volume of $L \mapsto \infty$, only the non-symmetric phase solution will exist, since the symmetric phase solution has an infinite energy. This is due to the symmetric boundary condition $f(\pi/2) = \pi/2$, which results in the skyrmion having a small but finite energy density on the rim of this disc and since this rim has an infinite radius in this limit it has an infinite energy.

Thus, in this limit only the non-symmetric phase solution will exist and this corresponds to the usual skyrmion on flat space, R^3, with the physical vacuum boundary condition on the rim of this disc. On the other side of this disc there will be a region of trivial vacuum field. This is analogous to the infinite volume limit of $S^3_{phy}(L)$ corresponding to the usual flat space hedgehog.

However, as the volume of space is decreased, while still in the limit $y \mapsto \infty$, the radius of the rim will reduce to a finite value. Thus, at some finite value of L, the symmetric phase limit should also exist and for values of L up to 1.6, we numerically found only symmetric solutions to exist. These symmetric solutions correspond to two half skyrmions, each separately within a spherical surface whose radius is equal to the radius of the disc's rim. This being the case, we can see that this limit has already been described by Goldhaber and Manton [9] as half skyrmions in flat space.

He found there to be an optimal radius, r_0, of this spherical boundary surface which corresponds to a value of $L_0 = 1.037$ and gives an energy $E_0 = 1.015 \times 12\pi^2$, for two such half skyrmions. Employing our approximate conformal ansatz, (4.3.25), we can take this limit of our ellipse numerically. We find, for a value of the rim radius r_0, with $L_0 = 1.037$, the value of E_0 to be equal to Manton's value, to the same number of significant figures were quoted by him. Thus, we see that in this limit our conformal ansatz provides a good approximation to the true solution. Moreover, this result certainly suggests that since the half skyrmion concept is important in understanding flat space arrays, that the skyrmion on a disc offers an even better model than the $S^3_{phy}(L)$ model of dense skyrmionic matter.

In the $y \mapsto \infty$ limit, our results suggest that only the symmetric phase will persist, as the high curvature at the pole forces the non-symmetric skyrmion to the $\mu = \pi/2$ points. Our contour plots, Figures (4.4.1) and (4.4.3), suggest the

178

energy of this skyrmion, which sits on a cylindrical region of space, will be about $1.03 \times 12\pi^2$ and this value will be insensitive to the value of L. However, one must be careful in taking this limit, as for large enough values of L, the skyrmion will clearly localise about a pole. In the $y \mapsto \infty$ limit the curvature behaves like:

$$R \sim -\frac{y^{1/3}}{L^2}. \qquad (4.4.6)$$

Thus, in the infinite volume limit, when y increases faster than L^6, the resulting curvature is infinite at all points of space. When y increases slower than this, the curvature will tend to zero over the whole of space (except at the poles) and the usual flat space skyrmion will result. However, in the limit when y increases as L^6, a finite curvature of space will result (again except at the poles). Thus, in this limit we expect both phases to coincide. This limit should correspond to a skyrmion on a cylinder.

Concluding, we see that the local curvature acts as an effective non-isotropic compressor on dense skyrmionic matter, where the isotropic compression is produced by the volume. Thus we see, that the effect of isotropic bulk compression and expansion of skyrmionic matter, does indeed have an analogue in the elliptical deformations of $S^3_{phy}(L)$, just as changing the volume of physical space is analogous for isotropic compression and expansion.

As we have already noted, at the delocalising phase transition point, $L = L_c = \sqrt{2}$ for the trivial map on $S^3_{phy}(L)$, an infinitesimal conformal transformation of the fields will be the mode of steepest descent. Moreover, as we have also seen in

Section 4.1, a finite version of this conformal map, (4.1.19), gives a good approximation to the true solutions energy for all values of L above $\sqrt{2}$. We also noted that such a generalised finite conformal mapping exists on the ellipse (4.3.25) and that at the $L = L_c = \sqrt{2}$ point, the infinitesimal version of this mapping gives the softest mode for elliptical space deformation. Thus, it is of interest to compare this finite form with the true solution for varying values of y.

Figure (4.4.12) shows the symmetric ($\alpha = 1$) version of this ansatz, (solid line), and the exact solution, (dashed line), at a value of $L = 1.4$ and for values of y in the range 9.9 to -9.9 from $\mu = 0$ to $\pi/2$. Since the ansatz is exact at the end point and the point $\mu = \pi/2$, the maximal discrepancy occurs in the region $\mu \sim \pi/4$ (and $\mu \sim 3\pi/4$). At $y = 0$, this ansatz reduces to the exact solution. At $y = -9.9$ it is also indistinguishable from the exact solution, agreeing with our suggestion that as $y \mapsto -\infty$ it becomes exact. This is analogous to the fact, that in flat space the usual discrepancy in a conformal-like ansatz occurs in the skyrmion tail, but for this half skyrmion on flat space, the $\sigma = 0$ boundary condition does not require such a tail behaviour and indeed, as $y \mapsto -\infty$, the flat space half skyrmion results.

For small values of y the ansatz is also indistinguishable at values of 0.975 and -1.067. As y increases however, a large discrepancy develops, so that at a value of $y = 9.9$ the ansatz is significantly different from the true solution near $\mu = \pi/4$. This is because the ansatz does not compensate correctly for the large local curvature effect present on such a needle-like surface. Hence, in
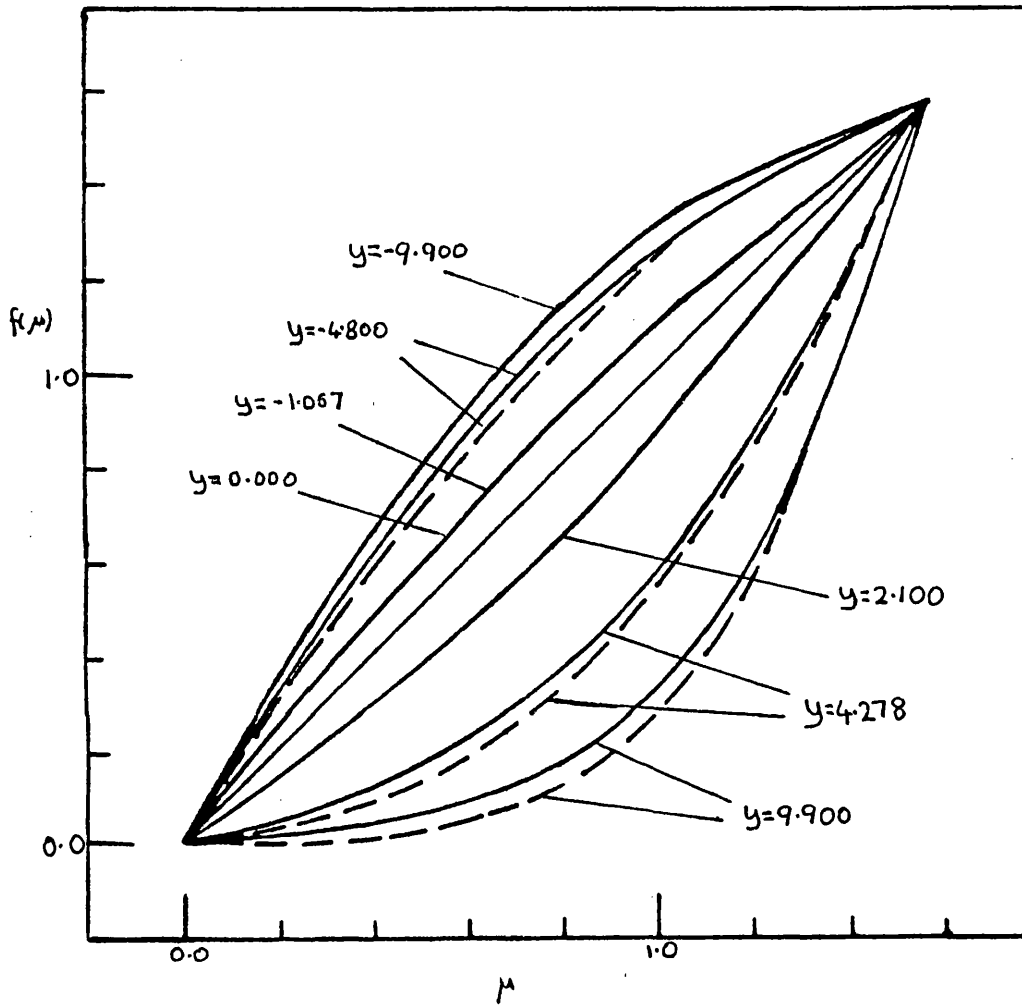
Figure (4.4.12): Plots of the profile function $f(\mu)$ in the symmetric phase, at $L = 1.4$ for various values of y. The solid lines correspond to the approximate finite conformal ansatz given in expression (4.3.25),while the dashed lines correspond to exact numerical solutions.

conclusion, we suspect this ansatz or an extended version as Jackson et al [10] considered, might be able to reproduce much of the data presented here. Moreover, as argued by Jackson et al in the case of their $S^3_{phy}(L)$ ansatz, such forms give clues to the type of ansatz required to reproduce flat space array results.

4.5 A Skyrmion On A More General Closed Surface

Having found there to be many interesting features of dense skyrmionic matter on an ellipse and some justification for the belief that local curvature effects mock the flat space array environment, we shall now finally consider a skyrmion on a more general shaped closed surface.

We have in mind to allow the shape of physical space to vary as well as the mapping, so as to minimise the energy. As we have already mentioned, such a general calculation will have pathological elements, since there are no terms in the Skyrme energy functional for a static field, (4.1.8), which determine the shape of space. Our numerical calculations will reveal this problem and we will present some consequences and a possible resolution to this problem.

We shall consider a $B = 1$ hedgehog on a closed surface, parameterised as:

$$r^2 = x^2 + y^2 + z^2 + w^2, \qquad (4.5.1)$$

with r, the radius of this three dimensional surface, embedded in R^4 which can vary from point to point. (x, y, z, w) are Cartesian coordinates of R^4.

To simplify our numerical calculations, we choose to constrain this three

surface such that in polar coordinates (μ, θ, ϕ), its radius function r depends only on μ. This allows us to evoke the hedgehog ansatz as a sensible mapping. Thus, the polar coordinates and the Cartesian coordinates in R^4 of this surface are related by:

$$
\begin{aligned}
w &= r(\mu)\cos\mu, \\
x &= r(\mu)\sin\mu\cos\theta, \\
y &= r(\mu)\sin\mu\sin\theta\cos\phi, \\
z &= r(\mu)\sin\mu\sin\theta\sin\phi,
\end{aligned}
\qquad (4.5.2)
$$

where r is a function of μ alone.

In order to fix the centre of this surface we choose to impose the condition on $r(\mu)$, that

$$
r(0) = r(\pi). \qquad (4.5.3)
$$

Moreover, since we are naturally only interested in smooth manifolds, we are interested in surfaces satisfying the smoothness boundary conditions

$$
r \sim L_0 + \beta\mu^2 \qquad\qquad \mu \sim 0 \qquad (4.5.4)
$$

and

$$
r \sim L_0 + \gamma(\pi - \mu)^2, \qquad\qquad \mu \sim \pi \qquad (4.5.5)
$$

where $2L_0$ is the length of the shape along the w-axis and the constants β, γ determine the quadratic behaviour at the poles of the three surface.

As stated, we can now sensibly consider a skyrmion in the standard hedgehog form given by,

$$\sigma = \cos f,$$

$$\pi_x = \sin f \cos \theta,$$

$$\pi_y = \sin f \sin \theta \cos \phi,$$

$$\pi_z = \sin f \sin \theta \sin \phi, \qquad (4.5.6)$$

where the profile function of f is taken to be a function of μ only. Here, $B = 1$ boundary conditions are identical to those given in equation (4.3.11) and the end point behaviour of the profile is also assumed to be of the form given in equation (4.4.1) for the profile function of the ellipse.

The metric on physical space is now observed to be diagonal with elements,

$$\left(\dot{r}^2 + r^2, r^2 \sin^2 \mu, r^2 \sin^2 \mu \sin^2 \phi\right) \qquad (4.5.7)$$

and the measure given by,

$$r^2(\dot{r}^2 + r^2)^{1/2} \sin^2 \mu \, d\mu \, d\theta \, d\phi. \qquad (4.5.8)$$

The deformation matrix is also diagonal with eigenvalues:

$$\lambda_1^2 = \frac{\dot{f}^2}{\dot{r}^2 + r^2} \qquad (4.5.9)$$

and

$$\lambda_2^2 = \lambda_3^2 = \frac{\sin^2 f}{r^2 \sin^2 \mu}, \qquad (4.5.10)$$

184

where $\dot{f}$ and $\dot{r}$ denote derivatives with respect to μ. Thus, the Skyrme Model's static energy functional, given in equation (4.1.8), takes the form:

$$E = 4\pi \int_0^\pi d\mu L^2 \sin^2 \mu (\dot{r}^2 + r^2)^{1/2} \left(\frac{\dot{f}^2}{\dot{r}^2 + r^2} + \frac{2\sin^2 f}{r^2 \sin^2 \mu} \right)$$
$$+ 4\pi \int_0^\pi d\mu L^2 \sin^2 (\dot{r}^2 + r^2)^{1/2} \frac{\sin^2 f}{r^2 \sin^2 \mu} \left(\frac{2\dot{f}^2}{\dot{r}^2 + r^2} + \frac{\sin^2 f}{r^2 \sin^2 \mu} \right), \qquad (4.5.11)$$

here we have also performed the trivial θ, ϕ integrations.

Since we require the functional forms of f and r, which minimise this energy functional, the resulting Euler Equations will be a coupled set of two equations which will both be ordinary second order differential equations. However, such a minimisation procedure results in a pathological problem. The resulting equations and the boundary conditions for f and r, give more matching parameters than matching conditions. Even after including a Lagrange multiplier, multiplying a volume term to fix the volume of physical space, the problem is not resolved. This of course reflects our failure to have extended the model to include a term which will dictate the shape of physical space.

Thus, we choose to find approximate minimal energy 'solutions' for r and f by choosing variational forms for these functions and minimising the energy with respect to the parameters within these forms. Clearly this represents a reasonably well defined problem. However, we must expect that the pathology may once more rear its head. This technique however, will reveal the nature of this pathology and leads us to further insight in to the nature of the Skyrme functional.

185

We thus choose the convenient, four parameter Fourier type forms for r and f given by:

$$r(\mu) \;=\; L_0\{1 + \sin\mu(c_1\sin\mu + d_1\sin 2\mu + c_2\sin 3\mu + d_2\sin 4\mu)\},$$

$$f(\mu) \;=\; \mu + a_1\sin\mu + b_1\sin 2\mu + a_2\sin 3\mu + b_2\sin 4\mu. \qquad (4.5.12)$$

These forms automatically satisfy our boundary conditions. Moreover, we can control the symmetry of space about the equator $\mu = \pi/2$, by the c coefficients in $r(\mu)$ and the non-symmetric phase by the a coefficients.

We further require to minimise r and f for fixed volumes of physical space. Thus, the volume

$$V = \int \sqrt{g} \qquad (4.5.13)$$

is chosen initially and then by calculating the integral (4.5.13), we can then choose L_0, such that the space has the required volume.

The resulting numerical parameter minimisation was performed using the Minew Cern minimisation package. For direct comparison with the ellipse we shall employ the variable L given in equation (4.3.19).

For the values of L up to and equal to 1, the trivial mapping of $S^3_{phy}(L)$ is known to be an absolute minimum of the energy at a given volume in this range. Thus, the eight parameters were found to be zero at these values of L with $L = L_0$. Beyond $L = 1$ the shape of space changes significantly and the pathology rears its head once more.

Since we know that skyrmions prefer to sit on a sphere of radius $L = 1$, that is on regions of space with curvature -6, as we increase L beyond this value this is exactly the behaviour we find. Thus, as we increase the volume, two regions of space develop. One region being taken up by a trivial vacuum and the other is spherical with radius of 1 and on which the skyrmion takes the identity mapping form. Moreover, the shape of the region of space with the trivial vacuum is completely undetermined by the Skyrme energy functional and there is an infinite degeneracy of shape 'solutions' here. This behaviour is similar to a balloon with a weak point, which when blown up expands only at its weak point, though in this case in an arbitrary fashion. This is of course our pathology at work. The energy of such a structure will be equal to the lower bound for all values of L equal and above 1 and thus the volume becomes ineffective in expanding the skyrmion.

Thus, at a value of $L = 1.3$, our variational minimisation gives the shape and mapping depicted in Figure (4.5.1). Here we have chosen to represent the shape on the Cartesian axis. Choosing the $\theta = 0$ cross-section, we plot the value of w against $x = (x^2 + y^2 + z^2)^{1/2}$. As the angle μ varies, the value of $f(\mu)$ at the corresponding point on the cross-section varies over a unit circle and the points on these circles are represented by the lines protruding from the smooth curve. Thus, it leads to a revealing pictorial representation of the data for a hedgehog solution.

Examination of Figure (4.5.1) shows the upper and lower halves of space are
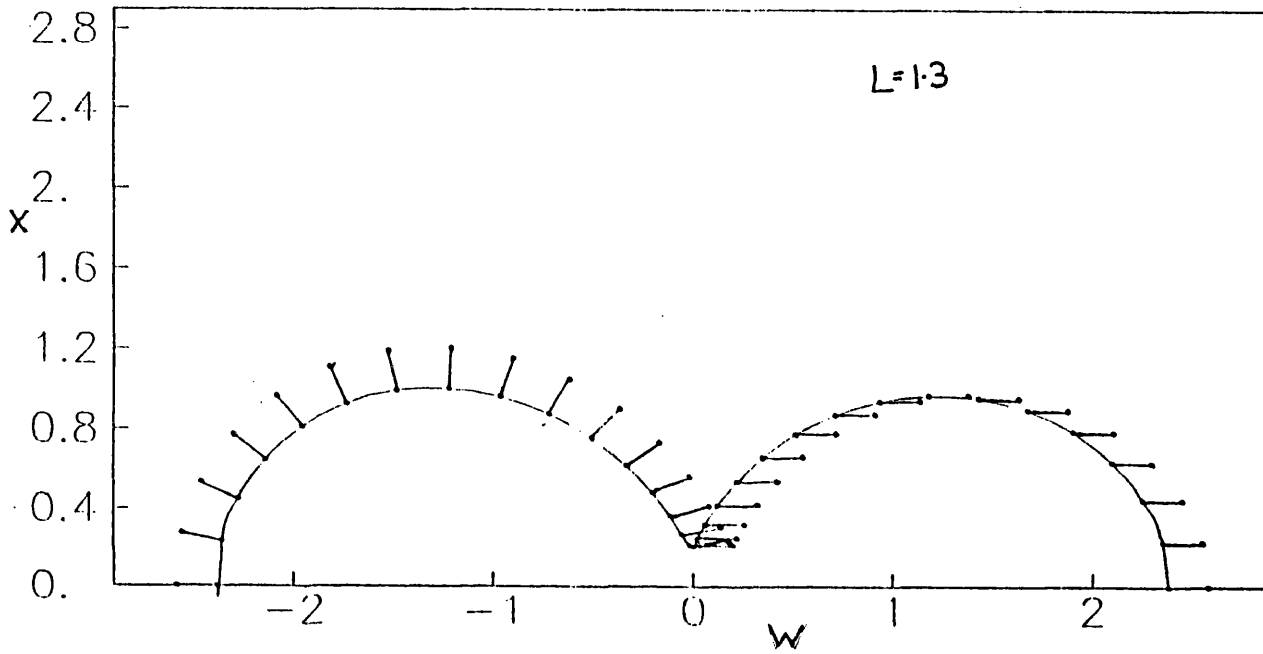
Figure (4.5.1): Plot of the $\theta = 0$ cross section through physical space in the (w, x) plane of R^4, (see equation 4.3.3), at $L = 1.3$. The spines indicate the hedgehog skyrmion's 'profile angle' $f(\mu)$, relative to the w axis at a point of physical space and at a corresponding value of μ. The angle μ, defining a point in space at $\theta = 0$, is measured about the origin from the w axis.

both approximately spherical, with radius ~ 1 and joined at $\mu = \pi/2$ by a sharp 'pinch'. On the lower half of space the hedgehog is 'radial' and hence approximately takes the identity map form. On the lower half of space f is approximately zero and the trivial vacuum with zero baryon density exists. The smoothness and nature of the upper half of space is a consequence of our parametric form and not a consequence of the model. As we expected, this structure gives an energy very close to the lower bound with value $1.003 \times 12\pi^2$.

This phenomena is thus the analogue of the phase separation phenomenon of dense crystalline matter as its average baryon density is increased, discussed by Kugler et al [11]. As we apply a piston to expand dense baryonic matter, there are two regions of space that exist, one with a skyrmion and one with the trivial vacuum. Thus it would appear, that a skyrmion is rigid against such an expansion. However, as already pointed out, since we have not incorporated kinetic effects and the skyrmions are heavily localised, we expect zero point motions and quantum corrections to be important. Hence, the branch of the energy curve which connects the rarified and dense forms of skyrmionic matter may well be important as a transitive phase of matter.

In Section 4.2, we previously demonstrated, that as the volume of space increases, the sphere with trivial skyrmion mapping is stable to perturbation in both the map and shape of space up to $L = \sqrt{2}$. Thus, this phase separation is not in contradiction with our previous results, since here the type of deformations occurring are not smooth and this phase transition is first order and beyond the

189

region of our perturbative, second order analysis. Moreover, our elliptical space calculation also shows a first order phase transition at a value of $L \sim 1.2$, for the needle-like shape, if we do not constrain the size and hence locality of the metric perturbation of $S^3_{phy}(L)$.

We thus have a rather negative result from these observations and can see that our calculation does not reveal a wealth of interesting shapes of physical space, as global volume effects are not able to overcome the effect of the optimal local curvature. Also, we have not achieved our natural requirement of considering only smooth physical spaces, since we will always have a pinch region.

In order to resolve this difficulty we could imagine adding various terms to the energy, such as the square of the Ricci tensor or its derivative squared, to stop pinching and thus, regions of high curvature. However, this would significantly change the model and has little physical justification. Thus, we choose to try and simply constrain the local curvature such that it is always negative.

The Ricci tensor is diagonal for this metric, with two of its elements less than or equal to the third. Thus, we choose to demand that this third element, the R_{11} component, be less than or equal to zero, so that all three elements of the Ricci tensor will be less than or equal to zero. Thus the resulting space will have definite negative curvature. We also note that the regions of space where R_{11} is zero, will be cylindrical.

Thus, we choose to include the following term in the energy,

$$\lambda \int \sqrt{g} (|\ R_{11}\ | + R_{11})^2.\qquad (4.5.14)$$

This integral is positive semi-definite and vanishes for R_{11} less than or equal to zero. The Lagrange multiplier is then increased to large values, typically $10,000$, in order to force R_{11} to be less than or equal to zero and hence the local curvature scalar to be negative definite.

The resulting minimisation problem is well defined, however in practice, it is some what unstable. This constraint is very active as L is increased, with large regions of space developing with $R_{11} = 0$, as we might have expected. In effect, we have erected a steep wall across an energy surface in a region of steep descent towards an infinite degeneracy of minimum energy shapes, which are undetermined by the energy functional. Thus, across the wall we expect a whole variety of shapes to still persist, each lying on a local path of steepest descent.

Presumably our variational forms smooth this effect out and we find that there appear to be three predominant symmetries in the shape that space prefers, with the constraint of equation (4.5.14) imposed. Figures (4.5.2) to (4.5.7) show these structures at values of $L = 1.3$ and 1.5.

In the first case, Figures (4.5.2) and (4.5.3), physical space can be considered to be divided by the mapping in three distinct regions. At the $\mu = 0$ end (or the $\mu = \pi$ end) of space, we have a hemispherical three surface of radius of about 1, with optimal curvature $R = -6$, on which the hedgehog is seen to be

191

Figure (4.5.2): Plot of the $\theta = 0$ cross section through a non-symmetrical physical space in the (w, x) plane of R^4, at $L = 1.5$. Here the constraint $R_{11} \leq 0$ was imposed. The angle $f(\mu)$, at a point of physical space is measured relative to the w axis and is indicated by the spines.

Figure (4.5.3): Plot of the $\theta = 0$ cross section through a non-symmetrical physical space in the (w, x) plane of R^4, at $L = 1.3$. Here the constraint $R_{11} \leq 0$ was imposed. The angle $f(\mu)$, at a point of physical space is measured relative to the w axis and is indicated by the spines.
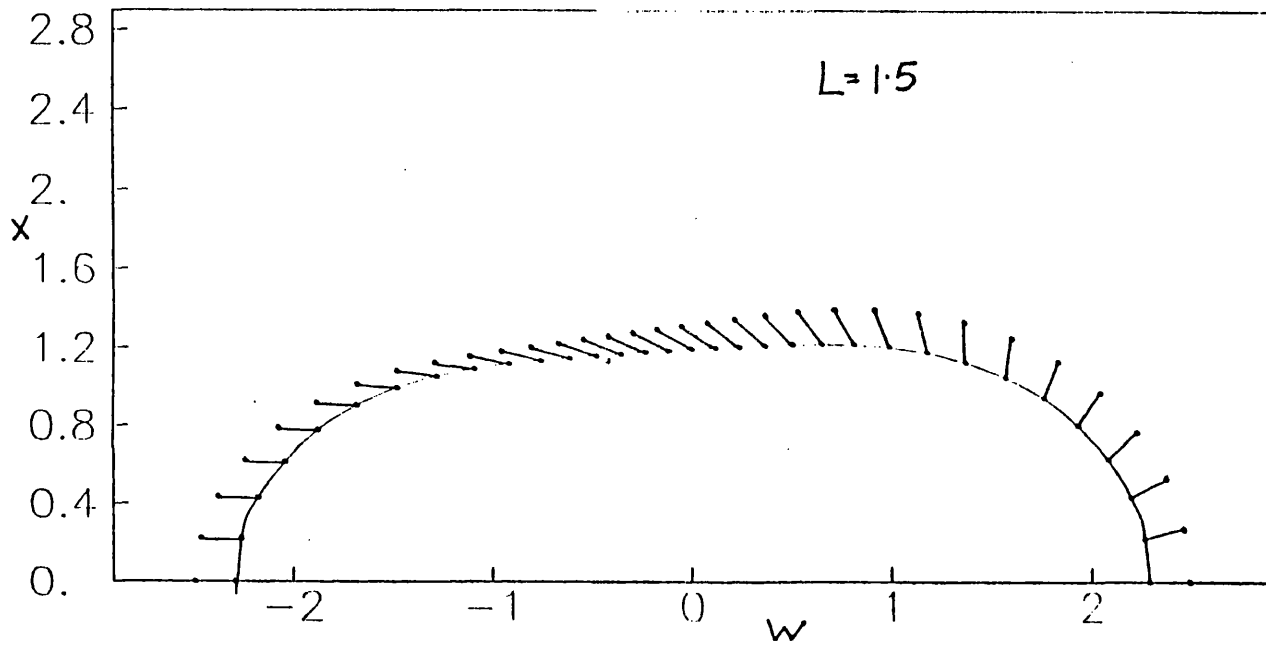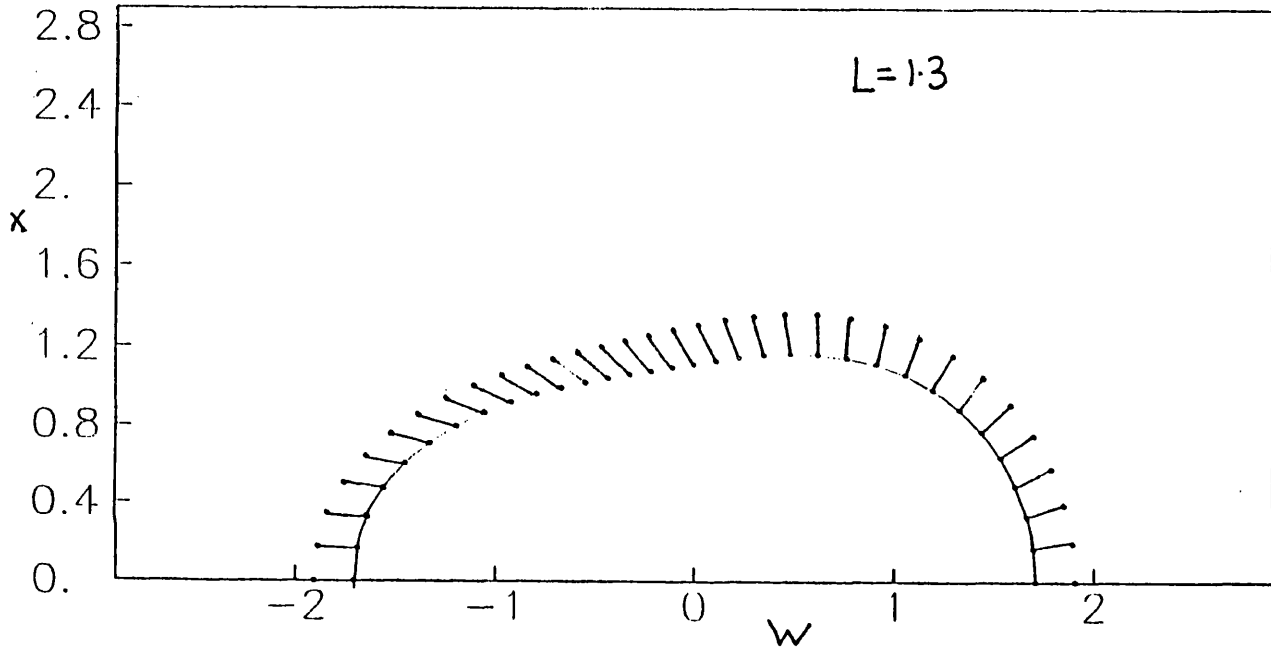
Figure (4.5.4): Plot of the $\theta = 0$ cross section through a 'buckled' non-symmetrical physical space (see text) in the (w,x) plane of R^4, at $L = 1.5$. Here the constraint $R_{11} \leq 0$ was imposed. The angle $f(\mu)$, at a point of physical space is measured relative to the w axis and is indicated by the spines.

Figure (4.5.5): Plot of the $\theta = 0$ cross section through a 'buckled' non-symmetrical physical space (see text) in the (w,x) plane of R^4, at $L = 1.3$. Here the constraint $R_{11} \leq 0$ was imposed. The angle $f(\mu)$, at a point of physical space is measured relative to the w axis and is indicated by the spines.
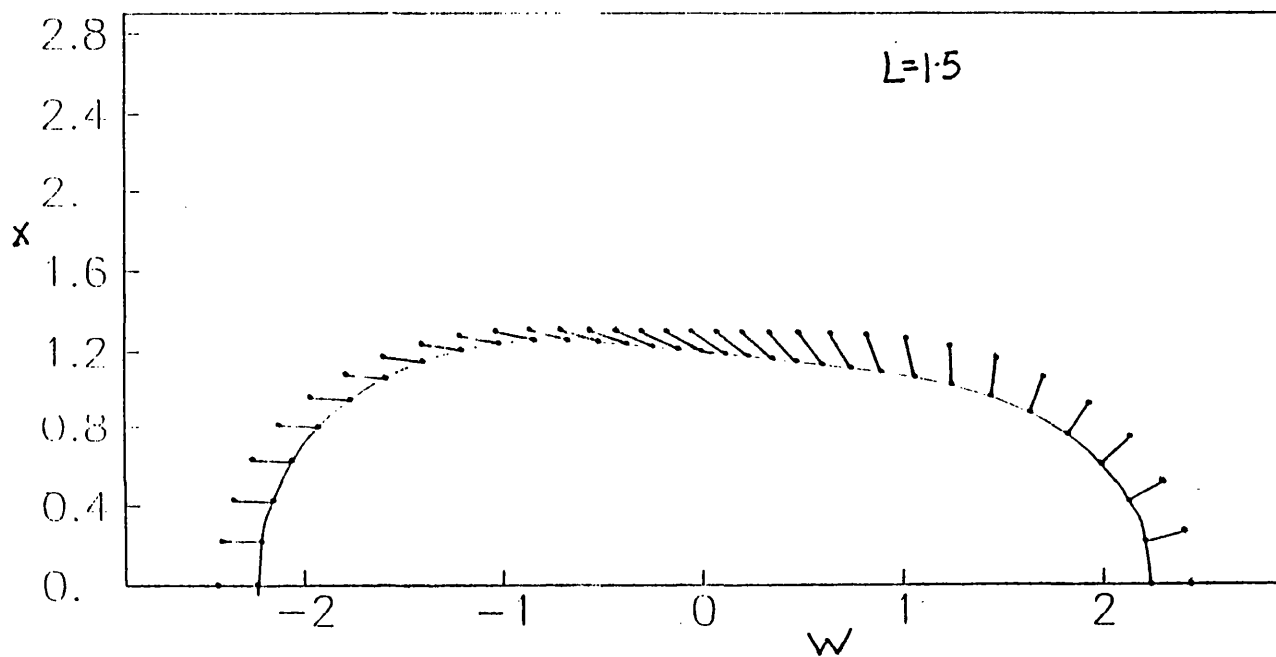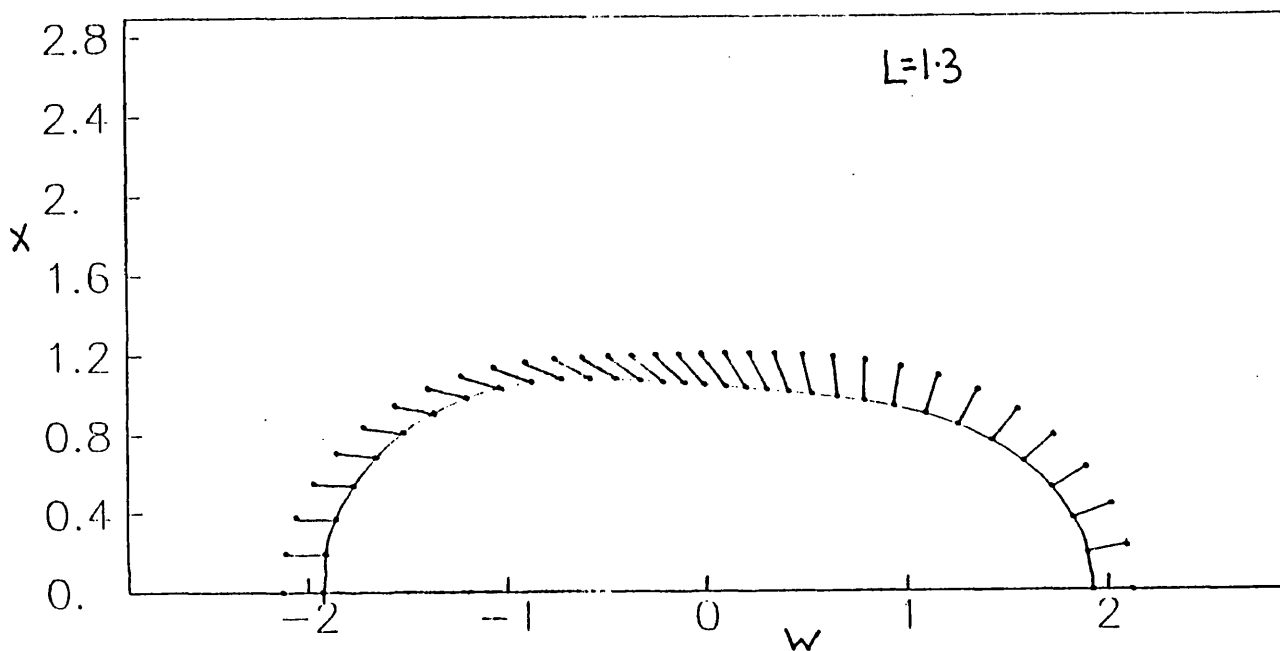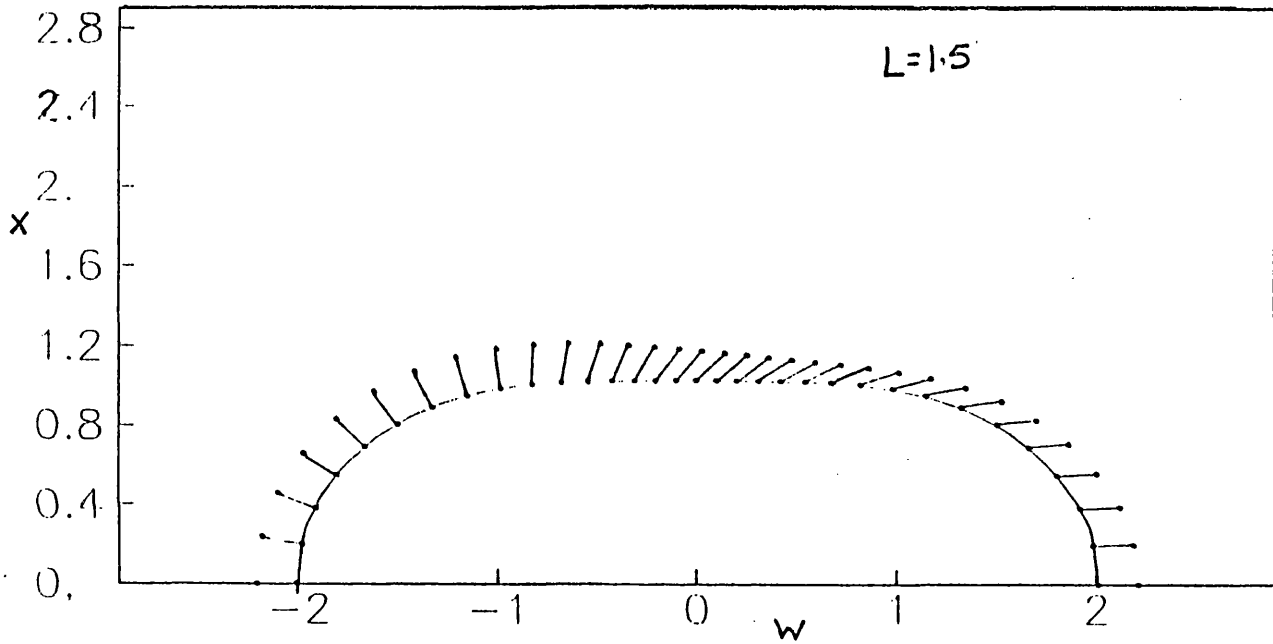
Figure (4.5.6): Plot of the $\theta = 0$ cross section through a symmetrical physical space in the (w,x) plane of R^4, at $L = 1.5$. Here the constraint $R_{11} \leq 0$ was imposed. The angle $f(\mu)$, at a point of physical space is measured relative to the w axis and is indicated by the spines.

Figure (4.5.7): Plot of the $\theta = 0$ cross section through a symmetrical physical space in the (w,x) plane of R^4, at $L = 1.3$. Here the constraint $R_{11} \leq 0$ was imposed. The angle $f(\mu)$, at a point of physical space is measured relative to the w axis and is indicated by the spinor.
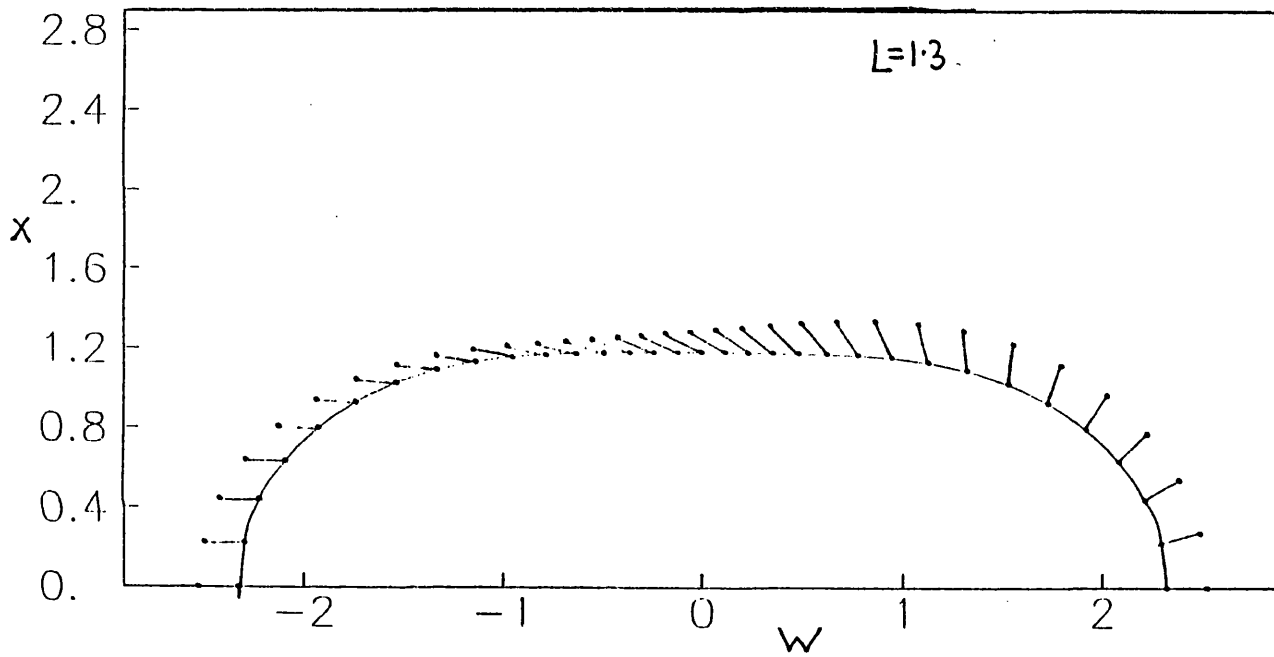
radial, corresponding to the identity mapping in this region. There is thus a half skyrmion in this region. On the adjacent 'bucket' region, with $R_{11} = 0$, the other half of the skyrmion exists with its baryon density depleting as μ increases. This can be seen by noting that as the angle μ varies, the angle $f(\mu)$ on this surface reduces towards its trivial vacuum value. Finally, on the other end we have a second hemisphere, whose radius depends on the amount of volume it is required to take up, in order to avoid excessive stretching of the skyrmion and on which no baryon density exists and the field takes its trivial vacuum value of $f = \pi$, (or $f = 0$). Note that this structure is a non-symmetric skyrmion. Indeed, since space is non-symmetrical, it makes little sense to consider a symmetric phase skyrmion.

The second case, Figures (4.5.4) and (4.5.5), is similar, except now the 'bucket' region, with $R_{11} = 0$, grows in width towards the $\mu = \pi$ pole, but it still has half a skyrmion stretch over it. The vacuum hemisphere now has a larger radius than the trivial $L = 1$ region. Thus, the structure involves less stretching of the skyrmion than the previous case and has an energy which is slightly less than those of Figures (4.5.2) and (4.5.3) at corresponding values of L.

The final situation, Figures (4.5.6) and (4.5.7), consists of the case where both the vacuum and identity regions have identical radii and a cylindrical $R_{11} = 0$ region, with a half skyrmion between them. Only in this case is the space symmetrical and hence a symmetrical mapping sensible. However, the large gains

of the non-symmetrical mapping structure at the π pole with optimal curvature, avoids this possibility.

The energies of these three structures are plotted against varying values of L shown in Figure (4.5.8). The energy of the trivial map of the sphere is also included, (solid line). As observed, the second type space, (dot-dashed line), is more favourable than the first, (dashed line), at all volumes due to the reduced stretch of the skyrmions that result. The symmetric third option, (dot-dot-dashed line), is seen to be the most stable of the three for values of L of below about 1.5. Above this value, the increasing volume of space and the resistance of the half skyrmion to stretching over the cylindrical region, results in its being preferable for space to buckle in to the second type of shape depicted in Figures (4.5.4) and (4.5.5). Around a value of $L = 1.25$, all three options become indistinguishable and all three undergo a first order phase transition to the identity mapping of $S^3_{phy}(L)$, as indicated by the plot. This occurs at an energy of about $1.03 \times 12\pi^2$. The volume and the energy at the phase transition point and its first order nature, are all consistent with the result for the sphere, subject to our less general elliptical deformations. The reason for the linearity of the non-symmetric phase plot, is however unclear.

In conclusion, our results suggest that three very similar structures exist in the non-symmetric phase and that these are similar to the needle-type elliptical structure in both energies, critical points and shape. Thus, the much simpler elliptical calculation seems to have most of the features of the more general
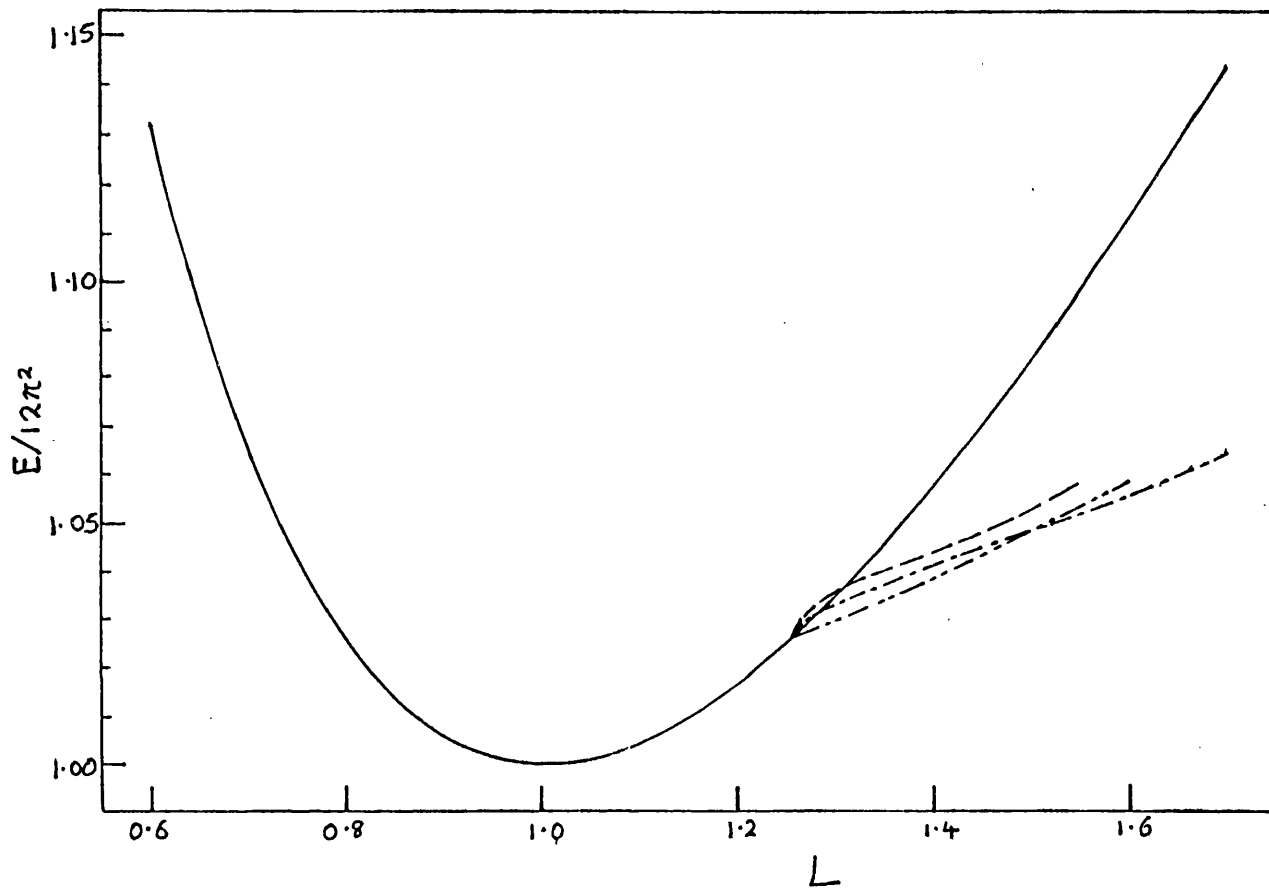
Figure (4.5.8): Plots of $(energy)/12\pi^2 = E/12\pi^2$ versus L of a hedgehog solution on various shaped spaces. The solid line indicates the trivial map skyrmion on the sphere. The non-symmetric spaces, with the skyrmion localised about the narrowest region, (dashed line) and the symmetric, (dot-dashed line), shapes are depicted merging at the common first order phase transition point.

skyrmions on negatively curved closed surfaces. However, in this instance we see that skyrmions split in to halves as a direct consequence of the $R_{11} \leq 0$ constraint, with half a skyrmion on a $R_{11} = 0$ 'bucket' three surface and half on a $R = -6$ hemisphere.

Finally we should note, that by allowing general unconstrained deformation of this sphere to a negative curved three surface, we have not observed the $S^3_{phy}(L)$ local stability up to $\sqrt{2}$ we predicted. This can be rectified by simply controlling the size of the space deformation as in the elliptical case. To achieve this the parameters of $r(\mu)$, (4.5.12), are re-expressed in terms of a new set of parameters, $(\alpha, \beta, \gamma, \delta)$,

$$
\begin{aligned}
c_1 &= \alpha \cos \beta, \\
d_1 &= \alpha \sin \beta \cos \delta, \\
c_2 &= \alpha \sin \beta \sin \delta \cos \gamma, \\
d_2 &= \alpha \sin \beta \sin \delta \sin \gamma.
\end{aligned}
\tag{4.5.15}
$$

Fixing the value of the parameter, α, and hence the maximum magnitude of $r(\mu)$, the three remaining parameters lie within a three dimensional spherical surface of radius α, embedded within a four dimensional parameter space. We can now increase the value of α form zero ($S^3_{phy}(L)$) and vary the remaining independent parameters β, δ, γ and the four parameters in $f(\mu)$, (4.5.12), to obtain minimal energy configurations. In Figures (4.5.9) and (4.5.10), we plot the minimum energy obtained as the magnitude of α is increased from zero at
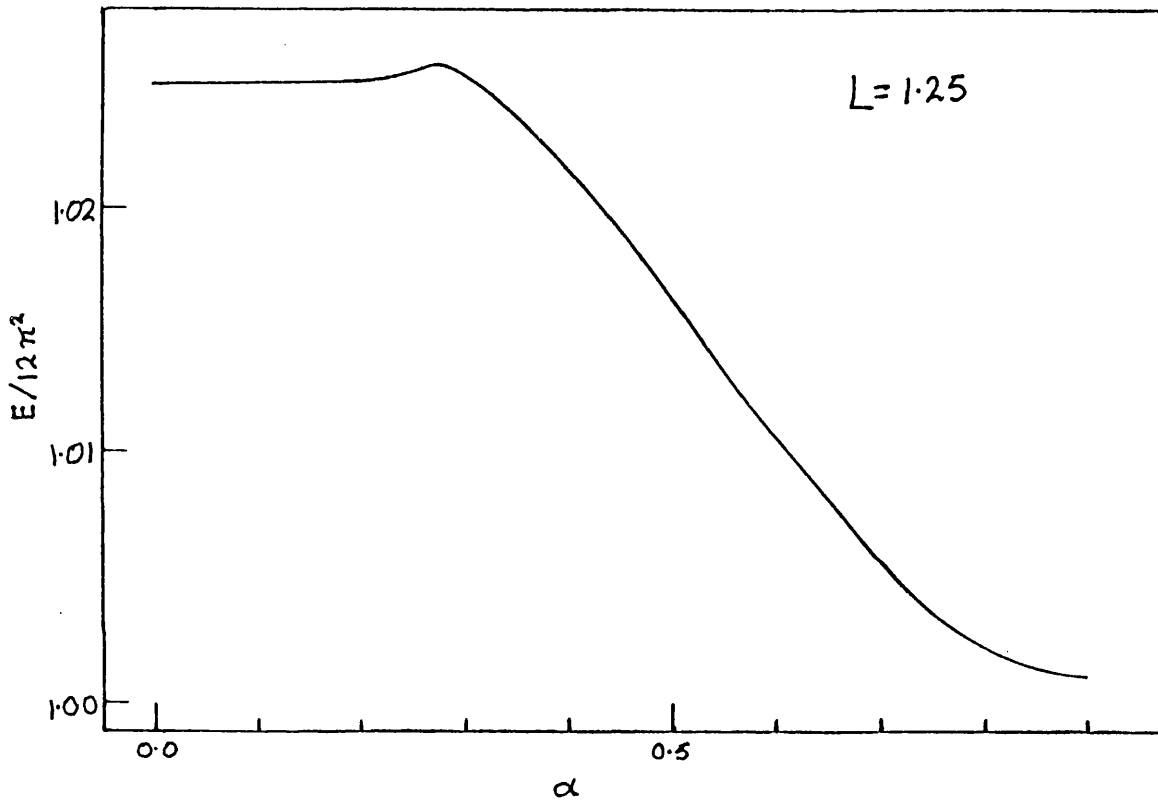
Figure (4.5.9): Plot of $(energy)/12\pi^2$ of the hedgehog versus the parameter α, (see equation (4.5.15)), at $L = 1.25$, with the curvature of physical space unconstrained.
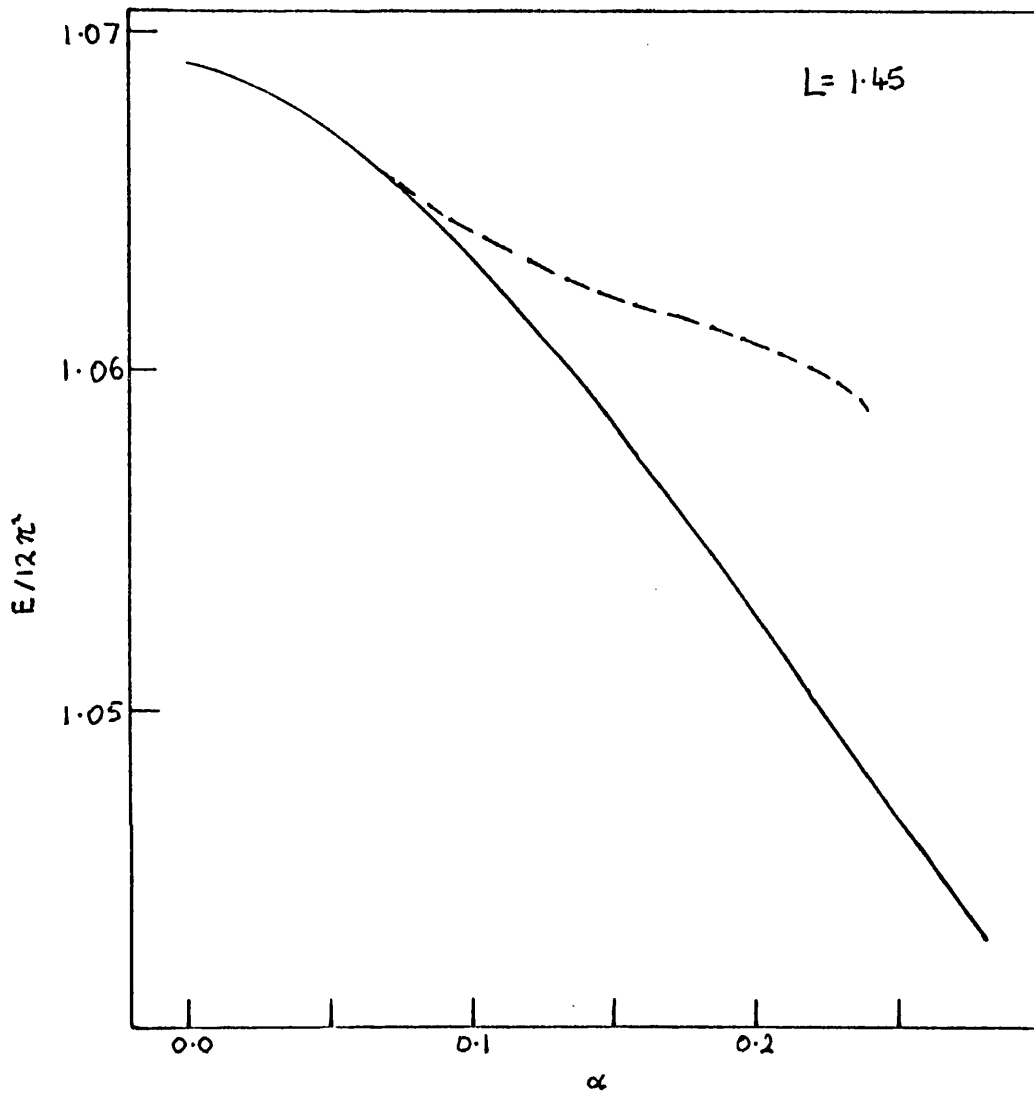
Figure (4.5.10): Plot of $(energy)/12\pi^2$ of the hedgehog versus the parameter α, (see equation (4.5.15)), at $L = 1.45$, with the solid line corresponding to the curvature of physical space unconstrained, while the dashed line corresponds to the constraint $R_{11} \leq 0$ being imposed.

$L = 1.25$ and 1.45 (note differing scale sizes in these two figures). In Figure (4.5.9), at $L = 1.25$, we see that the sphere is indeed stable as α is increased up to 0.3. Beyond this value, the energy falls steeply towards the lower bound as α approaches a value of 1. Here we have dropped the curvature constraint of (4.5.2), and the $\alpha \sim 1$ surface will look similar to that in Figure (4.5.1). In Figure (4.5.10), we see that at a volume of $L = 1.45$, the sphere is completely unstable as α moves from zero, which is a local maximum. Indeed, we see our results confirmed the sphere's stability to a value of $L = L_d = \sqrt{2}$. On this plot we have included a second branch, (dashed line), which has a higher energy and corresponds to the turning on of the curvature constraint of (4.5.14). Thus, in the region of $\alpha < 0.06$ the constraint has no effect and the deformation size is insufficient to produce positive curvature. Beyond this point the two curves branch smoothly, the curve with no constraint falling more sharply. Thus, as we expected, the constraint cuts through a region of steep descent in parameter space and is therefore very active.

References

[1] H.Forkel, A.D.Jackson, M.Rho, C.Weiss and A.Wirzba,

"Chiral Symmetry Restoration and the Skyrme Model", Stony Brook

preprint (1989)

[2] L.Castillejo, P.S.J.Jones, A.D.Jackson, J.J.M.Verbaarschot, A. Jackson

Nucl. Phys. A501 (1989) 801

[3] N.S.Manton, Commun. Math. Phys. 111 (1987) 469

[4] G.M.Loss Math. Phys. Lett 14 (1987) 149

[5] V.V.Novozhilov 'Foundations of the Non-Linear Theory of Elasticity'

Rochester N.Y. Graylock Press (1953)

[6] A.Jackson, A.D.Jackson, A.S.Goldhaber, G.E.Brown and L.C. Castillejo

Phys. Lett. 154B (1985) 101

[7] N.Manton and P.J.Ruback Phys. Lett. B181 (1986) 137

[8] A.Wirzba and H.Bang 'The Mode Spectrum and the Stability Analysis of

Skyrmions on a 3-Sphere'

Nordita preprint (1990)

[9] A.S.Goldhaber and N.S.Manton Phys. Lett. B198 (1987) 231

[10] A.D.Jackson, C.Weiss, A.Wirzba and A.Lande,

"Accurate Variational Forms for Multi-Skyrmion Configurations" Stony

Brook preprint (1988)

[11] M.Kugler and S.Shtrikman, Phys. Lett. B208 (1988) 491

CHAPTER 5

CHIRAL BAGS WITHIN
DENSE SKYRMIONIC MATTER

5.1 Introduction

In Chapter 3 we reviewed the current status of the Skyrme Model's predictions for dense baryonic matter. This showed that the model can be used to describe baryonic matter in a static crystalline form, which consists of a periodic skyrmion array. A variety of crystalline arrays have thus far been investigated, all of which have been found to have similar general characteristics. In particular, all have been shown to give considerable gains in binding energy at high densities over that of an array of isolated iso-rotated hedgehogs. Their minimal energy field configurations all occur at densities which are considerably higher than those at which 'normal' nuclear matter exists. At these high densities, these skyrmion crystals have been shown to condense to half skyrmions arrays.

Our numerical investigation involving the fcc array of skyrmions, demonstrated that the most likely candidate for the classical ground state configuration of crystalline skyrmionic matter, is the condensed fcc array, which corresponds to a simple cubic array of half skyrmions. Its minimal energy field configura-

tion, has an energy per unit baryon, which is 3.8% above the lower bound. As Manton et al [1] demonstrated, in flat space this bound cannot be saturated and thus, the close vicinity of this cubic half skyrmion array's energy to the bound, leads us to believe that this may well represent the absolute minimal energy, static crystalline field configuration. The corresponding high density of this field configuration, as we have already argued, may well be decreased when 1-loop quantum corrections are included and its density may well approach realistic nuclear matter densities.

In this chapter, we wish to propose further possible investigations involving this minimal energy crystal of Skyrme matter, which would reveal the particular nature of this crystal and lead to a better understanding of the physical interpretations that should be attached to its existence. As we outlined in Chapter 3, Klebanov [2] proposed that such arrays should represent neutron matter and he demonstrated how this could be achieved using naive semi-classical quantization techniques for quantizing the crystal's isospin-rotational modes. However, we have in mind the possibility of the crystal representing dense nuclear matter, which contains both neutrons and protons, as well as higher resonance states. We shall not tackle the question of electromagnetic interactions, which as Klebanov noted, would lead to divergent electrostatic contributions to the energy of the crystal per particle.

We believe that the possibility of the crystal being composed of α-particle like structures is an appealing one and would moreover, be of great interest.

Such an α-particle picture of nuclear matter, for cubic half skyrmion crystals, is however, at this time based only on intuition and a belief that the Skyrme Model might give a ground state within the $B = 4$ sector, with quantum numbers of the α-particle. This belief does have some basis however. Firstly, we know that in the $B = 2$ sector, the model gives a ground state configuration, which as a consequence of the particular axial symmetry present in the field configuration, has the quantum numbers of the deutron [3]. Secondly, this configuration was arrived at numerically [4] by considering the field deformation which occurs as two optimally orientated hedgehogs are brought together. Since hedgehogs represent generalised baryons containing both nucleons and deltas, it is seen that the resulting deutron bound state at high densities can be considered as being composed of all the dominant particles known to determine a deutron's physical properties.

As we have already pointed out, the $B = 4$ minimal energy configuration has also been obtained by Carson et al [5] and has also been found to possess a high degree of symmetry. Of further relevance here, is their observation, firstly, that within the Skyrme Model this may represent an α-particle and secondly, that the cubic point group symmetry this field configuration possesses is also present with our half skyrmion cubic field configuration [5]. Therefore, there exists the possibility of this half skyrmion crystal being composed of the $B = 4$ units, which may represent the generalised classical α-particle of the Skyrme Model. However, this consistency of symmetry is not easily transformed in to

209

the actual field configuration we have numerically discovered. In particular, it is not obvious how Carson's (et al) $B = 4$ field configuration, with the physical $U(\vec{x}) = 1$ boundary condition at spatial infinity, might be related to a crystalline field configuration with its twisted periodic boundary conditions, (3.2.13) and (3.3.3). It is true however, that the baryon density plots for this minimal energy crystalline fcc field given by Kugler et al [6] and the Carson et al [5] minimal energy $B = 4$ configuration, are similar. In particular, both are cubical and have similar numbers of regions of depleted baryon density. Given that the relation between these two fields remains to be more precisely established and that the actual pion field configuration of the $B = 4$ configuration, has not yet been presented by Carson et al, the question of the relation between the two field configurations remains an open one which we shall not consider here.

Nevertheless, we can still construct arguments which can be expected to hold independently of Carson's (et al) actual field arrangement and without an explicit relation between the two systems.

As we have seen in Chapter 3, our fcc crystal's low densities can be pictured as being composed of four types of iso-rotated spherical hedgehog skyrmions centred on the points of an fcc lattice, such that neighbouring skyrmions have their pion fields relatively iso-rotated about their line of centre by an angle π.

Specifically, we can describe the uncondensed phase fcc array in terms of the fcc cube. If the eight hedgehogs at the vertices of this cube are taken to be unrotated, then those on the faces are iso-rotated about an axis perpendicular

to the face on which they lie, by an angle π. A representative cell of the fcc crystal is thus an octant of this fcc cube and is itself a cubic cell, with the four different types of skyrmion centred on four of its vertices forming a tetrahedron, (see Figure (3.1.3a)). Periodic repetitions of these tetrahedral units generate the full fcc lattice arrangement.

Since the Skyrme Model Lagrangian is invariant under a constant global isospin rotation of a field configuration, there exists an infinite degeneracy of equivalent crystalline field configurations. By performing a global iso-rotation of our fcc lattice arrangement, we can obtain an equivalent crystal in which the tetrahedral symmetry of these representative units is explicit. Specifically, a global iso-rotation of the fcc arrangement by an angle $2\pi/3$, about an axis $x = y = z$ passing through the centre of this tetrahedron and the vertex on which the unrotated hedgehog sits, results in an arrangement in which the hedgehogs within the cell are iso-rotated by an angle $2\pi/3$ and each characterised by the direction of the axis about which it is iso-rotated. The resulting arrangement has each of the four skyrmions, which together form a tetrahedral unit within this representative cell, iso-rotated about an axis passing from the centre of the tetrahedron to the vertex point on which it sits, by an angle $2\pi/3$. Thus, the resulting pion field arrangement is explicitly seen to possess tetrahedral symmetry. It is important to note, that these iso-rotations do not affect the σ-field. The arrangement, though equivalent to that which we considered before, reveals much about the manner in which the pion field direction distorts as one increases the density of the crystal.

With this picture, we see that as the density of the crystal is increased, by decreasing the lattice space a of the fcc cube, the hedgehogs forming the tetrahedral unit within the representative cell, approach each other along the axis about which they are respectively iso-rotated. Since along these axes the pion fields remain unrotated and point outwards from the hedgehogs at the centre, we clearly see the manner in which the $B = 4$ hedgehog units approach each other as the lattice spacing is decreased.

An identical tetrahedral arrangement of four hedgehogs in the low density limit of the $B = 4$ sector, will clearly also be an optimum field arrangement. However, in this sector, a product of the minimal energy $B = 2$ fields at large separations, would be more bound than this tetrahedral field at correspondingly low densities. However, this tetrahedral arrangement should still be a local extremum of the energy of the $B = 4$ configurations at all densities. At high densities, bringing these spherical hedgehogs together along the respective axes of rotation, will result in large field deformations as the hedgehog fields overlap and should result in the true $B = 4$ configuration of Carson et al, which they suggested might represent an α-particle. Thus, in this manner, we suggest that our minimal energy, cubic half skyrmion crystal represents an array of α-particles at high densities. However, this crystal's periodic boundary conditions make establishing its association with the $B = 4$ solution non-trivial.

This picture also suggests, that at a density below that at which the minimal energy cubic half skyrmion field configuration exists, the cubic half skyrmion ar-

ray will be less bound than a crystal composed of optimally separated, tetrahedral $B = 4$ units, separated by regions of trivial vacuum. The tensor interaction of these $B = 4$ units should of course be weak, if they do indeed represent physical α-particles. Thus, at a fixed baryon density below that of the minimal density, allowing the crystalline field to break the periodic fcc boundary condition, we might expect that a simple cubic arrangement of α-particle like structures would condense out, separated by regions of trivial vacuum. However, the manner in which this condensation would occur is not clear, as the relation between the crystal's twisted boundary condition and the $B = 4$ physical boundary condition is not yet established.

It is clear though, that the $B = 4$ tetrahedral units within the crystal would slide along the four axes of the tetrahedron which pass through its centre and its four vertices. Thus, we can picture this condensation as being due to the fact that a tetrahedral unit has a definite density at which it prefers to be and when the baryon density of the crystal is decreased, these units remain rigid. In order to decrease the density, they slide along the four axes of symmetry of the tetrahedron and the exteriors of these tetrahedral $B = 4$ units are surrounded by regions of space in which the baryon density is zero. In this manner the baryon density of the whole cube is reduced. However, the twisted boundary condition of the condensed fcc crystal will no longer hold. Presumably, as the density is decreased, the fields at the edges of the $B = 4$ tetrahedral units smooth out, becoming spherical in order to match smoothly with the regions of trivial vacuum

213

at their exterior. Hence we suspect, that as the baryon density of the crystal decreases, these $B = 4$ units within the condensed fcc array would correspond to that of the $B = 4$ configuration discovered by Carson et al [5].

Given the belief that fcc skyrmionic matter may be composed of α-particle like structures, we wish in this chapter to present an alternative method by which the particle content of this crystal might be deduced. We wish here to consider the possibility of explicitly including quark degrees of freedom, which we expect to be relevant at short distances within a baryon. Thus, within dense baryonic matter we might expect this to be a necessary step in the development of a realistic physical model of dense baryonic matter. The inclusion of quark degrees of freedom can be achieved by invoking the Chiral Bag Model, which provides an elegant two phase description of a baryon.

In the Chiral Bag Model a baryon is described in terms of quarks at short distances within its core and these are assumed to be confined within a spherical bag. At the exterior of this bag a meson cloud exists. These two phases are coupled at the bag surface by the requirement that the axial current be continuous. Thus, the resulting model is chiral invariant. In the interior, perturbative Q.C.D. governs the dynamics of the quarks, which interact via gluons, though these gluonic effects are usually ignored. In the exterior region, the desire to incorporate the P.C.A.C. hypothesis correctly within this model and hence its resulting successful low energy pion theorems, leads one to incorporate the dominant low energy pion degrees of freedom, realised as the Goldstone modes of

broken Chiral Symmetry. Thus, at the exterior of the bag the mesons dynamics are taken to be governed by the Non-Linear Sigma Model. To stabilise the bag at the tree level, against collapsing to a point in a chiral symmetric manner, it has been both customary and of interest to generalise this effective mesonic Lagrangian by including Skyrme's fourth order term.

In the next section we shall present the details of this model and briefly review some of the recent results.

The inclusion of explicit quark degrees of freedom within crystalline skyrmionic matter, through the Chiral Bag Model, has already been considered by some authors [7][8][9]. The inclusion of quarks should partially cure the low energy restriction of the Skyrme's effective Lagrangian with its limited number of mesons. These attempts to extend the description of Skyrme matter, employed the Wigner-Seitz approximation. Wurst et al [9] considered cutting spherical holes out of a crystalline skyrmionic field, which satisfied Klebanov's cubic boundary condition. They considered placing free massless Dirac fermions, the quarks, inside spherical bags and ignored gluonic interactions. This approach is only valid if the spacing between neighbouring skyrmions is large, because only then is the array composed of approximately spherical skyrmions. The imposition of spherical bag symmetry places strong constraints on the deformation of the crystalline configuration. As a result, their Wigner-Seitz approach was unable to describe high density baryonic matter, since spherical symmetry of the bag was inconsistent with that of the simple cubic lattice arrangement. This

resulted in the Wigner-Seitz lattice having an energy which was always greater than that of the corresponding free skyrmion field configuration and thus there was no binding. Thus, their imposition of spherical symmetry, which was a mere calculational convenience, prevents their lattice calculation from giving insights in to the relevance of quark degrees of freedom at high densities.

Clearly what is relevant here, is to allow the shapes of the bag surfaces to deform as the density of the crystal increases. Thus, for our fcc crystal at low densities the spherical shaped bag would be relevant, but at high densities, the shape of this bag would be expected to mirror the symmetry of the mesonic field configuration, which has cubic symmetry. However, a calculation in which the shape of the bag is allowed to deform smoothly and continuously, is certainly beyond the realms of realistic possibility. Yet what we are most interested in here, is not understanding the manner in which these bags deform as the density increases, but the nature of the minimal energy half skyrmion arrangement at high densities.

We therefore wish to consider cubic, or more generally, square based prisms cut out of our minimal energy cubic crystals of half skyrmions, as we shall later show. These have an advantage over spherical bags in that they can be placed together to fill the whole space, whereas a sphere would require a tortuous bag shape deformation in order for the bags to fill space. The details of the consistent shape that can be cut of the minimal energy field configuration will be presented in Section 5.3. We note here simply, that given such an inclusion of explicit

quarks via the Chiral Bag Model, will not only reveal the particular nature of this matter, but might also provide us with an understanding of quark deconfinement at high densities.

We might thus envisage a Chiral Bag Model description of nuclear matter, composed of nucleons interacting through pions and with the acknowledged quark substructure of nucleons explicitly included. A second advantage of extending our model to include quarks through the Chiral Bag Model, is that we can expect that since it interpolates between the two extreme limits of the Skyrme Model and the M.I.T. Bag Model, it will incorporate the successes of them both. The manner in which this is achieved will be seen in the next section.

5.2 The Chiral Bag Model

In recent years the Chiral Bag Model [10] has emerged to provide an elegant, two phase description of a nucleon, in which the nucleons central quark core is coupled to an external meson field through continuity of the axial vector current. This model has been shown to provide the exciting possibility of understanding the relationship between the two distinct extremes of the bag and soliton models of baryons.

Originally the M.I.T. Bag Model [11] set out to describe hadrons solely in terms of their quark substructure. This model of hadronic substructures was developed in a manner which incorporated many of the phenomenological features

of high energy hadronic physics. A baryon is described as an extended object, a bag, in to which three valence quarks are placed.

The results of deep inelastic scattering experiments have revealed that within a hadron, quarks or partons move freely over short distances. However, no free quarks exist in the physical particle spectrum. Thus, the M.I.T. Bag Model describes a baryon as composed of three quarks, bound inside a confining closed surface. Outside of this bag the quarks attain an infinite mass and are thus prevented from existing in this, the exterior region.

The physical basis of the confining mechanism which prevents quarks from being observed in asymptotic channels, is not understood. However, since within a hadron quarks interact through the eight gauge bosons of Q.C.D., the gluons presumably provide the 'glue' which binds them within the hadron. In this way, the Bag Model imposes quark confinement by fiat. In so doing, it is supposed that non-perturbative effects of Q.C.D. result in a two phase structure. The bag represents a bubble within which quarks and gluons interact perturbatively, in a manner governed by Q.C.D.. These bubbles exist within the 'normal' phase, which has a non-perturbative vacuum structure and in to which colour electric fields cannot penetrate.

The original M.I.T. Bag Model only attempted to describe the perturbative phase and imposed colour confinement by demanding that the (colour) vector current across the bag surface vanishes.

$$n_\mu \bar{\psi} \gamma^\mu \psi \,|_{BOUNDARY} = 0. \qquad (5.2.1)$$

218

Here ψ is taken to be an iso-scalar, that is, a four component Dirac spinor, describing the quark field and n_μ is the outward unit normal to the bag surface. The linearised version of this boundary condition,

$$-i\hat{n} \cdot \vec{\gamma}\psi(x) \, |_{BOUNDARY} = \psi(x) \, |_{BOUNDARY}, \qquad (5.2.2)$$

uniquely solves boundary condition (5.2.1), the usual M.I.T. boundary condition. The bag is usually taken to be a sphere of radius R, with the boundary given by $r = R$. With the linearised boundary condition, the quarks within the bag are prevented from escaping from it. It is a trivial consequence of Gauss' theorem, that within the bag only colour singlet contributions of quarks and gluons can exist.

The perturbative phase is believed to have a higher vacuum energy density than the normal phase and thus, bubbles will not expand to fill all of the space. Therefore, a constant measuring of the excess energy density of the hadronic phase is usually introduced. This results in the bag size becoming a physical quantity, relevant to the distance scales at which quarks confine. However, this interpretation of the bag radius, R, being a physical quantity, is not taken over in the Chiral Bag Model generalisation, as we shall see later.

The dynamics of the quarks and gluons within the spherical cavity are determined by perturbative Q.C.D., subject to the confining boundary condition (5.2.2). Initially the gluon effects, as well as the quark masses, are neglected. The dynamics of the free massless quarks are then determined by the massless

219

Dirac Equation. It is then possible to obtain a complete analytic solution to the Dirac Equation, subject to boundary condition (5.2.2), for a spherical bag. By including quark masses and gluonic interactions, the resulting model has been shown to give a good fit to the low lying hadronic spectra [12]. In particular it gives the correct ordering of the spectra.

The M.I.T. Bag Model of a hadron however, has some short comings, particularly with respect to its description of low energy nuclear physics. For example, since all the nucleon's physical properties are confined by boundary condition (5.2.2), in order to study the interaction of nucleons it was necessary to consider the complex process of bag fission and fusion [13]. Moreover, since quarks are confined their currents are discontinuous at the bag surface. Thus, the quarks vector axial current is not conserved. Hence, the M.I.T. Bag Model is not chiral symmetric and makes no attempt to incorporate the success of the low energy phenomenology of Chiral Symmetry. As a result, the M.I.T. Bag Model is only relevant and successful in describing hadronic substructure and thus, strong interaction processes at short distances.

The Chiral Bag Model thus emerged, to overcome the short comings of the M.I.T. Bag Model. The former provides a model of a nucleon with not only an explicit quark substructure, but also an exterior pionic cloud through which nucleons interact. The Chiral Bag Model, as developed by Vento et al[10], was based on the P.C.A.C. hypothesis. Thus, the Chiral Bag Model has an exterior pionic field which, by demanding axial current conservation across the bag

220

boundary, is consistently unified with the quark fields on the boundary of the cavity.

The Chiral Bag Model's generalisation of the confining linear boundary condition (5.2.2) reads,

$$-i\hat{\vec{n}} \cdot \vec{\gamma}\psi(x) \mid_{BOUNDARY} = e^{-if_\pi \vec{\theta} \cdot \vec{\tau}\gamma_5}\psi(x) \mid_{BOUNDARY}, \qquad (5.2.3)$$

where $\psi(x)$ is now taken to be an iso-scalar composed of up and down quarks. Here, $\vec{\theta}(x)$ is the external pion field which is excluded from penetrating the bag. The boundary condition is $SU(2)_L \times SU(2)_R$ chiral invariant. It couples the internal up and down quark fields to the iso-triplet vector pion fields at the bag surface, via a γ_5 vertex. On physical grounds one expects that the external pionic fields should be the Goldstone Bosons of Chiral Symmetry, as realised in the Goldstone mode. Thus, in the initial version of the Chiral Bag Model, the external pion dynamics were taken to be governed by the Non-Linear Sigma Model. We can thus interpret the unitary matrix $U = e^{if_\pi \vec{\theta} \cdot \vec{\tau}\gamma_5}$, appearing in the boundary condition (5.2.3), as the result of a Yukawa coupling of the quarks to the pion fields of the Non-Linear Sigma Model.

Inside the bag, neglecting gluonic interaction, quarks obey the massive Dirac equation,

$$(i\gamma^\mu \partial_\mu - m)\psi(x) = 0. \qquad (5.2.4)$$

Now, differing choices of $\vec{\theta}$ at the boundary, give different boundary conditions, (5.2.3), on the bag surface. Thus, differing choices of the pionic field strength at

the bag surface, result in different solutions to the Dirac equation and hence to theories with different physical content.

Deviations from Chiral Symmetry are treated perturbatively, based on the observation that both the pions and the quark current masses are small. Thus, the masses of the free quark field in the Dirac equation, (5.2.4), are usually neglected, to be included later as perturbative effects.

As we have already noted, in addition to the linear boundary condition (5.2.3) on the bag surface, in order to maintain Chiral Symmetry, the Chiral Bag Model imposes the condition that the vector axial current be continuous across the boundary surface. This condition reads,

$$\hat{n} \cdot \vec{A}^a[\psi] \mid_{BOUNDARY} = \vec{n} \cdot \vec{A}^a[\sigma, \vec{\pi}] \mid_{BOUNDARY} . \tag{5.2.5}$$

The vector axial current of the iso-scalar quark field is given by:

$$A^a_\mu[\psi] = \bar{\psi}\gamma_\mu\gamma^5\frac{\tau^a}{2}\bar{\psi}. \tag{5.2.6}$$

The form of the axial current for the σ and $\vec{\pi}$ fields, depends on the explicit Chiral Symmetric Model we employ to govern the dynamics of the external pion degrees of freedom. Here we wish to consider a version of the Chiral Bag Model, in which the bag is stable at the tree level against collapse of the bag to a point and also to incorporate the pure Skyrme Model description of a baryon as a soliton. Thus, we shall employ the Skyrme Lagrangian to govern the external pion dynamics. The axial current for the $\sigma, \vec{\pi}$ fields can be represented in terms

222

of the 2×2 unitary field U and this has the form:

$$A^i_\mu[U] = i \frac{f^2_\pi}{4} Tr(\tau^i \{U, \partial_\mu U^+\}) - i \frac{1}{32e^2} Tr(\tau^i \{U, \partial_\nu U^+\}) Tr(L^\nu L_\mu)$$

$$+ i \frac{1}{32e^2} Tr[\tau^i \{U, \partial_\mu U^+\}] Tr[L_\nu L^\nu]. \quad (5.2.7)$$

The Chiral Bag Model we have outlined, determined by equations (5.2.3), (5.2.4), (5.2.5) and the Skyrme Lagrangian, is explicitly $SU(2)_R \times SU(2)_L$ chirally symmetric and since it incorporates the Non-Linear Sigma Model's pions in the Goldstone mode, it is seen to unify the success of low energy soft pion theorems with the success of the M.I.T. Bag Model in describing a hadronic substructure.

Having discussed and justified the dynamics and relevant boundary conditions of the Chiral Bag Model, we shall briefly indicate the types of exact solution which have been obtained for a spherical confining bag of radius R. However, before doing so it is interesting to note that this model does indeed interpolate between the M.I.T. Bag and the pure Skyrme Models. This observation is based on the fact that as we vary the size of the bag radius, the pionic field strength $\vec{\theta}$, at the surface, varies smoothly. Thus, in the limit when $| \vec{\theta}(R) | = 0$, the two flavour Chiral Bag boundary condition, (5.2.3), reduces to one flavour. The M.I.T. condition (5.2.2) and the M.I.T. Bag Model results. In the limit of zero bag size, we have pionic degrees of freedom throughout the whole of space and the model reduces to the Skyrme Model.

For a spherical bag, complete analytic solutions to the Dirac Equation for the massless quark fields are available when the external Skyrme field is assumed to

be of the hedgehog form:

$$U(\vec{x}) = e^{i f_\pi \vec{\tau} \cdot \hat{\vec{\theta}}(r) |\vec{\theta}|},$$ (5.2.8)

which describes a single baryon in the pure Skyrme Model limit. At the spherical

bag surface, $r = R$, the iso-vector pion field strength, $\vec{\theta}$, is normal to the surface

and has a constant magnitude.

It is now obvious that the M.I.T. Bag limit will correspond to the magnitude

of the iso-vector field strength, being zero on the bag surface when the bag has

an infinite radius. The pure skyrmion limit, resulting when the bag has zero size,

will correspond to the limit of $| \vec{\theta} |= \pi$ at the bag surface.

On substituting the hedgehog ansatz for the external pion field (5.2.8), in to

the linear boundary condition, we obtain;

$$-i \hat{\vec{n}} \cdot \vec{\gamma} \psi(x) \mid_{r=R} = (\sin \theta(r) - \hat{\vec{r}} \cdot \vec{\tau} \cos \theta(r) \gamma_5) \psi(x) \mid_{r=R} .$$ (5.2.9)

This condition is such that it does not commute with $\vec{J} = \vec{L} + \vec{S}$ or $\vec{T}$ separately,

but with them taken together to form the grand-spin generator:

$$\vec{K} = \vec{L} + \vec{T} + \vec{S}.$$ (5.2.10)

The chiral boundary condition, (5.2.9), which is sphere symmetric, thus couples

the isospin directions to spatial directions and results in the grand-spin generator,

(5.2.10), being a good quantum number. Thus, spinor solutions to the Dirac

Equation (5.2.4), will be partially characterised by (K, k_z).

224

An analytic general solution to the massless Dirac Equation, in spherical co-ordinates, which satisfies the chiral boundary conditions, can easily be obtained. The lowest energy solution is given by:

$$\psi_{(r)}^{T} = \frac{N}{\sqrt{4\pi}}(ij_0(\omega r) \quad \vec{\sigma} \cdot \vec{r} j_1(\omega r)) \, \nu \, e^{-i\omega t}, \qquad (5.2.11)$$

where the spin-isospin state,

$$\nu = \frac{1}{\sqrt{2}}(- \mid \uparrow d > + \mid \downarrow u >), \qquad (5.2.12)$$

satisfies

$$(S + I) \mid \nu >= 0 \qquad (5.2.13)$$

and has the quantum number 0^+.

Since parity commutes with the Dirac Hamiltonian, there are two opposite parity states, $j \pm l$ for a fixed value of j. Thus, for $K = 0$, there is another state, with the quantum numbers 0^-, which has higher energy.

The hedgehog ansatz, (5.2.8), enables us to take the non-linearity of the exterior Skyrme Lagrangian in to account. The resulting equation of motion which determines the $\sigma, \vec{\pi}$ fields is the non-linear second order differential equation, (1.1.25), for the profile function, with $f(r)$ replaced by $\theta(r)$. The boundary condition at spatial infinity, (1.1.15), taken with the equation of motion, implies that $\mid \vec{\pi} \mid$ tends to zero as α/r^2 asymptotically. This coefficient, α, determines, through the equations of motion, the values of $\theta(r)$ and $\dot{\theta}(r)$ at the bag boundary, $r = R$. The linear boundary condition (5.2.9), subsequently determines the

225

Dirac spinor solution to the Dirac Equation. The conservation of axial current condition, (5.2.5), at the bag boundary, then determines the coefficient α. Note that since the value of α determines the pion field at spatial infinity, its value should be related to $g_{\pi NN}$ and its subsequent determination through the continuity of axial current at the bag surface, is the mechanism by which α is chosen, so that the Goldberg-Treiman relation holds for the hedgehog field.

Initially Vento et al [10] considered putting three valence quarks in to the 0^+ ground state, (5.2.11), with the Non-Linear Sigma Model determining the exterior σ and $\vec{\pi}$ fields. However, as we have already pointed out, there are distinct advantages to be gained by employing the Skyrme Lagrangian in the exterior regions, as this leads to a bag which is stable against collapsing to a point at the tree level, which their version does not. Vento et al found that the total energy of the system, the bag plus the exterior pion clouds, is close to that of the nucleon mass for a wide range of bag radii from $1.5Fm$ down to $0.5Fm$.

In order to complete the construction of the Chiral Bag Model it is necessary to include quark vacuum effects. Indeed, a consistent construction of the Chiral Bag Model necessarily requires these 1-loop effects to be included in the quark sector [14]. The model suffers many defects when these effects are ignored. The most serious of these is that the baryon number takes unphysical, non-integer values, as noted by Rho et al [15]. The vacuum correction to the valence quark contributions have been shown to correct this defect.

To understand this difficulty we note that the exterior σ, $\vec{\pi}$ fields, should have

associated to them, the usual baryon number, B, given by the field's winding number. However, since we have a bag cut out of this field, its contribution to the baryon number will be less than unity and is given by;

$$B = \frac{1}{\pi}(\theta - 1/2\sin 2\theta), \qquad (5.2.14)$$

for a hedgehog field where θ is the value of the chiral angle at the bag surface. When this is added to the three valence quarks contribution of unity to the baryon number, we see that this model gives a baryon number which is greater than unity and not an integer. The resolution of this lies in the presence of the mesonic fields exterior to the bag, which modify the bag boundary condition for the quarks in the negative energy sea, as well as for the valence quarks. This leads to a vacuum quark contribution to the baryon number which is precisely equal and opposite to that from the mesons. This result has been demonstrated numerically, by evaluating mode sums of the quark vacuum contributions [14].

The mechanism by which this cancellation occurs can be understood by considering the effect of increasing the value of chiral angle $\theta(r)$ at the bag surface. In the M.I.T. Bag Model limit, $\theta = 0$, the solution to the Dirac Equation produces an energy mode spectrum which takes both positive and negative values. In this limit its spectrum is symmetric about zero energy. As the strength of the pion field at the bag surface grows, the lowest positive energy valence quark states drop in energy and eventually cross zero energy and become negative; the other modes oscillate in energy but do not change sign. It is this spectral flow which

227

provides the mechanism for the fractional cancellation of the baryon number of the vacuum and of the exterior meson field.

Another case in which the need to include vacuum contributions is essential, is seen when one considers the Hamiltonian. Without the quark vacuum's contributions, the Hamiltonian is not bounded from below. To see this, we note that the energy scales with the inverse bag radius and thus by decreasing the size of the bag we can make the energy arbitrarily large and negative with Sigma Model exterior pion field. This is resolved by considering the Casimer energy, which treats the 'fallen' negative energy valence states in a unified fashion with the rest of the Dirac negative energy sea and thereby restores the positivity of the Hamiltonian.

It has been shown that on incorporating these vacuum effects with the Skyrmion exterior field, a successful 'Cheshire Cat' picture emerges for the Chiral Bag Model. That is, the low energy physical observable becomes independent of the bag radius. This has been found to be the case for the model's predictions of the baryonic mass, r.m.s. baryon radius, g_a and the $N - \Delta$ mass splitting.

This independence of the physical observables from the bag radius, has long been known to be exactly satisfied for various $(1 + 1)$-dimensional models [16] in which explicit bosonization of fermionic fields is possible and the physical equivalence of both phase descriptions can be demonstrated. However, in $(1 + 3)$ dimensions we expect such a phenomenon will only approximately exist, since the Skyrme Model is believed only to represent a truncated version of the 'true'

mesonic Lagrangian believed to correspond to Q.C.D. at low energies.

Thus, the Chiral Bag Model provides an instructive and consistent model of a nucleon which interpolates between the Skyrme and M.I.T. Bag Models. However, the necessity to include quark vacuum effects explicitly, for consistency, requires one to evaluate mode sums of the negative energy sea. Unfortunately, such sums in general have ultra violet divergences and the low energy nature of this model results in its not giving a guidance as to how these divergences should be removed, or even a unique prescription for isolating finite pieces. However, Jackson and Vepstas [17] have shown that a minimal type subtraction scheme, based on physical arguments, results in a consistent Chiral Bag Model in which all physical quantities are explicitly finite. Thus, the Chiral Bag Model has matured in to a consistent physical model of a baryon.

5.3 Chiral Bags Within A Dense Skyrmionic Crystal

We have seen in the previous section, that it is natural to attempt to extend the Skyrme Model by including explicit quark degrees of freedom in a chirally symmetric manner and that this can be achieved by employing the Chiral Bag Model. Thus, in this section we shall attempt to extend the Skyrme Model's description of dense crystalline baryonic matter presented in Chapter 3, by including quarks through the Chiral Bag Model. The resulting two phase model of baryonic matter, will have the same baryonic interaction, via the tensor force,

at the exterior of the bags that we investigated for a pure skyrmionic crystal. Due to the presence of interior quark degrees of freedom, we expect results in significant hard core repulsions between baryons as they approach each other in dense baryonic matter.

It is clear from the outset, such a generalisation will increase the complexity of the calculational procedure which would be required to obtain exact numerical results, since here we have a two phase model which is governed by different dynamical equations. In order to simplify our argument, which will be of a suggestive nature, we shall confine our consideration to the fcc condensed half skyrmion crystal at high densities. The twisted boundary conditions determining the symmetries of this field configuration were given in Chapter 3, in equations (3.2.13) and (3.3.3). Since this configuration has the lowest energy of all the crystalline Skyrme fields so far considered, it is clear that this is the most interesting candidate array that we can study.

Since for this field configuration we have to hand the accurate analytic forms, (3.6.1), for the true minimal energy field configuration, we shall make use of these. This ansatz is not a true solution to the Skyrme Model's Euler Equation, thus, this configuration's vector axial current is not exactly conserved. However, this ansatz does possess all of the symmetries of the true minimal energy field configuration and gives a very accurate estimate of its minimum value of energy. Hence, we believe that it is reasonable for us to make use of this analytic form and moreover, to assume that with the introduction of quarks the field distortions

are insignificant.

Thus, from the outset we shall assume that the exterior pionic fields are fixed and given by equation (3.6.1) and that we can introduce quarks by cutting holes in to this field and that employing the Chiral Bag boundary condition on the surfaces of these bags has little effect on these exterior fields. The latter assumption seems reasonable, since we expect the exterior fields to at least maintain the symmetry of the true soliton field. As we noted, conservation of axial current will not now be achieved when we employ this ansatz, however, its deviation from being conserved, we also expect to be of secondary importance.

In order to place quarks within this crystalline mesonic field, we have first to decide the shapes and positions at which we wish to cut holes in to the skyrmion field. Clearly in this matter, the symmetry of the field configuration is our guiding principle.

Since our fcc half skyrmion crystalline field configuration corresponds to a simple cubic crystalline array of half skyrmions, it seems natural to make these cuts at the cubic Weigner-Seitz cells of this lattice. This belief is further strengthened by noting that these surfaces are those on which the value of the sigma field vanishes identically for this ansatz. Thus, on these surfaces $\vec{\theta}$ would have a constant magnitude of $\pi/2$. This is similar to the spherical bag, with an exterior hedgehog field, for which the chiral angle has a constant value on the bag surface. These cubical bags however, have an advantage, they possess the desirable property that they join together smoothly to fill the whole of space. Thus, at

high densities, as the density of baryonic matter varies, these cubical bags meet smoothly and we could avoid considering deformation in the shape of the bag surface.

Thus, we see that on grounds of symmetry it seems both natural and desirable to cut cubic cavities out of our simple cubic fcc crystalline skyrmion field along the planes on which the σ field zero vanishes. For the ansatz (3.6.1), we see these mutually orthogonal planes are given by $x = \frac{l}{4}$, $y = \frac{m}{4}$ and $z = \frac{n}{4}$, where l, m and n take odd integer values.

As has already been implied, we might also consider expanding and decreasing the size of these cubes so that on the bag surface the value of the sigma field will no longer be zero and also the magnitude of the chiral angle, θ, for ansatz (3.6.1), will vary over the bag surface. However, care must be taken in choosing such surfaces, which are only piece-wise continuous. In general such surfaces will lead, for a fixed background mesonic field, to inconsistency with the Chiral Bag boundary conditions.

In particular, the Chiral Bag Model boundary condition (5.2.5), expressing the conservation of axial current across the bag surface, cannot in general be satisfied for such shapes. This difficulty arises because we have fixed the background mesonic field and we have not allowed it to respond when the quarks are included within the cavities which are cut out of it.

To see that this is the case, we note that at the discontinuous points of a piece-wise continuous surface, the normal to the surface is undefined. These points

will form lines which are the edges of our cubes. Since the conservation of axial current boundary condition (5.2.5), explicitly involves the normal at all points on the surface of the bag, at these discontinuous points the normal component to the surface of the axial current must vanish for consistency. The normal to the surface also occurs in the confining boundary condition (5.2.3) and consistency here will require that the quark field $\psi(x)$, vanish at these discontinuous points. This implies that all the components of the axial current of the quark field vanish at these points. Thus we see, that for the fixed mesonic fields, in order for the axial current boundary condition to be satisfied, the normal component to the surface of the axial current must vanish at any discontinuous points on the bag surface.

Hence, we are not free to cut arbitrary shaped cavities out of the fixed background mesonic field. Moreover, if we choose our half skyrmion cubes as the cavities, the axial current normal to the surface must vanish on the discontinuous edges of the cubes.

Thus, before we can fix the shapes and locations of the cavities, we must first establish at which points of space the components of the axial currents for the mesonic field must vanish. We shall therefore consider the nine components of the axial vector current, (5.2.7), of the mesonic fields. For this purpose we employ the ansatz given in equation (3.6.1). To simplify matters considerably, we can note that for our purposes, we only require the points at which the components of the axial current $A^i_\mu(\vec{x})$, vanish. Here μ is the spatial index and i the isospin

index. From this it is simple to deduce that the only terms which vanish in the axial current's components come from components of the quantity

$$L_\mu^i(\vec{x}) = \frac{i}{2}Tr(\tau^i U^+ \partial_\mu U) = -(\pi^i \partial_\mu \sigma - \sigma \partial_\mu \pi^i) \qquad (5.3.1)$$

and also that

$$A_\mu^i(\vec{x}) \sim L_\mu^i(\vec{x}). \qquad (5.3.2)$$

Thus, employing our crystalline ansatz (3.6.1), we can deduce the zeros of the nine components $A_\mu^i(\vec{x})$, by noting that they behave as

$$A_1^1 \sim \cos\eta\cos\varsigma \qquad A_1^2 \sim \xi\sin 2\eta\cos\varsigma \qquad A_1^3 \sim \sin\xi\cos\eta\sin 2\varsigma,$$

$$A_2^1 \sim \sin 2\xi\sin\eta\cos\varsigma \qquad A_2^2 \sim \cos\xi\cos\varsigma \qquad A_2^3 \sim \cos\xi\sin\eta\sin 2\varsigma,$$

$$A_3^1 \sim \sin 2\xi\cos\eta\sin\varsigma \quad A_3^2 \sim \cos\xi\sin 2\eta\sin\varsigma \quad A_3^3 \sim \cos\xi\cos\eta, \qquad (5.3.3)$$

where $\xi = 2\pi x/a$, $\eta = 2\pi y/a$ and $\varsigma = 2\pi z/a$ and where $a/2$ is the size of the half skyrmion cube, or alternatively a is the lattice spacing of the fcc lattice.

Let us concentrate on a representative half skyrmion cube, centred at the origin and defined by;

$$\frac{\pi}{2} \geq \xi, \eta, \varsigma \geq \frac{-\pi}{2}. \qquad (5.3.4)$$

On the surface of this cube, the value of the σ field is zero and within this cube there is a half skyrmion with $B = 1/2$.

Examining the form of the axial current's components $A_a^i(\vec{x})$, it is simple to deduce that the scalar product $\vec{a}.\vec{A}^i(\vec{x})$, where $\vec{a}$ is some spatial vector, vanishes

only at the points which the three functions $\cos \xi \cos \nu, \cos \xi \cos \varsigma$ and $\cos \nu \cos \varsigma$, simultaneously vanish, that is to say, on the edges of the half skyrmion cubes. Hence, for the fixed half skyrmion background field (3.6.1), these lines define the only points at which discontinuities in the bag surface can occur.

Hence, we have found that the half skyrmion cubes, which naturally exist within the fcc condensed field configuration, represent the simplest 'elementary' cavities which can be cut out of the field and that they are consistent with both the Chiral Bag boundary conditions and with the symmetry of the skyrmionic field.

For a spherical bag of radius R and an exterior spherical hedgehog field, we have seen in the previous section that the bag radius can be continuously varied without deforming the shape of the bag. However, for our cubical bag of length $a/2$, with the meson field fixed as we decrease the cubic bag's volume, on the edges of the cube the axial current of the mesonic field through the bag surface will no longer vanish and hence we can no longer satisfy the Chiral Bag boundary consistently. A resolution of this problem, with fixed background field (3.6.1), is provided by smoothly deforming the cube at its edges so that there are no discontinuous points on the bag surface. Indeed, symmetry suggests that in doing so, one should choose bag surfaces which have the same shape as the surfaces on which the value of the σ field is constant. However, here we do not wish to consider the complex process of deforming the shape of our cubic bag. Alternatively, we could simply demand that the pion fields on the bag

surface remain fixed as we increase the volume of our cube. However, this would correspond to decreasing the baryon density of the crystal and will not give the expected independence of the physical quantities on the bag size and hence would not lead to results consistent with the 'Cheshire Cat' philosophy.

However, there does exist an alternative method of changing the bag size while keeping the background field fixed and also maintaining consistency with the Chiral Bag boundary conditions. This can be seen by noting that $\hat{\vec{n}}.\vec{A}^i(\vec{x})$, where $\hat{\vec{n}}$ is the outward normal to the bag surface, vanishes in general on the edges of our cube. Hence, if we increase the length of this cube in one direction, while keeping the other two lengths fixed, this scalar product will vanish on the edges of this square based prism. Thus, we can expand the size of our cube in one direction only, but we have of course, three degenerate choices of direction. Thus, we expect the analogue of the bag radius, R, of a spherical bag, to be the length of this square based prismoidal bag within the condensed fcc crystal.

Summarising, we have discovered that rectangular bags can exist within our condensed half skyrmion fcc array and that their existence is non-trivial. Moreover, we expect the length of this rectangular bag to provide the analogue of the bag radius R of a spherical bag.

Thus, we can imagine fixing one of the faces of this cubic bag at $x = -a/4$ and sliding the opposite face along the x axis for example. As the length of the bag increases successively by $a/2$, the value of the σ field on the surface will become zero, while on the other fixed surfaces it will remain fixed at zero. The

pure skyrmion limit will be obtained when the length of this rectangular bag is reduced to zero. Moreover, we can even allow two opposite sides of this bag to simultaneously slide. If we were to keep the length of the bag fixed and allow the bag to slide, then this would correspond to allowing our bag to translate through crystalline skyrmionic matter.

Thus, it seems natural at this point to propose a well defined calculation in which we solve the free massless Dirac Equation for the interior quark wave function of lowest positive energy, subject to the Chiral Bag boundary conditions on the surface of this cubical bag. To simplify the calculation it should be reasonable to employ the ansatz (3.6.1), to give the pionic field strength on the bag surface. We expect the error induced by this approximation, of freezing the exterior pionic field, to be of secondary importance. The solutions to the Dirac Equation will be dependent on the length of our rectangular bag.

Given the cubic symmetry of the pionic field at the exterior of this rectangular bag, one might expect that an approximate separable solution to the Dirac Equation exists, at least in the case where the value of σ on all the bag surface is constant and zero. This corresponds to the situation when whole half skyrmion cubes have been cut out of the half skyrmion field. In this case the linear boundary condition, (5.1.2), takes its simplest form. For the spherical bag, the ground state quark wave function when $\sigma = 0$ on the bag surface, has a constant upper component and a vanishing lower component and has zero energy.

However, for a rectangular bag, a separable solution to the Dirac Equation

will not, unfortunately, exist. This follows from the observation, that at the corners of the rectangular bag, the quark wave function not only has to vanish, but must also have double zeros. This being the case, there seems no hope of finding simple solutions to the Dirac Equation within these rectangular bags by analytic means and hence numerical techniques will be required at this point.

The solution to this Dirac Equation, should however, enable us to determine the ground state wave function of the quarks. Placing three valence quarks in to this ground state should enable us to determine the particle content of the cubic bag. This would indeed provide an interesting insight in to the nature of the minimum energy fcc half skyrmion lattice.

We noted in the previous section, that the Chiral Bag Model provides a consistent model of a baryon only when quark vacuum effects are included. This observation will clearly apply to our chiral bag within crystalline skyrmionic matter. For example, if we imagine placing three valence quarks within the chiral bag defined in equation (5.3.1), then this would correspond to removing half a baryon from the mesonic field, but replacing it with three valence quarks whose baryon number is unity. Thus, naively, the crystal's baryon number rises by $B = 1/2$. Moreover, as we vary the length of the rectangular bag, the mesonic contribution to the baryon number would smoothly vary, while the contribution to the baryon number of the three valence quarks would remain fixed at unity. Thus, again naively, the baryon number which is clearly a physical observable would smoothly depend on the length of our rectangular bag. The resolution to

this paradox for a spherical bag, was that the negative energy sea within the bag also carries baryon number charge. The baryon number carried by the negative energy sea is negative and was found to be exactly equal in magnitude to that of the exterior pion field.

For our rectangular bag, we thus require that a similar mechanism exist by which the baryon number of the valence quarks, the exterior mesonic field and the interior quark vacuum remain fixed on an integer value. Thus, in order to see whether this cancellation occurs, it is sensible at this stage to reproduce the arguments which led to the miraculous baryon number cancellation and see if they apply to our rectangular bag.

The simplest manner in which this can be achieved is to consider the half skyrmion bag defined in equation (5.3.1). Here we shall keep the size of the cubic bag fixed. The directions of the pionic fields on the surface of the bag are now fixed and given by our ansatz or for that matter, the true minimal energy configuration. We ignore all other regions of space where the exterior pionic fields should exist and now vary the chiral angle, θ. That is to say, the mesonic field on the surface is given by

$$U_\theta = \cos\theta + \hat{\vec{\pi}}.\vec{\tau}\sin\theta, \qquad (5.3.5)$$

where $\hat{\pi}^i$ is the unit vector pion field on the bag surface, given by ansatz (3.6.1) and θ is the chiral angle which has a constant value on the bag surface and which we vary between 0 and π. Clearly, we must still demand that on the edges of the

cube, the value $\hat{\vec{n}}.\vec{A^i}(\vec{x})$ vanishes, in order to maintain consistency. This can be achieved by setting the value of $\vec{n}.\vec{\nabla}\theta$ at the edges of the surface to zero. Thus, we should also vary on the surface the value of $\vec{n}.\vec{\nabla}\theta$ as we vary the value θ, while always keeping its value at the edges fixed at zero.

This vanishing of the axial current at the corners is clearly seen by considering for example, on the surface $\xi = \pi/2$, the quantity

$$\hat{\vec{x}}.\vec{L^i}(U_\theta) = \hat{\pi}^i\partial_x\theta + \frac{\sin 2\theta}{2}\partial_x\hat{\pi}^i, \qquad (5.3.6)$$

where L_a^i is given by equation (5.3.1). At the edges of this face it is trivial to demonstrate from (3.6.1), that $\partial_x\hat{\pi}^i$ vanishes and hence we require $\partial_x\theta$ vanish at the edges and similarly for other faces. This then leads to the axial current normal to the faces of the cube vanishing at the edges of the cube. In the case of θ, given by $\cos^{-1}\sigma$, where σ is given in equation (3.6.1), we see the condition $\vec{n}.\vec{\nabla}\theta$ was trivially satisfied.

Having established the manner in which we can vary the chiral angle, θ, at the surface, while keeping it constant over the whole of the surface, we now have the analogue of the usual spherical bag.

In the case of a spherical bag, when $\theta = 0$ on the bag surface, the M.I.T. boundary condition results and formally the model reduces to the M.I.T. Bag Model, while in the case of $\theta = \pi$ we have a pure skyrmion field surrouding a cubic bag with zero baryon number.

Thus, the value of the chiral angle at the surface of the bag should determine

240

the Dirac spinor solutions to the Dirac Equation. Moreover, these solutions will have energies which vary smoothly with θ. Thus, we characterise the solution and energy by the value of θ on the bag surface. Therefore, if we say $\psi_\theta(\vec{x})$ is a solution to the Dirac Equation, satisfying the Chiral Bag boundary conditions at a specific value of θ on the surface, then this Dirac spinor has the form

$$\psi_\theta^T = (\phi \quad \chi)e^{i\omega_\theta t}. \tag{5.3.7}$$

This solution will have associated with it a set of quantum numbers which serve to characterise this state. These quantum numbers will typically be analogues of angular momentum quantum numbers and 'radial' quantum numbers which determine the number of nodes the solution has. A cubic shaped bag does not have good angular momentum quantum numbrers and so in this case, the analogue of angular momentum quantum operators will be non-local.

In the case of a spherical bag with an external hedgehog field, the angular momentum quantum numbers are (K, k_z) and its purity $(-1)^L$. For each value of these quantum numbers there is a countable infinity of state with radial quantum numbers.

For the spherical bag, for $\theta = 0$, the M.I.T. Bag solutions have an energy spectrum for a given angular momentum quantum number, which is symmetric about zero energy. However, for non-zero values of θ on the surface, the spectrum is no longer symmetric. Thus, as we already observed, as θ varies on the surface there is a spectral flow of the energy spectrum. As θ increases from zero, the

energy of the lowest positive energy states, with a given set of angular momentum quantum numbers, reduces, until at $\theta = \pi/2$ it becomes zero. As θ continues to increase it then sinks in to the negative energy sea, until at a value of $\theta = \pi$ its energy is equal and opposite to its value at $\theta = 0$. The energies of the higher radial modes sink down to the energy of the next lowest state as θ increases from 0 to π. Thus, as θ varies from 0 to π the number of modes is conserved and moreover, the mode spectrum is invariant for the spherical bag, with respect to the transformation $\theta \mapsto \pi - \theta$.

It is this spectral flow which is responsible for the baryon number of the negative energy sea exactly cancelling the baryon number of the exterior mesonic field. To see this we must carefully define the baryon number of the interior quark vacuum. To calculate the vacuum contribution we have to perform a regulated mode sum, defined by;

$$B(\theta) = -\frac{1}{2} \, lim_{\lambda \to 0} \, \Sigma_n \, sign \, (\omega_n) e^{-|\lambda E_n|} \, |_\theta \, . \qquad (5.3.8)$$

For the spherical bag, we see that this spectral flow, as θ is increased from zero, results in $B(\theta)$ becoming increasingly negative and in this manner the vacuum contribution cancels the increasing mesonic field contribution to the baryon number, leaving the three valence quarks with unit baryon number, to wholly account for the baryon number. This mode sum has been explicitly performed by Goldstone and Jaffe [18], who confirm the result

$$B(\theta) = -\frac{(\theta - 1/2 \sin 2\theta)}{\pi}, \qquad (5.3.9)$$

242

which we see is the exact result required for the complete cancellation of the contribution of the exterior mesonic field, (5.2.4).

At $\theta = \pi/2$, the lowest energy mode has zero energy and in this case, the contribution of the negative energy sea to the baryon number is exactly minus one half. Thus, we see that the existence of a zero mode at $\theta = \pi/2$ is an important characteristic of the spectral flow.

Thus, for our cubic bag, we imagine that there will also be a zero mode when $\theta = \pi/2$. We wish here, to examine the conditions under which this zero mode might exist at $\theta = \pi/2$ for our cubic bag. Firstly, we can expect that as the value of θ on the bag surface is varied, no modes with the same angular like quantum numbers will cross. Given that ψ_θ, (5.3.4), is a solution satisfying the Chiral Bag boundary conditions, it is simple to deduce that

$$\psi_{-\theta}^T = (-\chi \quad \phi)e^{+i\omega_\theta t} \qquad (5.3.10)$$

will also be a solution. Note that the energy of this solution is of equal but opposite sign to that of ψ_θ. Similarly, in the massless quark limit there will also be a solution,

$$\psi_{\pi+\theta}^T = (\chi \quad \phi)e^{-i\omega_\theta t}. \qquad (5.3.11)$$

This solution has the same energy as ψ_θ. We see from this, that if we can identify these two solutions as having the same angular quantum numbers, then we have proven that the energy spectrum is invariant under the transformation $\theta \mapsto \theta + \pi$ and this is indeed the case for a spherical bag.

243

If this were also true for a cubical bag, we see that we would only need to demonstrate that as θ increases from 0 to π, all modes spiral down in energy, in order to obtain the result that there exists a zero mode at some value of θ between 0 and π. Hence, given that ψ_θ is a solution, then in the massless limit so is

$$\psi_{\pi-\theta}^T = (\phi \quad -\chi)e^{i\omega_\theta t}, \qquad (5.3.12)$$

which has an energy which is equal and opposite to that of the ψ_θ state. Thus, we see that if we can establish that the transformation $\theta \mapsto \pi - \theta$ does not change the lowest energy mode's quantum numbers, then we could identify this solution with ψ_θ. This would then imply

$$\psi_{\pi/2}^T = (\phi \quad 0), \qquad (5.3.13)$$

with $\omega_{\pi/2} = 0$. This is indeed the case for the spherical bag.

Thus, if we could identify these two solutions as having the same quantum numbers, we could reproduce the arguments which resulted in the baryon number cancellation by the negative energy sea. These arguments are most appealing and certainly identify the necessary requirement for such a cubic bag model to give a sensible value for the baryon number. However, the arguments required to establish whether or not a state can be identified with the state obtained by the transformation $\psi_\theta \mapsto \psi_{\pi-\theta}$, will depend on the nature and characteristics of the solution to the Dirac Equation within the cubic bag.

Thus, to summarise, we have presented appealing arguments which certainly

present a mechanism by which these cubic bags within skyrmionic matter could be included consistently. Moreover, although mode sum would be required to evaluate vacuum contributions to physical quantities, we feel that if we could establish the existence of a zero mode, when $\theta = \pi/2$ on the surface, then this would be sufficient evidence for one to believe these arguments. This model would then enable us to establish the particle content of these skyrmionic crystals and give us a real physical interpretation as to what its existence corresponds to.

References

[1] N.S.Manton and P.Ruback, Phys. Lett. B181, 137

[2] I.Klebanov, Nucl. Phys. B262 (1985) 133

[3] E.Braaten and L.Carson, Phys. Rev. D56 (1986) 1897

[4] J.J.Verbaarschot, T.S.Walhout, J.Wambach and H.W.Wyld,
Nucl. Phys. A468 (1987) 520

[5] E.Braaten, S.Townsend and L.Carson,
'Novel Structures of Multisolitonic Solutions in the Skyrme Model'
Uni. of Minnesota preprint (1984)

[6] M.Kugler and S.Shtrikman, Phys. Lett. B208 (1988) 491

[7] B.Banerjee N.K.Glendening and V.Sone

[8] M.Kutschera, C.J.Pethich and D.G.Ravenhall

[9] G.E.Brown, A.D.Jackson and E.Wurst, Nucl. Phys. A468 (1985) 450

[10] V.Vento, M.Rho, E.M.Nyman, J.H.Jun and G.E.Brown

[11] A.Chodos, R.L.Jaffe, K.Johnson, C.B.Thorn and V.F.Weiskoff,
Phys. Rev. D9 (1974) 3471

[12] A.Chodos, R.L.Jaffe, K.Johnson and C.B.Thorn,
Phys. Rev. D10 (1974)

T.Deyrand, R.L.Jaffe, K.Johnson and J.Kiskies

Phys. Rev. D12 (1975) 2060

[13] C.deTar, Phys. Rev. D17 (1978) 323

C.deTar, Phys. Rev. D19 (1979) 145

[14] L.Vepstas, 'Casimer Effect in the Chiral Bag Model' Ph.D. Thesis

Stony Brook

[15] M.Rho, A.S.Goldhaber and G.E.Brown, Phys. Rev. Lett. 519 (1983) 747

[16] S.Nadkarmi, H.B.Neilson and I.Zahed, Nucl. Phys. B253 (1985) 308

[17] A.D.Jackson and L.Vepstas, 'Justifying the Chiral Bag' preprint

Stony Brook

[18] J.Goldstone and R.L.Jaffe, Phys. Rev. Lett. 517 (1983) 1518

CHAPTER 6

CONCLUSION

6.1 General Conclusions

In the previous chapters, we have detailed at great length the many interesting features of Skyrmionic matter. In particular we have concentrated on describing and understanding the nature of infinite crystalline arrays of skyrmionic matter and the dense skyrmionic matter on a physical space with locally varying curvature.

At this stage we shall only briefly summarise the many conclusions which we have already drawn within this thesis.

We have seen that in its crystalline form, skyrmionic matter has some general features which are independent of the specific form of array on which the skyrmions are located. The most significant feature appears to be the existence of a phase transition as the density of skyrmionic matter is increased, which is in general of second order. This phase transition corresponds to skyrmionic matter, which at low densities is localised about the points of a lattice, becoming an array of half skyrmions at high densities which has an increased delocalising nature. Moreover, dense crystalline skyrmionic matter has a 'jelly like' charac-

ter, being relatively incompressible though easily deformed. We have also seen that the most stable form of crystalline skyrmionic matter so far discovered is a condensed, simple cubic array of half skyrmions.

Considering a single skyrmion on a closed surface and varying the volume of the surface, we can vary the average baryon density of the skyrmion. The simple three sphere model demonstrates that this effective manner of increasing or decreasing the volume of the skyrmion at high densities, causes the energy of the skyrmion to rise sharply as a result of its resistance to either isotropic compression or expansion. Thus, as we continue to increase to volume of physical space, there comes a point at which it is preferable for the skyrmion to localise about a point rather than continue to stretch itself over the whole of space. Beyond this point, increasing the volume of the sphere becomes ineffective in stretching the skyrmion and the skyrmion chooses to remain unstretched as the volume further increased, by localising about a point. This simple characteristic of skyrmionic matter accounts for the observed, striking similarities of the delocalising phase transitions which occur in both crystalline arrays of skyrmions and for a skyrmion on a three sphere.

However, the observation that dense crystalline skyrmionic matter is easily deformed has no analogue for a skyrmion on a three sphere, since in this case there is no method by which we can effectively and simply exert non-isotropic deformations on the skyrmion. To resolve this difficulty, we show that the relevant variable which can perform such non-isotropic deformations of skyrmion matter

is the local curvature of space and by simply placing the skyrmion on a space with varying local curvature, we can generate these deformations in an effective manner. Thus, we soon discovered that on a surface of varying curvature, the skyrmion very much prefers to sit on a region of space with the curvature of a three sphere of radius 1 and if forced to choose between regions of space of higher and lower curvature, it chooses the regions of low curvature. Thus, the gross features of our results for a skyrmion on an elliptically shaped three surface, revealed that if the shape of the sphere is changed to a space in which the curvature is lower in one region than the other, then the skyrmion responds by localising itself on that region of space and this process does not cost an undue amount of much energy. Thus we see once more, that this generalised model of a skyrmion on a three sphere provides a simple analogue to crystalline skyrmionic matter in that skyrmionic matter on an ellipse is resistant to expansion though easily deformable and as with crystalline skyrmionic matter has a 'jelly like' character.

This brief review of the many detailed arguments and results for the varying forms of dense skyrmionic matter that we have considered, demonstrates clearly the manner in which a simple geometrical picture of a the topological skyrmion can be used in order to understand the many complex results which we have presented and thus leads one to conclude that such a simple geometric picture of a skyrmion is both natural and important in this understanding of the relevance of skyrmions to baryonic matter.

LIST OF TABLES AND FIGURES

CHAPTER 3

CHAPTER 4